



Electroweak radiative B-decays as a test of the Standard Model and beyond

Andrey Tayduganov

► To cite this version:

Andrey Tayduganov. Electroweak radiative B-decays as a test of the Standard Model and beyond. Other [cond-mat.other]. Université Paris Sud - Paris XI, 2011. English. NNT : 2011PA112195 . tel-00648217

HAL Id: tel-00648217

<https://theses.hal.science/tel-00648217>

Submitted on 5 Dec 2011

HAL is a multi-disciplinary open access archive for the deposit and dissemination of scientific research documents, whether they are published or not. The documents may come from teaching and research institutions in France or abroad, or from public or private research centers.

L'archive ouverte pluridisciplinaire **HAL**, est destinée au dépôt et à la diffusion de documents scientifiques de niveau recherche, publiés ou non, émanant des établissements d'enseignement et de recherche français ou étrangers, des laboratoires publics ou privés.



LAL 11-181
LPT 11-69

THÈSE DE DOCTORAT

Présentée pour obtenir le grade de

Docteur ès Sciences de l'Université Paris-Sud 11

Spécialité: PHYSIQUE THÉORIQUE

par

Andrey Tayduganov

**Désintégrations radiatives faibles de mésons B
comme un test du Modèle Standard et au-delà**

**Electroweak radiative B -decays as a test of the
Standard Model and beyond**

Soutenue le 5 octobre 2011 devant le jury composé de:

Dr.	J. Charles	Examineur
Prof.	A. Deandrea	Rapporteur
Prof.	U. Ellwanger	Président du jury
Prof.	S. Fajfer	Examineur
Prof.	T. Gershon	Rapporteur
Dr.	E. Kou	Directeur de thèse
Dr.	A. Le Yaouanc	Directeur de thèse
Dr.	M.-H. Schune	Examineur

Contents

Résumé	7
Abstract	9
Introduction	11
1 Flavour physics in the Standard Model and beyond	13
1.1 The Standard Model	13
1.2 Motivation for New Physics beyond the Standard Model	17
1.3 $b \rightarrow s\gamma$ in the SM	19
1.3.1 Photon polarization of the quark level $b \rightarrow s\gamma$ process in the SM	20
1.3.2 Possible contamination of “wrong” chirality contribution due to the \mathcal{O}_2 term	25
1.4 Photon polarization with new physics	27
1.4.1 Extra source of flavour violation in MSSM	28
1.4.2 Mass Insertion Approximation	29
2 The $B \rightarrow K_1\gamma \rightarrow (K\pi\pi)\gamma$ decay and polarization measurement	31
2.1 How to measure the polarization: basic idea	31
2.2 Photon polarization determination with $B \rightarrow K_1\gamma$ decay	32
2.3 Master formula for $\overline{B} \rightarrow \overline{K}_1\gamma \rightarrow (\overline{K}\pi\pi)\gamma$ decays	35
2.3.1 Master formula	35
2.3.2 Derivation of the master formula	37
2.3.3 Hadronic parameters	41
2.4 Determination of λ_γ in the DDLR method	43
2.4.1 The previous method of Gronau <i>et al.</i>	43
2.4.2 Application of the DDLR method for the λ_γ determination	44
3 Strong interaction decays of the K_1-mesons	49
3.1 Overview of the previous K_1 -decay studies	49
3.1.1 Experimental overview	49
3.1.2 Theoretical overview	50
3.2 Theoretical model	52
3.2.1 The mixing of the kaon resonances	53

3.2.2	3P_0 Quark-Pair-Creation Model	54
3.2.3	The issue of the damping factor	58
3.3	How to compare the theoretical model computation with the experimental data?	59
3.3.1	The K -matrix formalism	60
3.3.2	Observed problems in the K -matrix analysis	63
3.4	Numerical results	68
3.4.1	Fit of parameters γ and θ_{K_1}	69
3.4.2	Model predictions for partial widths	71
3.4.3	Prediction of signs of decay amplitudes and the “off-set” phase issue	73
3.4.4	The issue of the $\kappa\pi$ channel	78
4	Sensitivity studies of the polarization measurement with $B \rightarrow K_1(1270)\gamma$ in the DDLR method	81
4.1	Statistical error on the polarization parameter	81
4.2	Theoretical uncertainties of the hadronic model and error on the polarization parameter	85
4.2.1	Theoretical uncertainty due to the K_1 mixing angle	86
4.2.2	Theoretical uncertainty due to the “off-set” phase δ_ρ	87
4.3	Discussion on the importance of the D -waves and the cut-off	90
5	Future prospects of the photon polarization measurement	93
5.1	Comparison to the other methods	93
5.1.1	Up-down asymmetry of GGPR	93
5.1.2	The angular analysis of $B \rightarrow K^*\ell^+\ell^-$	93
5.1.3	Methods invoking CP -asymmetries	97
5.2	New physics constraints combining various methods of the polarization determination	98
6	Conclusions	103
6.1	The general method of Gronau <i>et al.</i> : a critical view	103
6.2	Improvement of statistical errors by the DDLR method	105
6.3	The treatment of the full system of the K_1 -decays	105
6.3.1	Critical view of the experimental analyses of the K_1 -system of strong decays	105
6.3.2	A semi-theoretical treatment of the K_1 -system of strong decays	106
6.4	Theoretical errors on the polarisation measurement	106
6.5	The need for improvements of our experimental knowledge and some future prospects	106
A	Renormalization and running of the Wilson coefficients	109
A.1	Renormalization and operator mixing	109
A.2	$b \rightarrow s\gamma$ at Leading Logarithmic Approximation	110

B	Watson's theorem	115
C	K-matrix formalism	117
C.1	General formalism for the overlapping resonances	117
C.2	Relation of the couplings in the K -matrix method and the quark model . .	120
C.3	Watson's theorem: another view	123
C.4	Re-interpreting the ACCMOR result	124
D	QPCM	129
D.1	Spacial integrals in QPCM	129
D.2	Fixing the relative signs for tree-body decay	130
D.2.1	Clebsch-Gordan coefficients	130
D.2.2	Determination of the relative sign of $g_{K^*K\pi}$ and $g_{\rho\pi\pi}$	131
D.3	Partial Wave Amplitudes	132
D.4	Phase space convention	133
E	Some notes on statistics	135
E.1	Maximum likelihood method	135
E.2	General DDLR method	136
	Bibliography	141
	Acknowledgements	147

Résumé

La désintégration radiative du méson B en méson étrange axiale, $B \rightarrow K_1(1270)\gamma$, a été observée récemment avec un rapport d'embranchement assez grand que $B \rightarrow K^*\gamma$. Ce processus est particulièrement intéressant car la désintégration du K_1 dans un état final à trois corps nous permet de déterminer la polarisation du photon, qui est surtout gauche (droit) pour $\overline{B}(B)$ dans le Modèle Standard tandis que des modèles divers de nouvelle physique prédisent une composante droite (gauche) supplémentaire. Dans cette thèse, une nouvelle méthode est proposée pour déterminer la polarisation, en exploitant la distribution totale du Dalitz plot, qui semble réduire considérablement les erreurs statistiques de la mesure du paramètre de la polarisation λ_γ .

Cependant, cette mesure de la polarisation nécessite une connaissance détaillée de la désintégration forte $K_1 \rightarrow K\pi\pi$: c'est-à-dire l'ensemble complexe des différentes amplitudes d'ondes partielles en plusieurs canaux en quasi-deux-corps ainsi que leurs phases relatives. Un certain nombre d'expériences ont été faites pour extraire ces informations bien qu'il reste divers problèmes dans ces études. Dans cette thèse, nous étudions en détail ces problèmes en nous aidant d'un modèle théorique. Nous utilisons ainsi le modèle 3P_0 de création d'une paire de quarks pour améliorer notre compréhension des désintégrations fortes du K_1 .

A partir de ce modèle nous estimons les incertitudes théoriques : en particulier, celle venant de l'incertitude de l'angle de mélange du K_1 , et celle due à l'effet d'une phase "off-set" dans les désintégrations fortes en ondes- S . Selon nos estimations, les erreurs systématiques se trouvent être de l'ordre de $\sigma_{\lambda_\gamma}^{\text{th}} \lesssim 20\%$. D'autre part nous discutons de la sensibilité des expériences futures, notamment les usines SuperB et LHCb, pour λ_γ . En estimant naïvement les taux annuels d'événements, nous trouvons que l'erreur statistique de la nouvelle méthode est $\sigma_{\lambda_\gamma}^{\text{stat}} \lesssim 10\%$, ce qui est deux fois plus petit qu'en utilisant seulement les distributions angulaires simples.

Nous discutons également de la comparaison avec les autres méthodes de mesure de la polarisation en utilisant les processus tels que $B \rightarrow K^*e^+e^-$, $B_d \rightarrow K^*\gamma$ et $B_s \rightarrow \phi\gamma$, pour la détermination du rapport des coefficients de Wilson $C_{7\gamma}'^{\text{eff}}/C_{7\gamma}^{\text{eff}}$. Nous montrons un exemple de contraintes possibles sur $C_{7\gamma}'^{\text{eff}}/C_{7\gamma}^{\text{eff}}$ dans plusieurs scénarios de modèles supersymétriques.

Mots clés: Modèle Standard, au-delà du Modèle Standard, interaction faible, physique du B , désintégration radiative de meson- B , polarisation de photon, propriétés de meson- K_1 , modèle des quarks, matrice- K , asymétrie CP , supersymétrie.

Abstract

Recently the radiative B -decay to strange axial-vector mesons, $B \rightarrow K_1(1270)\gamma$, was observed with a rather large branching ratio. This process is particularly interesting as the subsequent K_1 -decay into its three-body final state allows us to determine the polarization of the photon, which is mostly left(right)-handed for $\overline{B}(B)$ in the Standard Model while various new physics models predict additional right(left)-handed components. In this thesis, a new method is proposed to determine the polarization, exploiting the full Dalitz plot distribution, which seems to reduce significantly the statistical errors on the polarization parameter λ_γ measurement.

This polarization measurement requires, however a detailed knowledge of the $K_1 \rightarrow K\pi\pi$ strong interaction decays, namely, the complex pattern of various partial wave amplitudes into the several possible quasi-two-body channels as well as their relative phases. A number of experiments have been done to extract all these information while there remain various problems in the previous studies. In this thesis, we investigate the details of these problems. As a theoretical tool, we use the 3P_0 quark-pair-creation model in order to improve our understanding of strong K_1 -decays.

Finally we try to estimate some theoretical uncertainties: in particular, the one coming from the uncertainty on the K_1 mixing angle, and the effect of a possible “off-set” phase in strong decay S -waves. According to our estimations, the systematic errors are found to be of the order of $\sigma_{\lambda_\gamma}^{\text{th}} \lesssim 20\%$. On the other hand, we discuss the sensitivity of the future experiments, namely the SuperB factories and LHCb, to λ_γ . Naively estimating the annual signal yields, we found the statistical error of the new method to be $\sigma_{\lambda_\gamma}^{\text{stat}} \lesssim 10\%$ which turns out to be reduced by a factor 2 with respect to using the simple angular distribution.

We also discuss a comparison to the other methods of the polarization measurement using processes, such as $B \rightarrow K^*e^+e^-$, $B_d \rightarrow K^*\gamma$ and $B_s \rightarrow \phi\gamma$, for the determination of the ratio of the Wilson coefficients $C_{7\gamma}'^{\text{eff}}/C_{7\gamma}^{\text{eff}}$. We show an example of potential constraints on the $C_{7\gamma}'^{\text{eff}}/C_{7\gamma}^{\text{eff}}$ in several scenarios of supersymmetric models.

Keywords: Standard Model, beyond the Standard Model, weak interaction, B -physics, radiative B -decay, photon polarization, K_1 properties, quark model, K -matrix, CP asymmetry, supersymmetry.

Introduction

The radiative decay $b \rightarrow s\gamma$ has been extensively studied as a probe of the flavour structure of the Standard Model (SM) as well as new physics beyond the SM. While the majority of studies has been focused on the prediction of the decay rates of exclusive and inclusive $b \rightarrow s\gamma$ decays, there is one very interesting feature of this process which has attracted far less attention: in the SM, the emitted photon is predominantly left-handed in b , and right-handed in \bar{b} decays. This is due to the fact that the dominant contribution is from the chiral-odd dipole operator $\bar{s}_{L(R)}\sigma_{\mu\nu}b_{R(L)}$. As only left-handed quarks participate in weak interaction, this effective operator induces a helicity flip on one of the external quark lines, which results in a factor m_b for $b_R \rightarrow s_L\gamma_L$ and a factor m_s for $b_L \rightarrow s_R\gamma_R$. Hence, the emission of right-handed photons is suppressed by a factor m_s/m_b . This suppression can be relieved in some new physics models where the helicity flip occurs on an internal line, resulting in a factor m_{NP}/m_b instead of m_s/m_b . Unless the amplitude for $b \rightarrow s\gamma_R$ is of the same order as the SM prediction, or the enhancement of $b \rightarrow s\gamma_R$ goes along with the suppression of $b \rightarrow s\gamma_L$, the impact on the branching ratio is small since the two helicity amplitudes add incoherently. This implies that there can be a substantial contribution of new physics to $b \rightarrow s\gamma$ escaping detection when only branching ratios are measured. Therefore, the photon polarization measurement could provide a good test of the SM. In Chapter 1, after a mini-review of the SM, we present the basic theoretical knowledge needed for the polarization study in $b \rightarrow s\gamma$ such as operator product expansion. We also briefly discuss QCD effects and the consequent contamination from the right-handed polarization in exclusive processes.

Although the photon helicity is, in principle, a measurable quantity, it is very difficult to measure it directly. In this thesis we investigate one of the methods based on the study of the recently observed exclusive decay $B \rightarrow K_1(1270)\gamma$ followed by the three-body decay $K_1(1270) \rightarrow K\pi\pi$. Since the photon helicity is parity-odd and we measure only the momenta of the final state particles, one can form a triple product of three momenta like $\vec{p}_\gamma \cdot (\vec{p}_\pi \times \vec{p}_K)$ which is a pseudo-scalar and applying parity transformation it has the opposite sign for left- and right-handed photons. Therefore, this process is particularly interesting as the subsequent K_1 -decay into its three-body final state allows us to determine the polarization directly. In Chapter 2, we derive the master formula for the decay distribution of $B \rightarrow (K\pi\pi)_{K_1}\gamma$ and introduce a new method for the polarization determination. We propose a new variable, ω , to determine the polarization parameter λ_γ . The use of ω significantly simplifies the experimental analysis and allows us to include not only the angular dependence of the polarization parameter but also the three-body

Dalitz variable dependence to the fit.

In order to measure the polarization parameter λ_γ precisely, a sufficiently accurate modelling of the hadronic decays of $K_1 \rightarrow K\pi\pi$ is required. We first introduce the basic hadronic parameters required in our analysis, namely the various partial wave amplitudes into several possible quasi-two-body channels, as well as their relative phases. These parameters can, in principle, be determined by experimental measurements of the $K_1(1270) \rightarrow K\pi\pi$ decay. On the other hand, although the ACCMOR experiment had provided an extensive study of this decay, we find that the information one can extract from it is not accurate enough. In Chapter 3, we describe some of the problems encountered in our analysis, which include the strong phase between different intermediate resonance states and the controversial $K_1(1270) \rightarrow \kappa\pi$ channel. Being unable to obtain the hadronic parameters from the fundamental theory, we resort to combine experimental data and phenomenological models. In particular, combining the experimental results of the partial wave analysis of the K_1 -decays using the K -matrix formalism and the predictions of the 3P_0 quark-pair-creation model, we determine the phenomenological parameters of the model such as the K_1 mixing angle and the universal quark-pair-creation constant.

In Chapter 4, we estimate the sensitivity of the future experiments to λ_γ using Monte Carlo simulation and discuss statistical errors and theoretical uncertainties of the hadronic model. It turns out that the probability density function, or equivalently the properly normalized differential decay width distribution, is linearly dependent on the polarization parameter λ_γ : $W(\omega) = \varphi(\omega)(1 + \lambda_\gamma\omega)$. In principle, $\varphi(\omega)$ is a very complicated and unknown function which analytical form is very hard to derive. Thus, we use a numerical Monte Carlo method in order to simulate the ω -distribution. We find out that the inclusion of the full Dalitz information can improve the sensitivity by typically a factor of two compared to the pure angular fit. In Chapter 5, we discuss the sensitivity of the future experiments, namely the SuperB factories and LHCb to λ_γ , and compare our new method with the other methods of the polarization determination using different processes, such as $B^0 \rightarrow K^{*0}e^+e^-$, $B^0 \rightarrow K^{*0}(\rightarrow K_S\pi^0)\gamma$ and $B_s \rightarrow \phi\gamma$. Combining these different methods, we give an example of possible future constraints on the ratio of the Wilson coefficients $C'_{\tau\gamma}/C_{\tau\gamma}^{eff}$ in several scenarios of the Minimal Supersymmetric Standard Model.

We give our conclusions and perspectives for the future potential measurement of the photon polarization in Chapter 6. Some more technical aspects and details are discussed in the Appendices.

Chapter 1

Flavour physics in the Standard Model and beyond

1.1 The Standard Model

The Standard Model (SM) of strong, weak and electromagnetic interactions is a relativistic quantum field theory that describes all known interactions of quarks and leptons. The SM is made up of the Glashow-Weinberg-Salam model of the electroweak interactions and Quantum Chromodynamics (QCD). The SM is a gauge theory based on the gauge group $SU(3)_c \times SU(2)_L \times U(1)_Y$. The $SU(3)_c$ gauge group describes the strong colour interactions among quarks, and the $SU(2)_L \times U(1)_Y$ gauge group describes the electroweak interactions. At the present time three generations of quarks and leptons have been observed. The measured width of the Z boson does not permit a fourth generation with a massless (or light) neutrino. Many extensions of the minimal SM have been proposed, and there is evidence in the present data for neutrino masses, which requires new physics beyond the SM. Low-energy supersymmetry, dynamical weak symmetry breaking, extra dimensions, or something totally unexpected may be discovered at the next generation of high-energy particle accelerators.

The matter fields in the minimal SM are three families of spin-1/2 quarks and leptons, and a spin-zero Higgs boson, shown in Table 1.1. Q_L^i , u_R^i , d_R^i are the quark fields and L_L^i , e_R^i are the lepton fields. All the particles associated with the fields in Table 1.1 have been observed experimentally, except for the Higgs boson. The index i on the fermion fields is a family or generation index ($i = 1, 2, 3$), and the subscripts L and R denote left- and right-handed fields respectively,

$$\psi_L = P_L \psi, \quad \psi_R = P_R \psi \quad (1.1)$$

where P_L and P_R are the projection operators

$$P_L = \frac{1}{2}(1 - \gamma_5), \quad P_R = \frac{1}{2}(1 + \gamma_5) \quad (1.2)$$

Field	$SU(3)$	$SU(2)$	$U(1)$	Lorentz
$Q_L^i = \begin{pmatrix} u_L^i \\ d_L^i \end{pmatrix}$	3	2	1/6	(1/2, 0)
u_R^i	3	2	2/3	(0, 1/2)
d_R^i	3	2	-1/3	(0, 1/2)
$L_L^i = \begin{pmatrix} \nu_L^i \\ e_L^i \end{pmatrix}$	1	2	-1/2	(1/2, 0)
e_R^i	1	1	-1	(0, 1/2)
$\phi = \begin{pmatrix} \phi^+ \\ \phi^0 \end{pmatrix}$	1	2	1/2	(0, 0)

Table 1.1: Matter fields in the SM.

The $SU(2)_L \times U(1)_Y$ symmetry of the electroweak sector is not manifest at low energies. In the SM, the $SU(2)_L \times U(1)_Y$ symmetry is spontaneously broken by the vacuum expectation value of the Higgs doublet ϕ . The spontaneous breakdown of $SU(2)_L \times U(1)_Y$ gives mass to the W^\pm and Z^0 gauge bosons. A single Higgs doublet is the simplest way to achieve the observed pattern of spontaneous symmetry breaking, but a more complicated scalar sector, such as two doublets, is possible.

The terms in the SM Lagrangian density that involve only the Higgs doublet

$$\phi = \begin{pmatrix} \phi^+ \\ \phi^0 \end{pmatrix} \quad (1.3)$$

are

$$\mathcal{L}_{\text{Higgs}} = (D_\mu \phi)^\dagger (D_\mu \phi) - V(\phi) \quad (1.4)$$

where D_μ is the covariant derivative and $V(\phi)$ is the Higgs potential

$$V(\phi) = \mu^2 (\phi^\dagger \phi) + \lambda (\phi^\dagger \phi)^2 \quad (1.5)$$

For $\mu^2 < 0$ the Higgs potential is minimized when $\phi^\dagger \phi = -\mu^2/2\lambda$. This gives the vacuum expectation value in the standard form

$$\langle \phi \rangle = \begin{pmatrix} 0 \\ v/\sqrt{2} \end{pmatrix} \quad (1.6)$$

where $v = \sqrt{-\mu^2/\lambda}$ is real and positive.

The gauge covariant derivative acting on any field ψ is

$$D_\mu = \partial_\mu - ig_s A_\mu^a t^a - ig_2 W_\mu^i T^i - ig_1 B_\mu Y \quad (1.7)$$

where t^a ($a = 1, \dots, 8$) are the eight color $SU(3)$ generators, T^i ($i = 1, 2, 3$) are the weak $SU(2)$ generators, and Y is the $U(1)$ hypercharge generator. The generators are chosen to be in the representation of the field ψ on which the covariant generator acts. The gauge

bosons and the coupling constants associated with these gauge groups are denoted A_μ^a , W_μ^i and B_μ and g_s , g_2 and g_1 respectively. The kinetic term for the Higgs field contains a piece quadratic in the gauge fields when expanded about the Higgs vacuum expectation value. The quadratic terms that produce a gauge-boson mass are

$$\mathcal{L}_{\text{gauge boson mass}} = \frac{g_2^2 v^2}{8} (W^1 W^1 + W^2 W^2) + \frac{v^2}{8} (g_2 W^3 - g_1 B)^2 \quad (1.8)$$

where for simplicity of notation the Lorentz indices are suppressed. The charged W -boson fields

$$W_\mu^\pm = \frac{W_\mu^1 \mp i W_\mu^2}{\sqrt{2}} \quad (1.9)$$

have mass

$$M_W = \frac{g_2 v}{2} \quad (1.10)$$

It is convenient to introduce the weak mixing angle θ_W defined by

$$\sin \theta_W = \frac{g_1}{\sqrt{g_1^2 + g_2^2}}, \quad \cos \theta_W = \frac{g_2}{\sqrt{g_1^2 + g_2^2}} \quad (1.11)$$

The Z -boson field and photon field A are defined as linear combinations of the neutral gauge-boson fields W^3 and B :

$$\begin{aligned} Z_\mu &= W_\mu^3 \cos \theta_W - B_\mu \sin \theta_W \\ A_\mu &= W_\mu^3 \sin \theta_W + B_\mu \cos \theta_W \end{aligned} \quad (1.12)$$

The Z boson has a mass at tree level

$$M_Z = \frac{\sqrt{g_1^2 + g_2^2}}{2} v = \frac{M_W}{\cos \theta_W} \quad (1.13)$$

and the photon is massless.

The covariant derivative in Eq. (1.7) can be expressed in terms of the mass-eigenstate fields as

$$D_\mu = \partial_\mu - i g_s A_\mu^a t^a - i \frac{g_2}{\sqrt{2}} (W_\mu^+ T^+ + W_\mu^- T^-) - i \sqrt{g_1^2 + g_2^2} (T^3 - Q \sin^2 \theta_W) Z_\mu - i g_2 Q \sin \theta_W A_\mu \quad (1.14)$$

where $T^\pm = T^1 \pm i T^2$. The photon couplings constant in Eq. (1.14) leads to relation of the electric charge e and $g_{1,2}$ couplings: $e = g_2 \sin \theta_W$.

$SU(3)_c \times SU(2)_L \times U(1)_Y$ gauge invariance prevents bare mass terms for the quarks and leptons from appearing in the Lagrangian density. The quarks and leptons get mass

because of their Yukawa couplings to the Higgs field (colour indices are suppressed for simplicity):

$$\mathcal{L}_{\text{Yukawa}} = Y_u^{ij} \bar{u}_R^i \phi^T \epsilon Q_L^j - Y_d^{ij} \bar{d}_R^i \phi^\dagger Q_L^j - Y_e^{ij} \bar{e}_R^i \phi^\dagger L_L^j + \text{h.c.} \quad (1.15)$$

Since ϕ has a vacuum expectation value, the Yukawa couplings in Eq. (1.15) give rise to the 3×3 quark and lepton masses

$$M_u^{ij} = v Y_u^{ij} / \sqrt{2}, \quad M_d^{ij} = v Y_d^{ij} / \sqrt{2}, \quad M_e^{ij} = v Y_e^{ij} / \sqrt{2} \quad (1.16)$$

Neutrinos do not get mass from the Yukawa interactions in Eq. (1.15) since there is no right-handed neutrino field.

Any matrix M can be brought into diagonal form by separate unitary transformations on the left and right, $M \rightarrow \mathcal{U}_L M_{\text{diag}} \mathcal{U}_R^\dagger$, where \mathcal{U}_L and \mathcal{U}_R are unitary and M_{diag} is real, diagonal and non-negative. One can make separate unitary transformations on the left- and right-handed quark and lepton fields, while leaving the kinetic energy terms for the quarks, $\bar{Q}_L^i i \not{\partial} Q_L^i$, $\bar{u}_R^i i \not{\partial} u_R^i$ and $\bar{d}_R^i i \not{\partial} d_R^i$, and also those for the leptons, invariant. The unitary transformations are

$$\begin{aligned} u_L &= \mathcal{U}_L^u u'_L, & u_R &= \mathcal{U}_R^u u'_R, \\ d_L &= \mathcal{U}_L^d d'_L, & d_R &= \mathcal{U}_R^d d'_R, \\ e_L &= \mathcal{U}_L^e e'_L, & e_R &= \mathcal{U}_R^e e'_R. \end{aligned} \quad (1.17)$$

Here u , d and e are three-component column vectors (in flavour space) for the quarks and leptons, and the primed fields represent the corresponding mass eigenstates. The transformation matrices \mathcal{U} are 3×3 unitary matrices which are chosen to diagonalize the mass matrices:

$$\begin{aligned} \mathcal{U}_R^{u\dagger} M_u \mathcal{U}_L^u &= \text{Diag}(m_u, m_c, m_t) \\ \mathcal{U}_R^{d\dagger} M_d \mathcal{U}_L^d &= \text{Diag}(m_d, m_s, m_b) \\ \mathcal{U}_R^{e\dagger} M_e \mathcal{U}_L^e &= \text{Diag}(m_e, m_\mu, m_\tau) \end{aligned} \quad (1.18)$$

Diagonalizing the quark mass matrices in Eq. (1.18) requires different transformations of u_L and d_L , which are part of the same $SU(2)$ doublet Q_L . The original quark doublet can be rewritten as

$$\begin{pmatrix} u_L \\ d_L \end{pmatrix} = \begin{pmatrix} \mathcal{U}_L^u u'_L \\ \mathcal{U}_L^d d'_L \end{pmatrix} = \mathcal{U}_L^u \begin{pmatrix} u'_L \\ V_{\text{CKM}} d'_L \end{pmatrix} \quad (1.19)$$

where the Cabibbo-Kobayashi-Maskawa (CKM) mixing matrix V_{CKM} [1, 2] is defined as

$$V_{\text{CKM}} = \mathcal{U}_L^{u\dagger} \mathcal{U}_L^d \quad (1.20)$$

It is convenient to reexpress the SM Lagrangian in terms of the primed mass-eigenstate fields. The unitary matrices in Eq. (1.19) leave the quark kinetic terms unchanged. The Z and photon couplings are also unaffected, so *there are no flavour-changing neutral currents (FCNC) in the SM Lagrangian at tree level*. The W couplings are left unchanged by \mathcal{U}_L^u but not by V_{CKM} :

$$\frac{g_2}{\sqrt{2}} \bar{u}_L \gamma^\mu d_L W_\mu^+ = \frac{g_2}{\sqrt{2}} \bar{u}'_L \gamma^\mu V_{\text{CKM}} d'_L W_\mu^+ \quad (1.21)$$

As a result there are flavour-changing charged currents at tree level.

The CKM matrix V_{CKM} is a 3×3 unitary matrix, and so is completely specified by nine real parameters. Some of these can be eliminated by making phase redefinitions of the quark fields. The u and d quark mass matrices are unchanged if one makes independent phase rotations on the six quarks, provided the same phase is used for the left- and right-handed quarks of a given flavour. An overall phase rotation of all the quarks leaves the CKM matrix unchanged but the remaining five rotations can be used to eliminate five parameters, so that V_{CKM} can be written in terms of four parameters. One of the most convenient CKM parametrizations of V_{CKM} was introduced by Wolfenstein [3] which is defined by four parameters λ , A , ρ and η in the following way:

$$V_{\text{CKM}} = \begin{pmatrix} V_{ud} & V_{us} & V_{ub} \\ V_{cd} & V_{cs} & V_{cb} \\ V_{td} & V_{ts} & V_{tb} \end{pmatrix} = \begin{pmatrix} 1 - \lambda^2/2 & \lambda & A\lambda^3(\rho - i\eta) \\ -\lambda & 1 - \lambda^2/2 & A\lambda^2 \\ A\lambda^3(1 - \rho - i\eta) & -A\lambda^2 & 1 \end{pmatrix} + O(\lambda^4) \quad (1.22)$$

The analysis for leptons is similar to that for quarks, with one notable difference- because the neutrinos are massless, one can choose to make the same unitary transformation of the left-handed charged leptons and neutrinos.

1.2 Motivation for New Physics beyond the Standard Model

For the present moment the SM has been very successful in explaining a wide variety of existing experimental data. It covers a wide range of phenomena from low energy (less than a GeV) physics, such as kaon decays, to high energy (a few hundred GeV) processes involving real weak gauge bosons and top quarks. However, the SM is not satisfactory as the theory of elementary particles beyond the TeV energy scale. First of all, it does not explain the characteristic pattern of the mass spectrum of quarks and leptons. The second generation quarks and leptons are several orders of magnitude heavier than the corresponding first generation particles, and the third generation is even heavier by another order of magnitude. The quark flavour mixing CKM matrix also has a remarkable hierarchical structure, i.e. the diagonal terms are very close to unity and $\theta_{13} \ll \theta_{23} \ll \theta_{12} \ll 1$, where θ_{ij} denotes a mixing angle between the i -th and j -th generations. The observation of neutrino oscillations implies that there is also a

rich flavour structure in the leptonic sector. All of these masses and mixings are free parameters in the SM, but ideally they should be explained by some higher scale theory that could be responsible for this disparity.

The particles in the SM acquire masses from the Higgs mechanism. As is well known, the Higgs potential (1.5) is described by a scalar field theory, which contains a quadratic mass divergence due to the quantum corrections. This means that a Higgs mass of the order 100 GeV¹ is realized only after a huge cancellation between the bare Higgs mass squared μ^2 and the quadratically divergent mass renormalization, both of which are quantities of order Λ^2 where Λ is the cutoff scale of the theory. If Λ is of the order of the Planck scale ($M_{Pl} \sim 10^{19}$ GeV), then a cancellation of more than 30 orders of magnitude is required. This represents a fine-tuning which is often called the hierarchy problem. It would be highly unnatural if the SM was the theory valid at a very high energy scale, such as the M_{Pl} . Hence, the SM should be considered as an effective theory of some more fundamental theory, which most likely lies in the TeV energy region.

CP -violation is needed to produce the observed baryon number (or matter-antimatter) asymmetry in the universe. In the SM the complex phase of the CKM matrix (the V_{ub} and V_{td} matrix elements in Eq. (1.22) are complex) provides the only source of CP -violation, but models of baryogenesis suggest that it is quantitatively insufficient (for example, the V_{ub} and V_{td} contain the dominant source of the complex phase). This is another motivation to consider new physics models.

Several scenarios have been proposed for the physics beyond the SM. They introduce new particles, dynamics, symmetries or even extra-dimensions at the TeV energy scale. One of the most popular scenarios are the supersymmetric theories (SUSY). In SUSY one introduces a new symmetry between bosons and fermions, and a number of new particles (superpartners) that form supersymmetric pairs with the existing SM particles. The quadratic divergence of the Higgs mass term is then canceled out among the superpartners. The large extra space-time dimension models solve the problem by extending the number of spacetime dimensions beyond four. The Planck scale is diluted due to the large extra dimensions in the ADD-type models [6] since gravity is much more weaker because of this extra volume. In the Randall-Sundrum-type models [7] the hierarchy between the electroweak and Planck branes is diluted due to the exponential factor of the warped metric. Of course, this list is not complete and there exist many other proposed scenarios and models.

FCNC processes, such as $B - \bar{B}$ mixing and the $b \rightarrow s\gamma$ transition, provide strong constraints on new physics beyond the SM. If there is no suppression mechanism for FCNC processes, such as the Glashow-Iliopoulos-Maiani (GIM) mechanism [8] in the SM, the new physics contribution can easily become too large to be consistent with the experimental data. Therefore, the measurement of FCNC processes provides a good test of the flavour structure in new physics models. In chapter 5 we will illustrate one

¹The non-observation of the Higgs boson at LEP provides the lower bound at 95% CL: $m_{h_0} > 114.4$ GeV [4]. Quite recently CDF and DØ experiments at Tevatron excluded at 95% CL the range $158 < m_{h^0} < 173$ GeV [5]. A global fit of the electroweak precision data in the SM gives the upper bound at 95% CL: $m_{h^0} < 185$ GeV.

particular supersymmetric scenario and demonstrate the possible constraints on some SUSY parameters coming from the study of the $b \rightarrow s\gamma$ process.

1.3 $b \rightarrow s\gamma$ in the SM

The $b \rightarrow s\gamma$ process has played an important role in our understanding of the electro-weak interaction of the SM. The GIM mechanism shows that in the SM, FCNC such as $b \rightarrow s\gamma$ is forbidden at the tree level and only occurs through a loop level diagram. Inside of the loop, heavy particles, much heavier than b quark, can propagate. Therefore, the $b \rightarrow s\gamma$ process can be used to probe indirectly such heavy particles, namely top quarks in the case of SM or as yet unknown particles introduced by given models beyond the SM.

By now, the branching ratio of the inclusive $B \rightarrow X_s\gamma$ process is measured at a quite high precision ($\mathcal{B}(B \rightarrow X_s\gamma)_{\text{exp}} = (3.55 \pm 0.24 \pm 0.09) \times 10^{-4}$ [9]). The SM theoretical predictions for this observable are obtained at the next-to-next-to-leading order in QCD ($\mathcal{B}(B \rightarrow X_s\gamma)_{\text{th}} = (3.15 \pm 0.23) \times 10^{-4}$ [10]) and they are in relatively good agreement with the experimental value. However, these predictions have theoretical uncertainties coming from the CKM matrix element as well as various kinds of QCD corrections. As a result, even if we add some new physics contributions to the theoretical predictions, the total branching ratio often agrees with the experimental value within those theoretical uncertainties. While tremendous efforts in order to improve the precision of the theoretical prediction have been made so as to match the experimental precision, which could become even higher at future machines, it is necessary to investigate the characteristics of the particles inside the loop of the $b \rightarrow s\gamma$ process using another kind of observable. In this thesis, we discuss a measurement of the circular-polarization of the photon of the $b \rightarrow s\gamma$ process, which has the left- and right-handedness of the couplings of the interactions among the particles inside of the loop. In the SM, the fact that the W boson couples to left-handed quarks induces the photon polarization to be mostly left-handed. On the other hand, many new physics models contain new particles which couple differently from the SM. Therefore, the measurement of the photon polarization can be a useful tool to distinguish the interactions of the particles inside the $b \rightarrow s\gamma$ loop from the SM-like ones.

Although, there have been several proposals for how to measure this photon polarization, a precise measurement has not been achieved yet. In this chapter, we revisit the method proposed by Gronau *et al.* [11, 12] (the GGPR method in the following) using the exclusive $B \rightarrow K_{\text{resonance}}\gamma$ followed by the three-body decay of the $K_{\text{resonance}}$. Most interestingly, the Belle collaboration recently observed one of these decay channels, $B \rightarrow K_1(1270)\gamma \rightarrow (K\pi\pi)\gamma$, and found a relatively large branching ratio [13]

$$\mathcal{B}(B^+ \rightarrow K_1^+(1270)\gamma) = (4.3 \pm 0.9(\text{stat}) \pm 0.9(\text{syst})) \times 10^{-5} \quad (1.23)$$

which dominates over the decay to $K_1(1400)$, previously studied in detail by Gronau *et al.* [11, 12]. In this thesis, we introduce a new variable, ω , which was originally proposed by Davier *et al.* [14] for the τ polarization measurement at LEP (the DDLR method in the following). As we show later-on, the fact that the decay width of $B \rightarrow K_1\gamma \rightarrow (K\pi\pi)\gamma$

process depends only linearly on the polarization parameter λ_γ , allows us to use the variable ω in our study. The simplification in the fit by using ω makes it easier to include in the fit not only the angular dependence of the polarization parameter but also the three-body Dalitz variable dependence, which improves the sensitivity to the polarization parameter as also pointed out in [14]. On the other hand, the new radiative decay to $K_1(1270)\gamma$ instead of the $K_1(1400)\gamma$, implies a more complex pattern of hadronic decay channels, not only through $K^*\pi$, but also through $K\rho$ and a possible $\kappa\pi$. In this thesis, we discuss in detail the hadronic parameters required in this analysis. In particular, having various difficulties to extract them fully from the currently available experimental data, we attempt to evaluate them with the help of the so-called 3P_0 decay model.

1.3.1 Photon polarization of the quark level $b \rightarrow s\gamma$ process in the SM

In the SM, the quark level $b \rightarrow s\gamma$ vertex *without any QCD corrections* is given as:

$$\bar{s} \Gamma_\mu^{b \rightarrow s\gamma} b = \frac{e}{(4\pi)^2} \frac{g^2}{2M_W^2} V_{ts}^* V_{tb} F_2 \bar{s} i \sigma_{\mu\nu} q^\nu \left(m_b \frac{1 + \gamma_5}{2} + m_s \frac{1 - \gamma_5}{2} \right) b \quad (1.24)$$

where $q = p_b - p_s$ with p_b and p_s four-momentum of the b and s quark, respectively, F_2 is the loop function, whose expression can be found in [15]. If we fix the three momentum direction, namely the q direction, as $+z$ in the b quark rest frame (i.e. $q^\mu = (|\vec{q}|, 0, 0, |\vec{q}|)$) and define the right- and left-handed polarization vectors as

$$\varepsilon_{R,L}^\mu = \mp \frac{1}{\sqrt{2}} \begin{pmatrix} 0 \\ 1 \\ \pm i \\ 0 \end{pmatrix} \quad (1.25)$$

one can compute the helicity amplitude and demonstrate explicitly that

$$\bar{s}_L \sigma_{\mu\nu} q^\nu b_R \varepsilon_R^{\mu*} = \bar{s}_R \sigma_{\mu\nu} q^\nu b_L \varepsilon_L^{\mu*} = 0 \quad (1.26)$$

So we readily find that the first(second) term in Eq. (1.24) is non-zero only when we multiply by the left(right)-handed circular-polarization vector.

That means that the first term in Eq. (1.24), proportional to m_b , describes the $b_R \rightarrow s_L \gamma_L$ transition while the second one, proportional to m_s , describes the $b_L \rightarrow s_R \gamma_R$ transition². Since $m_s/m_b \simeq 0.02 \ll 1$, the photon in $b \rightarrow s\gamma$ in the SM is known to be predominantly left-handed.

²More intuitively, the outgoing photon polarization can be determined in the following way: due to the chiral structure of the W boson coupling to quarks the first term in Eq. (1.24) describes $b_R \rightarrow s_L$ transition; since $b \rightarrow s\gamma$ is a two-body back-to-back decay in the b -quark reference frame, due to the helicity conservation the photon must be left-handed. Correspondingly, the second term in Eq. (1.24) describes the right-handed photon emission.

Once we include the QCD corrections, other types of Dirac structure contribute and the above conclusion can be slightly modified. The result can typically be described in terms of the following effective Hamiltonian:

$$\mathcal{H}_{eff} = -\frac{4G_F}{\sqrt{2}}V_{ts}^*V_{tb}\left(\sum_{i=1}^6 C_i(\mu)\mathcal{O}_i(\mu) + C_{7\gamma}(\mu)\mathcal{O}_{7\gamma}(\mu) + C_{8g}(\mu)\mathcal{O}_{8g}(\mu) + \sum_{i=1}^6 C'_i(\mu)\mathcal{O}'_i(\mu) + C'_{7\gamma}(\mu)\mathcal{O}'_{7\gamma}(\mu) + C'_{8g}(\mu)\mathcal{O}'_{8g}(\mu)\right) \quad (1.27)$$

where C_i are the short-distance Wilson coefficients that can be calculated in perturbation theory, \mathcal{O}_i are the local long-distance operators which originate from diagrams in Fig. 1.1 and are given as follows:

Current-current:

$$\mathcal{O}_1 = (\bar{s}_{\alpha L}\gamma_\mu c_{\beta L})(\bar{c}_{\beta L}\gamma^\mu b_{\alpha L}), \quad \mathcal{O}'_1 = (\bar{s}_{\alpha R}\gamma_\mu c_{\beta R})(\bar{c}_{\beta R}\gamma^\mu b_{\alpha R}) \quad (1.28a)$$

$$\mathcal{O}_2 = (\bar{s}_{\alpha L}\gamma_\mu c_{\alpha L})(\bar{c}_{\beta L}\gamma^\mu b_{\beta L}), \quad \mathcal{O}'_2 = (\bar{s}_{\alpha R}\gamma_\mu c_{\alpha R})(\bar{c}_{\beta R}\gamma^\mu b_{\beta R}) \quad (1.28b)$$

QCD-penguins:

$$\mathcal{O}_3 = (\bar{s}_{\alpha L}\gamma_\mu b_{\alpha L})\sum_q(\bar{q}_{\alpha L}\gamma^\mu q_{\alpha L}), \quad \mathcal{O}'_3 = (\bar{s}_{\alpha R}\gamma_\mu b_{\alpha R})\sum_q(\bar{q}_{\alpha R}\gamma^\mu q_{\alpha R}) \quad (1.29a)$$

$$\mathcal{O}_4 = (\bar{s}_{\alpha L}\gamma_\mu b_{\beta L})\sum_q(\bar{q}_{\beta L}\gamma^\mu q_{\alpha L}), \quad \mathcal{O}'_4 = (\bar{s}_{\alpha R}\gamma_\mu b_{\beta R})\sum_q(\bar{q}_{\beta R}\gamma^\mu q_{\alpha R}) \quad (1.29b)$$

$$\mathcal{O}_5 = (\bar{s}_{\alpha L}\gamma_\mu b_{\alpha L})\sum_q(\bar{q}_{\alpha R}\gamma^\mu q_{\alpha R}), \quad \mathcal{O}'_5 = (\bar{s}_{\alpha R}\gamma_\mu b_{\alpha R})\sum_q(\bar{q}_{\alpha L}\gamma^\mu q_{\alpha L}) \quad (1.29c)$$

$$\mathcal{O}_6 = (\bar{s}_{\alpha L}\gamma_\mu b_{\beta L})\sum_q(\bar{q}_{\beta R}\gamma^\mu q_{\alpha R}), \quad \mathcal{O}'_6 = (\bar{s}_{\alpha R}\gamma_\mu b_{\beta R})\sum_q(\bar{q}_{\beta L}\gamma^\mu q_{\alpha L}) \quad (1.29d)$$

Magnetic penguins:

$$\mathcal{O}_{7\gamma} = \frac{e}{16\pi^2}m_b\bar{s}_{\alpha L}\sigma^{\mu\nu}b_{\alpha R}F_{\mu\nu}, \quad \mathcal{O}'_{7\gamma} = \frac{e}{16\pi^2}m_b\bar{s}_{\alpha R}\sigma^{\mu\nu}b_{\alpha L}F_{\mu\nu} \quad (1.30a)$$

$$\mathcal{O}_{8g} = \frac{e}{16\pi^2}m_b\bar{s}_{\alpha L}\sigma^{\mu\nu}t_{\alpha\beta}^a b_{\beta R}G_{\mu\nu}^a, \quad \mathcal{O}'_{8g} = \frac{e}{16\pi^2}m_b\bar{s}_{\alpha R}\sigma^{\mu\nu}t_{\alpha\beta}^a b_{\beta L}G_{\mu\nu}^a \quad (1.30b)$$

where α, β are the colour indices, $q_{R,L} = \frac{1 \pm \gamma_5}{2}q$, $\sigma^{\mu\nu} = \frac{i}{2}[\gamma^\mu, \gamma^\nu]$, t^a ($a = 1, \dots, 8$) are the SU(3) colour generators, $F_{\mu\nu}$ and $G_{\mu\nu}^a$ denote the electromagnetic and chromomagnetic field strength tensors correspondingly. The μ is the renormalization scale which is usually chosen as around m_b . One can notice that, making the Fourier transform

$$-\sigma^{\mu\nu}F_{\mu\nu} \rightarrow 2i\sigma_{\mu\nu}q^\nu \quad (1.31)$$

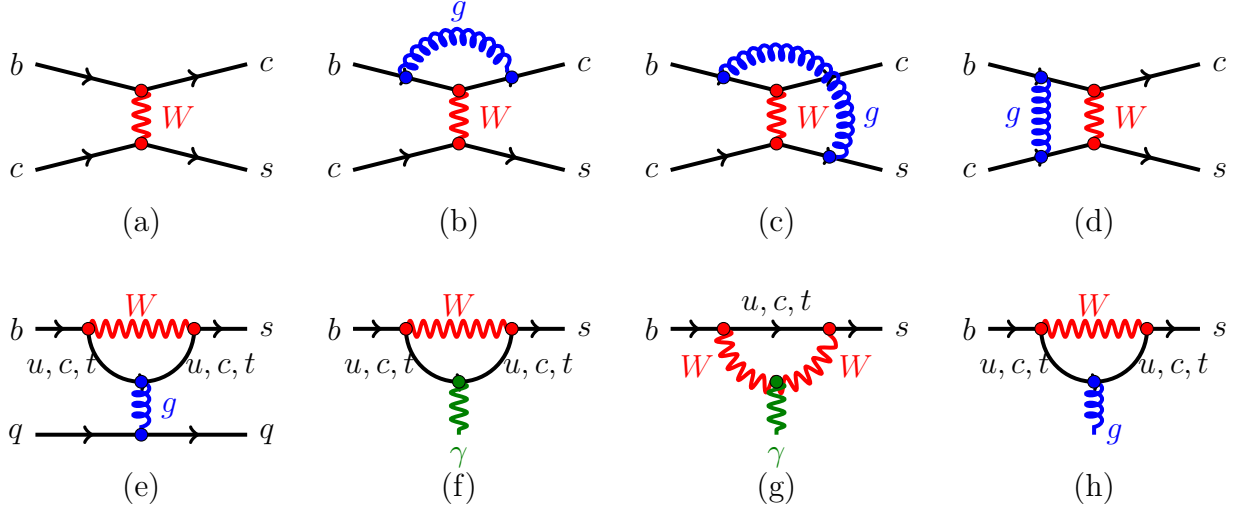


Figure 1.1: Typical diagrams in the full theory, from which the operators (1.28)-(1.30) originate: current-current (a) with QCD corrections (b, c, d); gluon penguin (e); electromagnetic photon penguin (f, g); chromomagnetic gluon penguin (h).

the dominant electromagnetic penguin operator $\mathcal{O}_{7\gamma}$ is equivalent to the first term in Eq. (1.24)³.

Note that in the SM \mathcal{O}'_i ($i = 1, \dots, 6$) have no contribution and hence $C'_i = 0$. The contribution of $\mathcal{O}'_{7\gamma}$ and \mathcal{O}'_{8g} is also negligible because $C'_{7\gamma}$ and C'_{8g} are suppressed due to the smallness of the strange quark mass

$$\frac{C'_{7\gamma}}{C_{7\gamma}} = \frac{C'_{8g}}{C_{8g}} = \frac{m_s}{m_b} \simeq 0.02 \quad (1.32)$$

At leading order (LO), one has to calculate and match the full end effective theory without taking into account QCD corrections and compute the anomalous dimension 8×8 matrix to order α_s . The corresponding leading logarithmic contribution is then obtained by calculating the tree-level matrix element of the $\mathcal{O}_{7\gamma}$ operator and one-loop matrix elements of four-quark operators $\{\mathcal{O}_1, \dots, \mathcal{O}_6\}$ ⁴ (see Fig. 1.2). Their effect can be absorbed into redefinition of the C_7 coefficient by introducing the so-called “effective” coefficient, $C_{7\gamma}^{eff}$ (for more details see Appendix A). So that the amplitude of the $b \rightarrow s\gamma$ can be written as

$$\mathcal{M}(b \rightarrow s\gamma)_{\text{LO}} = -\frac{4G_F}{\sqrt{2}} (C_{7\gamma}^{(0)eff}(\mu) \langle \mathcal{O}_{7\gamma}(\mu) \rangle + C_{7\gamma}'^{(0)eff}(\mu) \langle \mathcal{O}_{7\gamma}'(\mu) \rangle) \quad (1.33)$$

³The term proportional to m_s (the second term in Eq. (1.24)) is often neglected in this expression due to its smallness.

⁴In the naive dimensional regularization scheme the non-zero contributions come from $\mathcal{O}_{5,6}$ operators, while in the 't Hooft-Veltman scheme they all vanish (see Ref. [16] and references therein for more details).

where $C_{7\gamma}^{(0)eff}$ denotes the leading logarithmic approximation to $C_{7\gamma}^{eff}$. The renormalization scale μ is often chosen as of order of m_b .

The strong enhancement of $C_{7\gamma}^{(0)eff}$ by short-distance QCD effects can be seen using Eq. (A.19b). For instance, for $m_t = 170 \text{ GeV}/c^2$, $m_b = 5 \text{ GeV}/c^2$ and $\alpha_s^{(5)}(M_Z) = 0.118$, one obtains [16]

$$\begin{aligned} C_{7\gamma}^{(0)eff}(\mu_b) &= 0.695 C_{7\gamma}^{(0)}(\mu_W) + 0.085 C_{8g}^{(0)}(\mu_W) - 0.158 C_2^{(0)}(\mu_W) \\ &= 0.695(-0.193) + 0.085(-0.096) - 0.158 = -0.300 \end{aligned} \quad (1.34)$$

Thus, one observes a large enhancement with respect to $C_{7\gamma}^{(0)}(M_W) = -0.193$ due to the last term in Eq. (1.34) proportional to C_2 . Hence, the short-distance QCD corrections are very important for the $b \rightarrow s\gamma$ process.

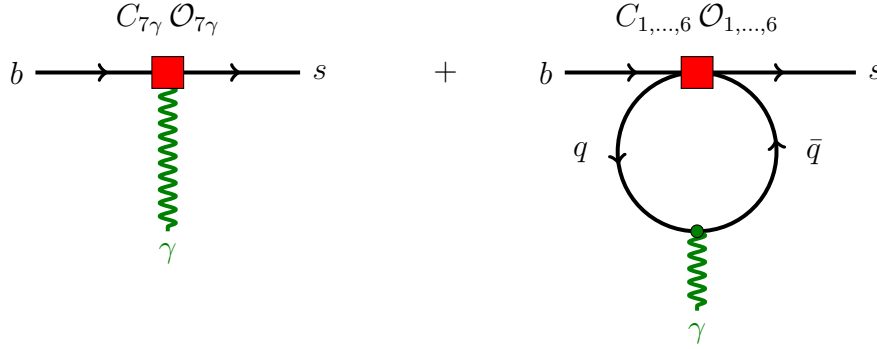


Figure 1.2: Leading order tree and one-loop level $O(\alpha_s^0)$ contributions to $b \rightarrow s\gamma$ of electromagnetic operator $\mathcal{O}_{7\gamma}$ and four-quark $\mathcal{O}_{1,...,6}$ operators respectively.

More recently, there has been a new development in computing the perturbative QCD corrections to the matrix element part [17, 18]. Such corrections are important particularly to cancel the renormalization scale dependence in Eq. (1.33). Examples of diagrams of such corrections are shown in Fig. 1.3 and 1.4. Most importantly, it turned out that the photon coming from these diagrams could potentially carry different polarization from that ones we expect from the $\mathcal{O}_{7\gamma}$ diagram. Many efforts to evaluate such effects have been made in the case of $B \rightarrow K^*\gamma$ [17, 18, 19, 20]. In the next section, we will follow the work by Khodjamirian *et al.* and Ball *et al.* based on the QCD sum rules and give some idea on the size of this “wrong” chirality contamination. However, it should be mentioned that there are some theoretical issues remaining on this issue⁵ and further

⁵For example, in Ref. [19, 20], authors made the dimensional estimate in the framework of the so-called Soft Collinear Effective Theory of the \mathcal{O}_2 contribution shown in Fig. 1.4 (left).

$$\frac{\mathcal{M}(\overline{B} \rightarrow \overline{K}^* \gamma_R)}{\mathcal{M}(\overline{B} \rightarrow \overline{K}^* \gamma_L)} \sim \frac{1}{3} \frac{C_2^{(0)}}{C_{7\gamma}^{(0)eff}} \frac{\Lambda_{QCD}}{m_b} \quad (1.35)$$

This result indicates up to 10% of “wrong” chirality contamination. However, as we will see, this value is much larger than other computations, such as the one we present in the next section.

theoretical works are required to reach to a more rigorous conclusion.

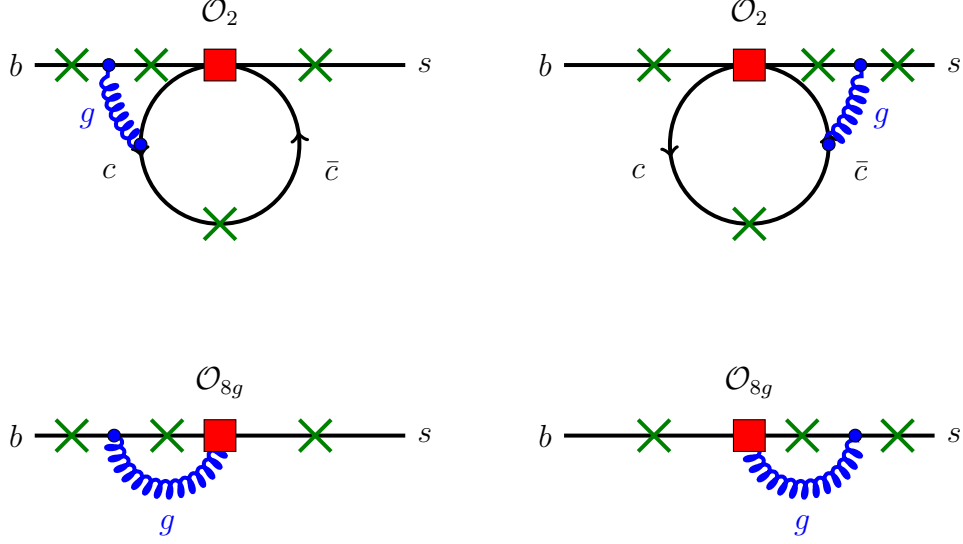


Figure 1.3: Next-to-leading order two- and one-loop level $O(\alpha_s)$ contributions to $b \rightarrow s\gamma$ of the four-quark \mathcal{O}_2 and the electromagnetic \mathcal{O}_{8g} operators respectively. The crosses indicate the places where the emitted photon can be attached.

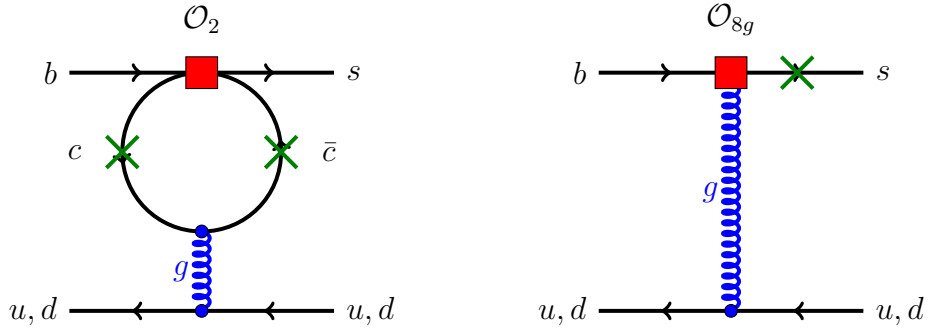


Figure 1.4: Next-to-leading order one-loop and tree level $O(\alpha_s)$ contributions to exclusive process $b \rightarrow s\gamma$ (e.g. $\bar{B} \rightarrow \bar{K}^*\gamma$) involving hard gluon exchange with spectator quark of four-quark \mathcal{O}_2 and chromomagnetic \mathcal{O}_{8g} operators respectively. The crosses indicate the places where the emitted photon can be attached.

1.3.2 Possible contamination of “wrong” chirality contribution due to the \mathcal{O}_2 term

In this subsection, we follow [21] and [22] to have a brief view of how the \mathcal{O}_2 contribution leads to the “wrong” chirality contribution in light-cone QCD sum rules⁶.

The theoretical description of the exclusive $b \rightarrow s\gamma$ decays involves both short- and long-distance contributions. In terms of the effective Hamiltonian the decay amplitude, for instance for the $\bar{B} \rightarrow \bar{K}^*\gamma$ decay, can be written as

$$\begin{aligned} \mathcal{M}(\bar{B} \rightarrow \bar{K}^*\gamma) = & -\frac{4G_F}{\sqrt{2}}V_{tb}V_{ts}^*\langle\bar{K}^*\gamma|C_{7\gamma}\mathcal{O}_{7\gamma} + C'_{7\gamma}\mathcal{O}'_{7\gamma} \\ & + i\varepsilon_{\gamma}^{\mu*}\sum_{i\neq 7}C_i\int d^4xe^{iqx}T\{j_{\mu}^{em}(x)\mathcal{O}_i(0)\}|\bar{B}\rangle \end{aligned} \quad (1.36)$$

A possibility to relieve the helicity suppression of right-handed photons is to consider an additional gluon emission resulting into three-particle final state $b \rightarrow s\gamma g$. The main effect comes from the $c\bar{c}$ resonances and is contributed by the \mathcal{O}_2 operator as depicted in Fig. 1.5. In the inclusive decay this is a bremsstrahlung correction and can be calculated in the perturbation theory. In the exclusive decays the emitted gluon can be either hard or soft. If it is hard, it attaches to the spectator quark (see Fig. 1.3), which induces $\mathcal{O}(\alpha_s)$ corrections. If it is soft (i.e. $|k_g^2| \ll 4m_c^2$), it must be interpreted as a parton in one of the external hadrons [21, 22]. The later case is beyond the perturbation theory. Thus, here we apply one of the non-perturbative QCD approaches called light-cone QCD sum rules.

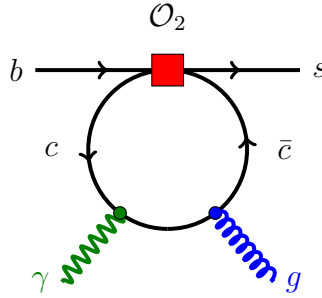


Figure 1.5: Dominant contribution to $b \rightarrow s\gamma g$. A second diagram with photon and gluon exchanged is implied.

Using the property

$$t_{\alpha\beta}^a t_{\gamma\delta}^a = -\frac{1}{2N_c}\delta_{\alpha\beta}\delta_{\gamma\delta} + \frac{1}{2}\delta_{\alpha\delta}\delta_{\beta\gamma} \quad (1.37)$$

⁶The original work on this line was performed by Khodjamirian *et al.* [21] where the local QCD sum rule is applied.

(where $N_c = 3$ is the number of colours) and performing the Fierz transformation, the dominant \mathcal{O}_2 operator can be rewritten as

$$\mathcal{O}_2 = \frac{1}{3} \underbrace{(\bar{c}_{\alpha L} \gamma_\mu c_{\alpha L})(\bar{s}_{\beta L} \gamma^\mu b_{\beta L})}_{\mathcal{O}_1} + 2(\bar{c}_{\alpha L} \gamma_\mu t_{\alpha\beta}^a c_{\beta L})(\bar{s}_{\rho L} \gamma^\mu t_{\rho\delta}^a b_{\delta L}) \quad (1.38)$$

Note that the \mathcal{O}_1 contribution vanishes for the on-shell photon due to its colour structure. Hence, only the second term of Eq. (1.38) contributes. Attaching a gluon to the charm loop and expanding the correlation function in Eq. (1.36) of the rewritten operator \mathcal{O}_2 (see the diagram in Fig. 1.5) in terms of the inverse powers of the charm quark mass, one obtains the effective quark-quark-gluon operator [21, 22]

$$\begin{aligned} \mathcal{O}_F &= i\varepsilon_\gamma^{\mu*} \int d^4x e^{iqx} T\{[\bar{c}(x) \gamma_\mu c(x)] \mathcal{O}_2(0)\} \\ &= -\frac{1}{48\pi^2 m_c^2} (D^\rho F^{\alpha\beta}) [\bar{s} \gamma_\rho (1 - \gamma_5) g_s \tilde{G}_{\alpha\beta}^a t^a b] + \dots \end{aligned} \quad (1.39)$$

where $F^{\alpha\beta} = i(q^\alpha \varepsilon^{\beta*} - q^\beta \varepsilon^{\alpha*})$ and the dots denote terms of higher order in $1/m_c$.

Two hadronic matrix elements can be parametrized in terms of three form factors, T_1 , L and \tilde{L} in the following way [22]:

$$\begin{aligned} \langle \bar{K}^* \gamma | \mathcal{O}_{7\gamma}^{(\prime)} | \bar{B} \rangle &= -\frac{e}{8\pi^2} m_b T_1^{(K^*)}(0) [\epsilon_{\mu\nu\rho\sigma} \varepsilon_\gamma^{\mu*} \varepsilon_{K^*}^{\nu*} p_{K^*}^\rho q^\sigma \\ &\quad \pm i\{(\varepsilon_\gamma^* \varepsilon_{K^*}^*)(p_{K^*} q) - (\varepsilon_\gamma^* p_{K^*})(\varepsilon_{K^*}^* q)\}] \end{aligned} \quad (1.40)$$

and

$$\begin{aligned} \langle \bar{K}^* \gamma | \mathcal{O}_F | \bar{B} \rangle &= \langle \bar{K}^* \gamma | (D^\rho F^{\alpha\beta}) [\bar{s} \gamma_\rho (1 - \gamma_5) g_s \tilde{G}_{\alpha\beta}^a t^a b] | \bar{B} \rangle \\ &= 2 \langle \bar{K}^* \gamma | \bar{s} \gamma_\mu (1 - \gamma_5) q^\mu g_s \tilde{G}_{\alpha\beta} b | \bar{B} \rangle \varepsilon_\gamma^{\alpha*} q^\beta \\ &= 2 \left(L \epsilon_{\mu\nu\rho\sigma} \varepsilon_\gamma^{\mu*} \varepsilon_{K^*}^{\nu*} p_{K^*}^\rho q^\sigma + i \tilde{L} [(\varepsilon_\gamma^* \varepsilon_{K^*}^*)(p_{K^*} q) - (\varepsilon_\gamma^* p_{K^*})(\varepsilon_{K^*}^* q)] \right) \end{aligned} \quad (1.41)$$

The $B \rightarrow K^*$ form factor T_1 and L, \tilde{L} are computed using the light-cone QCD sum rules. Note that L and \tilde{L} are functions of the three-particle (s -quark, spectator quark and gluon) K^* wave function. The difference between L and \tilde{L} comes e.g. from the different distribution amplitudes of the vector and axial vector wave functions of K^* . The T_1 form factor was computed in Ref. [23] and its updated value can be found in [24]

$$T_1^{(K^*)}(0) = 0.31 \pm 0.04 \quad (1.42)$$

and the most recent calculation by Ball and Zwicky [22] gives the values of L and \tilde{L} :

$$L = (0.2 \pm 0.1) \text{ GeV}^3, \quad \tilde{L} = (0.3 \pm 0.2) \text{ GeV}^3 \quad (1.43)$$

Writing explicitly the left- and right-handed polarization vectors of the photon and K^* , one finds that the operator \mathcal{O}_F induces corrections of $(L \pm \tilde{L})/(m_b m_c^2)$ to the left/right-handed amplitudes. Thus the amplitudes for the left- and right-handed photon emission in the $\bar{B} \rightarrow \bar{K}^* \gamma$ can be written as follows:

$$\mathcal{M}(\bar{B} \rightarrow \bar{K}^* \gamma_L) = -\frac{4G_F}{\sqrt{2}} C_L \langle \bar{K}^* \gamma_L | \mathcal{O}_{7\gamma} | \bar{B} \rangle \quad (1.44a)$$

$$\mathcal{M}(\bar{B} \rightarrow \bar{K}^* \gamma_R) = -\frac{4G_F}{\sqrt{2}} C_R \langle \bar{K}^* \gamma_R | \mathcal{O}'_{7\gamma} | \bar{B} \rangle \quad (1.44b)$$

where the new left/right-handed coefficients are defined as [22]

$$C_L = C_{7\gamma}^{(0)eff}(m_b) - C_2^{(0)}(m_b) \frac{L + \tilde{L}}{36m_b m_c^2 T_1^{(K^*)}(0)} \quad (1.45a)$$

$$C_R = C_{7\gamma}'^{(0)eff}(m_b) - C_2^{(0)}(m_b) \frac{L - \tilde{L}}{36m_b m_c^2 T_1^{(K^*)}(0)} \quad (1.45b)$$

Therefore, in addition to the small m_s/m_b contribution of $\mathcal{O}'_{7\gamma}$, there is potentially non-negligible right-handed pollution non-perturbative contribution. A numerical estimate for them is extremely important. Khodjamirian *et al.* [21] and later Ball and Zwicky [22] roughly agree on the magnitude of the non-perturbative contribution of the \mathcal{O}_2 operator. We quote the estimate for $B \rightarrow K^* \gamma$ using the form factors calculated by Ball and Zwicky:

$$\begin{aligned} C_L &= C_{7\gamma}^{(0)eff}(m_b) \times (1 + (0.02 \pm 0.01)) \\ C_R &= C_{7\gamma}'^{(0)eff}(m_b) \times \frac{m_s}{m_b} \times (1 - (0.17 \pm 0.18)) \end{aligned} \quad (1.46)$$

which gives the ratio

$$\frac{C_R}{C_L} \simeq \frac{m_s}{m_b} \times (0.8 \pm 0.2) \quad (1.47)$$

Therefore, the right-handed contribution is rather small and the non-perturbative correction is of the order of 20% decrease to the leading m_s/m_b term (in particular, this correction is important for the precise determination of the time-dependent CP asymmetry in $B \rightarrow K_S \pi^0 \gamma$ decay which is proportional to C_R/C_L). Note that this calculation has not been provided for the case of $B \rightarrow K_1 \gamma$. It should be noticed that C_R/C_L obtained by Khodjamirian *et al.* and by Ball and Zwicky is much smaller than the one estimated by Grinstein *et al.* in Eq. (1.35).

1.4 Photon polarization with new physics

When we consider the new physics contributions, the right-handed contribution can be significantly enlarged by different types of Dirac structure that those new physics models

can induce. It should be emphasized that there are many new physics models which can accommodate e.g. a large coefficient to the right-handed electro-magnetic operator $O'_{7\gamma}$ without contradicting the precise measurement of the inclusive $B \rightarrow X_s \gamma$ branching ratio as well as the time-dependent CP asymmetry of $B \rightarrow K_S \pi^0 \gamma$ [25, 26] (see Ref. [27, 28, 29, 30, 31, 32] for some examples of the constraints on the right-handed contribution obtained for specific new physics models).

1.4.1 Extra source of flavour violation in MSSM

Supersymmetric models are an example of new physics models beyond the SM at the TeV scale. The SUSY models are attractive not only because they solve the Higgs mass hierarchy problem. They can also be consistent with Grand Unification. This provides the unification of all three gauge couplings under the renormalization group running by the supersymmetric partners causing them to intersect at the same point at $M_{\text{GUT}} \simeq 10^{16}$ GeV.

General SUSY model contains sufficiently large number of parameters corresponding to the masses and mixings of the superpartners for each SM particle. Even in the Minimal Supersymmetric Standard Model (MSSM) the number is more than a hundred. These masses and mixing parameters are, at least partially, generated by the soft supersymmetry breaking mechanism, which is necessary to make all superpartners heavy enough such that they have not been detected at existing collider experiments. Therefore, in order to predict the masses and flavour mixing parameters of the SUSY particles one has to specify the mechanism of the SUSY breaking.

The MSSM is a minimal supersymmetric extension of the SM, containing a superpartner for each SM particle and two Higgs doublets (for the introduction to SUSY see for instance Ref. [33]). Its matter fields are organized in the chiral supermultiplets as

$$Q_i(3, 2, 1/6), \quad \bar{U}_i(\bar{3}, 1, -2/3), \quad \bar{D}_i(\bar{3}, 1, 1/3) \quad (1.48)$$

for the left-handed (Q) and right-handed (U , D) quark sector,

$$L_i(1, 2, -1/2), \quad \bar{E}_i(1, 1, 1) \quad (1.49)$$

for the left-handed (L) and right-handed (E) lepton sector, and

$$H_1(1, 2, -1/2), \quad H_2(1, 2, -1/2) \quad (1.50)$$

for the Higgs fields. As before, index $i = 1, 2, 3$ denotes a generation index. Under the condition of R -parity conservation, which is required to avoid a large proton decay rate, the superpotential can be written as

$$W_{\text{MSSM}} = Y_D^{ij} \bar{D}_i Q_j H_1 + Y_U^{ij} \bar{U}_i Q_j H_2 + Y_E^{ij} \bar{E}_i L_j H_1 + \mu H_1 H_2 \quad (1.51)$$

where Y_U^{ij} and Y_D^{ij} are quark Yukawa couplings. The soft SUSY breaking terms, induced by this superpotential, are

$$\begin{aligned}\mathcal{L}_{\text{soft}} = & (m_Q^2)_{ij} \tilde{q}_{Li}^\dagger \tilde{q}_{Lj} + (m_U^2)_{ij} \tilde{u}_{Ri}^\dagger \tilde{u}_{Rj} + (m_D^2)_{ij} \tilde{d}_{Ri}^\dagger \tilde{d}_{Rj} \\ & + (m_L^2)_{ij} \tilde{l}_{Li}^\dagger \tilde{l}_{Lj} + (m_E^2)_{ij} \tilde{e}_{Ri}^\dagger \tilde{e}_{Rj} \\ & + M_{H_1}^2 h_1^\dagger h_1 + M_{H_2}^2 h_2^\dagger h_2 - (B\mu h_1 h_2 + h.c.) \\ & + (A_U^{ij} \tilde{u}_{Ri}^\dagger \tilde{q}_{Lj} h_2 + A_D^{ij} \tilde{d}_{Ri}^\dagger \tilde{q}_{Lj} h_1 + A_E^{ij} \tilde{e}_{Ri}^\dagger \tilde{l}_{Lj} h_2 + h.c.) \\ & + \frac{M_1}{2} \tilde{B} \tilde{B} + \frac{M_2}{2} \tilde{W} \tilde{W} + \frac{M_3}{2} \tilde{g} \tilde{g}\end{aligned}\quad (1.52)$$

This soft SUSY breaking part of Lagrangian in MSSM consists of mass terms for scalar fields (\tilde{q}_{Li} , \tilde{u}_{Ri} , \tilde{d}_{Ri} , \tilde{l}_{Li} , \tilde{e}_{Ri} , h_1 , h_2), Higgs mixing terms, trilinear scalar couplings and gaugino (\tilde{B} , \tilde{W} , \tilde{g}) mass terms.

One can see from Eq. (1.52) that after the spontaneous symmetry breaking the squark mass can come from any combination of left- and right-handed couplings:

$$\begin{aligned}\mathcal{L}_{\text{soft}}^{\text{squark mass}} = & (m_Q^2)_{ij} \tilde{q}_{Li}^\dagger \tilde{q}_{Lj} + (m_U^2)_{ij} \tilde{u}_{Ri}^\dagger \tilde{u}_{Rj} + (m_D^2)_{ij} \tilde{d}_{Ri}^\dagger \tilde{d}_{Rj} \\ & + (v_2 A_U^{ij} \tilde{u}_{Ri}^\dagger \tilde{q}_{Lj} + v_1 A_D^{ij} \tilde{d}_{Ri}^\dagger \tilde{q}_{Lj} + h.c.)\end{aligned}\quad (1.53)$$

where $v_{1,2}$ are the vacuum expectation values of the Higgs fields. *Since the squark mass matrices (m_Q , m_U , m_D) and the trilinear couplings (A_U^{ij} , A_D^{ij}) are not diagonal in the quark basis, the squark propagators can change flavour and chirality (see Fig. 1.6).*

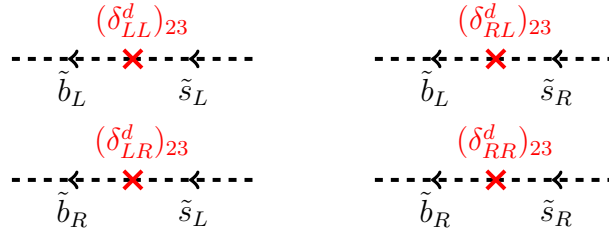


Figure 1.6: Flavour and chirality change in the squark propagators.

Once these new terms are introduced, the $b \rightarrow s\gamma$ process could receive a significantly new contribution. In particular, the chirality can be flipped on the squark propagator in the loop of $b \rightarrow s\gamma$ which can lead to a right-handed photon emission. As was discussed in detail in the previous sections, the right-handed suppression factor m_s/m_b comes from the left-handed coupling of W to quarks. However, if the loop contains right-handed coupling SUSY contribution (as an example, see Fig. 1.7), this suppression can be reduced.

1.4.2 Mass Insertion Approximation

As discussed in the previous subsection, the soft SUSY breaking terms which provide a new source of flavour violation, contain a huge number of parameters. In order to organize

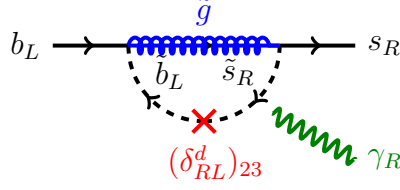


Figure 1.7: Example of one of the diagrams with the squark-gluino loop contribution to $b \rightarrow s\gamma$.

them, the so-called mass insertion approximation (MIA) [34] is used. In the MIA, one uses a basis where the fermion and sfermion mass matrices are rotated in the same way to diagonalize the fermion mass matrix (the super-CKM basis). In this basis, the couplings of fermions and sfermions to neutral gauginos are flavour diagonal, leaving the source of flavour violation in the off-diagonal terms of the sfermion mass matrix. These terms are described by $(\Delta_{AB}^q)_{ij}$, where A, B denote the chirality (L/R) and q indicate the (u/d) type. The sfermion propagator can be expanded as [31]

$$\langle \tilde{q}_{Ai} \tilde{q}_{Bj}^* \rangle = i(k^2 - m_{\tilde{q}}^2 - \Delta_{AB}^q)^{-1} \simeq \frac{i\delta_{ij}}{k^2 - m_{\tilde{q}}^2} + \frac{i(\Delta_{AB}^q)_{ij}}{(k^2 - m_{\tilde{q}}^2)^2} + \dots \quad (1.54)$$

where $m_{\tilde{q}}$ is the average squark mass. One assumes that $\Delta^2 \ll m_{\tilde{q}}^2$ so that the first term in expansion is sufficient. In this way, the flavour violation in SUSY models can be parametrized in a *model independent* way by dimensionless mass insertion parameters

$$(\delta_{AB}^q)_{ij} \equiv \frac{(\Delta_{AB}^q)_{ij}}{m_{\tilde{q}}^2} \quad (1.55)$$

which can be constrained by various flavour experiments.

Here we consider the gluino contribution to the $C_{7\gamma}^{(\prime)\bar{g}}$ Wilson coefficients. Then $C_{7\gamma}^{(\bar{g})}$ and $C_{7\gamma}^{\prime(\bar{g})}$ are written in terms of down-type mass insertion parameters as

$$C_{7\gamma}^{(\bar{g})} = -\frac{4\sqrt{2}\alpha_s\pi}{9G_F V_{tb} V_{ts}^* m_{\tilde{q}}^2} \left[(\delta_{LR}^d)_{23} \frac{m_{\tilde{g}}}{m_b} M_1(x) + (\delta_{LL}^d)_{23} \left(M_3(x) + (\delta_{LR}^d)_{33} \frac{m_{\tilde{g}}}{m_b} M_a(x) \right) \right] \quad (1.56a)$$

$$C_{7\gamma}^{\prime(\bar{g})} = -\frac{4\sqrt{2}\alpha_s\pi}{9G_F V_{tb} V_{ts}^* m_{\tilde{q}}^2} \left[(\delta_{RL}^d)_{23} \frac{m_{\tilde{g}}}{m_b} M_1(x) + (\delta_{RR}^d)_{23} \left(M_3(x) + (\delta_{RL}^d)_{33} \frac{m_{\tilde{g}}}{m_b} M_a(x) \right) \right] \quad (1.56b)$$

where $x = m_{\tilde{g}}^2/m_{\tilde{q}}^2$ and the loop functions M_i can be found in Ref. [35]. One can note that in SUSY models with large RL mixing the factor m_b is replaced by the internal gluino mass as can be seen from the first term in Eq. (1.56). As we will see in Chapter 5, this effect, often called chiral-enhancement, could lead to a dramatic enhancement of the right-handed photon emission in $b \rightarrow s\gamma$ process.

Chapter 2

The $B \rightarrow K_1 \gamma \rightarrow (K \pi \pi) \gamma$ decay and polarization measurement

In this chapter, we introduce our new method for the photon polarization measurement using the $B \rightarrow K_1 \gamma$ decay. In Section 2.1, the basic idea, first proposed by Gronau *et al.* [11], is discussed. It is explained why we need a three-body decay of the K_1 meson in order to have a direct measurement of the polarization. Section 2.2 contains the discussion of photon polarization determination using exclusive $B \rightarrow K_1 \gamma$ decay. In Section 2.3, the angular decay distribution of $B \rightarrow K_1 (\rightarrow K \pi \pi) \gamma$ is calculated and the master formula is derived. Section 2.4 considers a general introduction of the method, proposed by Davier *et al.* [14]. It is shown that a new introduced variable ω , which contains not only the angular but also the tree-body Dalitz variable information, turns out to be very sensitive to the photon polarization parameter λ_γ .

2.1 How to measure the polarization: basic idea

In this section, we first demonstrate why the $B \rightarrow K_1 \gamma$ decay is useful to determine the photon polarization, and why the other simpler mode such as $B \rightarrow K^* \gamma$ is not sufficient. One can not determine directly the polarization in the $B \rightarrow K^* (\rightarrow K \pi) \gamma$ decay by the following reason: since the photon helicity is parity-odd and we measure only the momenta of the photon and the final hadrons, we can not form a hadronic quantity that would be also parity-odd. Moreover, one can demonstrate that the decay plane $K - \pi$ is symmetric around helicity axis (i.e. the photon momentum direction) in the B reference frame (see Fig. 2.1); that means that we can not distinguish between left and right circular rotations. That is why the two-body decay of K^* provides no helicity information. That is not the case for the three-body decay of K_1 into $K \pi \pi$ final state, which is no longer symmetric around the photon direction. In this case one can form a triple product of three momenta like

$$\vec{p}_\gamma \cdot (\vec{p}_\pi \times \vec{p}_K) \tag{2.1}$$

which is a pseudo-scalar and applying parity transformation it has the opposite sign for left- and right-handed photons.

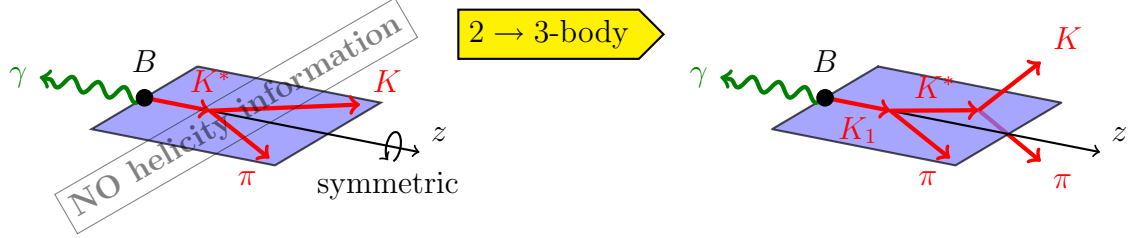


Figure 2.1: Comparison of the radiative B -decays involving two- and three-body decays of kaon resonance states.

On the other hand, it is known that the triple product is odd under time reversal and that the final state interactions break T -parity. Hence, the $K_1 \rightarrow K \pi \pi$ amplitude must involve a strong phase, coming from the interference of at least two amplitudes leading to a common tree-body final state. That could be an interference between two different charge states of $K^* \pi$ ($K^{*+} \pi^0$ and $K^{*0} \pi^+$ for instance), or between the $K^* \pi$ and $K \rho$ intermediate channels, or between their different partial S - and D -waves. According to Watson's theorem (for more details see Appendix B), the phase generated by the strong interactions coincides with the phases of the S -wave elastic scattering below the first threshold taken at the mass of the decaying particle [36]. Parametrization of the intermediate isobar states, K^* and ρ , in terms of Breit-Wigner forms provides a good estimation of the strong rescattering phases. The importance of the interference terms and the relative signs of the amplitudes will be discussed in detail later in Chapter 3.

2.2 Photon polarization determination with $B \rightarrow K_1 \gamma$ decay

The decay width of the exclusive decay $\bar{B} \rightarrow \bar{K}_1 \gamma$ can be written as

$$\mathcal{M}(\bar{B} \rightarrow \bar{K}_1 \gamma) = -\frac{4G_F}{\sqrt{2}} V_{ts}^* V_{tb} (C_L \langle \bar{K}_1 \gamma | \mathcal{O}_{7\gamma} | \bar{B} \rangle + C_R \langle \bar{K}_1 \gamma | \mathcal{O}'_{7\gamma} | \bar{B} \rangle) \quad (2.2)$$

Note that the left/right-handed coefficients $C_{L,R}$ in this equation are different from the ones determined by Eq. (1.45) for the $\bar{B} \rightarrow \bar{K}^* \gamma$ due to the difference in the $B \rightarrow K^*$ and $B \rightarrow K_1$ hadronic form factors and the unknown contribution of the long-distance effects of the \mathcal{O}_2 operator for $\bar{B} \rightarrow \bar{K}_1 \gamma$. *Therefore, we will neglect the long-distance \mathcal{O}_2 potential contribution in the following, but keeping in mind the theoretical uncertainty of the order of 10% to the right-handed polarization amplitude (see Eq. (1.35)).*

In the exclusive radiative B -decays the matrix elements of the electromagnetic penguin operator for the $\bar{B} \rightarrow \bar{K}_1$ transition can be parametrized in terms of the hadronic form

factors using the following convention:

$$\begin{aligned} \langle \bar{K}_1 | \bar{s} \sigma_{\mu\nu} (1 \pm \gamma_5) q^\nu b | \bar{B} \rangle &= T_2^{(K_1)}(q^2) [\varepsilon_{K_1\mu}^* (m_B^2 - m_{K_1}^2) - (\varepsilon_{K_1}^* \cdot p_B) (p_B + p_{K_1})_\mu] \\ &\quad + T_3^{(K_1)}(q^2) (\varepsilon_{K_1}^* \cdot p_B) \left[q_\mu - \frac{q^2}{m_B^2 - m_{K_1}^2} (p_B + p_{K_1})_\mu \right] \\ &\quad \pm 2T_1^{(K_1)}(q^2) \epsilon_{\mu\nu\rho\sigma} i \varepsilon_{K_1}^{\nu*} p_B^\rho p_{K_1}^\sigma \end{aligned} \quad (2.3)$$

with $T_1^{(K_1)}(0) = T_2^{(K_1)}(0)$ to avoid a kinematical singularity of the matrix element at $q^2 = 0$. Since the outgoing photon is on-shell, $q^2 = 0$ and $q_\mu \varepsilon^{\mu*} = 0$. Thus the second term in Eq. (2.3), proportional to $T_3^{(K_1)}$, vanishes when it is multiplied by $\varepsilon^{\mu*}$, and the hadronic matrix element is parametrized with only one form factor $T_1^{(K_1)}$ in radiative B -decays.

Due to the angular momentum conservation and the fact that B -meson is a pseudoscalar meson, helicity is conserved. Thus in order to determine the photon polarization it is sufficient to measure the polarization of K_1 through its three-body decay into $K\pi\pi$ final state. The angular distribution of this three-body decay carries the information of the K_1 polarization, $\varepsilon_{K_1}^{\nu*}$. Setting the helicity axis z along the K_1 direction in the B reference frame, the polarization vectors of K_1 will be determined by Eq. (1.25) while the photon polarization vectors will be obtained by a rotation (e.g. around x -axis) which takes the z -axis into the direction of \vec{q} so that

$$\varepsilon_{K_1 R, L}^\mu = \mp \frac{1}{\sqrt{2}} \begin{pmatrix} 0 \\ 1 \\ \pm i \\ 0 \end{pmatrix}, \quad \varepsilon_{\gamma R, L}^\mu = \mp \frac{1}{\sqrt{2}} \begin{pmatrix} 0 \\ 1 \\ \mp i \\ 0 \end{pmatrix} \quad (2.4)$$

Thus, fixing the momentum and the polarization vectors of the photon and K_1 in the B reference frame and using the parametrization (2.3), one obtains the matrix elements for the left- and right-handed operators

$$\langle \bar{K}_{1L} \gamma_L | \mathcal{O}_{7\gamma} | \bar{B} \rangle = \langle \bar{K}_{1R} \gamma_R | \mathcal{O}'_{7\gamma} | \bar{B} \rangle = i \frac{e}{8\pi^2} m_b (m_B^2 - m_{K_1}^2) T_1^{(K_1)}(0) \quad (2.5)$$

and

$$\langle \bar{K}_{1R(L)} \gamma_{R(L)} | \mathcal{O}_{7\gamma}^{(\prime)} | \bar{B} \rangle = \langle \bar{K}_{1L(R)} \gamma_{L(R)} | \mathcal{O}_{7\gamma} | \bar{B} \rangle = \langle \bar{K}_{1L(R)} \gamma_{R(L)} | \mathcal{O}'_{7\gamma} | \bar{B} \rangle = 0 \quad (2.6)$$

as expected from Eq. (1.26). As a result, we obtain

$$\Gamma(\bar{B} \rightarrow \bar{K}_{1L} \gamma_L) = \frac{\alpha G_F^2}{32\pi^4} |V_{ts}^* V_{tb}|^2 |C_L|^2 m_b^2 m_B^3 \left(1 - \frac{m_{K_1}^2}{m_B^2}\right)^3 |T_1^{(K_1)}(0)|^2 \quad (2.7a)$$

$$\Gamma(\bar{B} \rightarrow \bar{K}_{1R} \gamma_R) = \frac{\alpha G_F^2}{32\pi^4} |V_{ts}^* V_{tb}|^2 |C_R|^2 m_b^2 m_B^3 \left(1 - \frac{m_{K_1}^2}{m_B^2}\right)^3 |T_1^{(K_1)}(0)|^2 \quad (2.7b)$$

In the SM, $C_R/C_L \simeq C_{7\gamma}'^{eff}/C_{7\gamma}^{eff} \simeq m_s/m_b \ll 1$, thus, the photons are predominantly left(right)-handed polarized in $\bar{B}(B)$ decays. Although at leading logarithmic approximation (LLA) only electromagnetic penguin operator $\mathcal{O}_{7\gamma}$ contributes, one has always not to forget about the long-distance contribution of the other operators, especially of \mathcal{O}_2 , which can lead to an enhancement of the right(left)-handed photon emission in the $\bar{B}(B)$ decays up to 10% (as discussed in the end of Chapter 1).

If we could measure these two decay widths with different polarization separately, the ratio $|C_R/C_L|$ would provide a direct information of the right-handed current contribution of new physics in $b \rightarrow s \gamma$ process. However, experimentally, what we can only measure is the sum:

$$\Gamma(\bar{B} \rightarrow \bar{K}_1 \gamma) = \Gamma(\bar{B} \rightarrow \bar{K}_{1L} \gamma_L) + \Gamma(\bar{B} \rightarrow \bar{K}_{1R} \gamma_R) \quad (2.8)$$

As it has been explained in the previous sections, we use the kinematical information of the subsequent decay of K_1 in order to disentangle these two contributions. Assuming the narrow width of K_1 , one can write the total quasi-four body decay width by $\Gamma(\bar{B} \rightarrow \bar{K}_{1L} \gamma_L)$ and $\Gamma(\bar{B} \rightarrow \bar{K}_{1R} \gamma_R)$, respectively, followed by the three-body decay widths

$$\Gamma(\bar{K}_{1L} \rightarrow \bar{K} \pi \pi), \quad \Gamma(\bar{K}_{1R} \rightarrow \bar{K} \pi \pi) \quad (2.9)$$

Now, our decay widths can be written as:

$$\begin{aligned} \frac{d\Gamma(\bar{B} \rightarrow \bar{K}_1 \gamma \rightarrow (\bar{K} \pi \pi) \gamma)}{ds ds_{13} ds_{23} d\phi d\psi d \cos \theta} &\propto \sum_{\text{pol.}=L,R} \Gamma(\bar{B} \rightarrow \bar{K}_{1\text{pol.}} \gamma_{\text{pol.}}) \times \frac{d\Gamma(\bar{K}_{1\text{pol.}} \rightarrow \bar{K} \pi \pi)}{ds ds_{13} ds_{23} d\phi d\psi d \cos \theta} \\ &\times \frac{1}{(s - m_{K_1}^2)^2 + m_{K_1}^2 \Gamma_{K_1}^2} \end{aligned} \quad (2.10)$$

where $s = (p_1 + p_2 + p_3)^2$ is the off-shell "p²" of the K_1 and $s_{ij} = (p_i + p_j)^2$ with p_i to be the four-momentum of the final state mesons. The orientation of the $K \pi \pi$ decay system in the K_1 reference frame is determined by three angles θ, ϕ, ψ . The polar and azimuth angles, θ and ψ ¹ respectively, determine the orientation of the normal \vec{n} to the $K \pi \pi$ plane with respect to z -axis. Defining the $-z$ direction as the photon direction in the K_1 rest frame (see Fig. 2.2), the polar angle θ is given as $\cos \theta \equiv \left(\frac{\vec{p}_1 \times \vec{p}_2}{|\vec{p}_1 \times \vec{p}_2|} \right)_z$. The third angle ϕ defines the common rotation of \vec{p}_1 and \vec{p}_2 in the decay plane.

Here, the width of the K_1 is not really negligible ($\Gamma(K_1(1270)) = 90 \text{ MeV}/c^2$, $\Gamma(K_1(1400)) = 174 \text{ MeV}/c^2$ according to PDG [37]). Therefore, we present for completeness, in the following, a prescription that includes the initial state width of the K_1 decay into the three-body final state assuming the Breit-Wigner form, but which will not be used in practice. The Breit-Wigner factor is common for both polarizations and appears in modulus squared (therefore, its phase does not affect the crucial interference between different amplitudes).

¹Angle ψ is unobservable due to the rotation symmetry of the decay plane around the z -axis and is dropped out from the total squared amplitude as is demonstrated later in Eq. (2.17).

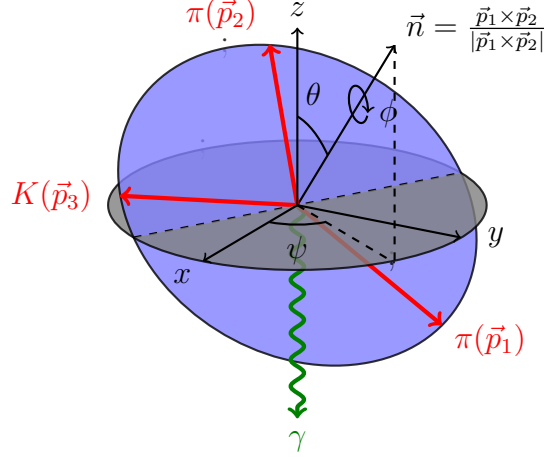


Figure 2.2: The $K_1 \rightarrow K \pi \pi$ decay plane in the rest frame of K_1 . Defining the $-z$ direction as the photon direction, the θ is given as $\cos \theta \equiv \left(\frac{\vec{p}_1 \times \vec{p}_2}{|\vec{p}_1 \times \vec{p}_2|} \right)_z$.

2.3 Master formula for $\bar{B} \rightarrow \bar{K}_1 \gamma \rightarrow (\bar{K} \pi \pi) \gamma$ decays

2.3.1 Master formula

In the following section, we will derive the master formula for the differential decay distributions of $B \rightarrow K_1 \gamma \rightarrow (K \pi \pi) \gamma$:

$$\begin{aligned} \frac{d\Gamma(\bar{B} \rightarrow \bar{K}_1 \gamma \rightarrow (\bar{K} \pi \pi) \gamma)}{ds ds_{13} ds_{23} d\cos \theta} &\propto \left\{ \frac{1}{4} |\vec{\mathcal{J}}|^2 (1 + \cos^2 \theta) + \lambda_\gamma \frac{1}{2} \text{Im}[\vec{n} \cdot (\vec{\mathcal{J}} \times \vec{\mathcal{J}}^*)] \cos \theta \right\} \\ &\times \frac{1}{(s - M_{K_1}^2)^2 + M_{K_1}^2 \Gamma_{K_1}^2} \end{aligned} \quad (2.11)$$

where $\mathcal{J}(s, s_{13}, s_{23})$ is the helicity amplitude of the $K_1 \rightarrow K \pi \pi$ decay. The “*photon polarization parameter*” λ_γ is defined as

$$\lambda_\gamma \equiv \frac{\Gamma(\bar{B} \rightarrow \bar{K}_{1R} \gamma_R) - \Gamma(\bar{B} \rightarrow \bar{K}_{1L} \gamma_L)}{\Gamma(\bar{B} \rightarrow \bar{K}_1 \gamma)} = \frac{|C_R|^2 - |C_L|^2}{|C_R|^2 + |C_L|^2} \quad (2.12)$$

which we want to extract. In the SM, $\lambda_\gamma \simeq 1(-1)$ for the $B(\bar{B})$ decays. It is clear from this master formula, that in order to determine λ_γ from the angular and the Dalitz plot analysis, we need a precise information on the helicity amplitude \mathcal{J} , which we will discuss in detail in this thesis.

Before closing this subsection, we make a comment on the master formula. In order to determine the polarization parameter λ_γ , we need non-zero value for $\text{Im}[\vec{n} \cdot (\vec{\mathcal{J}} \times \vec{\mathcal{J}}^*)]$, which requires the amplitude \mathcal{J} to contain more than one amplitude with a non-vanishing

relative phase. Such a condition can be nicely realised in this decay channel since when K_1 decays into three-body final states through more than one intermediate quasi-two-body channels, such as $K^* \pi$ and $K \rho$ (the different decay channels and the possible vector resonances for $K_1^+(1270/1400)$ and $K_1^0(1270/1400)$ are listed below in Eq. (2.13)), there is a non-vanishing relative strong phase originating from their Breit-Wigner forms (based on the isobar model)².

$$I : \quad K_1^+(1270/1400) \rightarrow \pi^0(p_1) \overbrace{\pi^+(p_2) K^0(p_3)}^{K^{*+}} \quad (2.13a)$$

$\underbrace{\hspace{10em}}_{\rho^+}$
 $\underbrace{\hspace{10em}}_{K^{*0}}$

$$II : \quad K_1^+(1270/1400) \rightarrow \pi^-(p_1) \overbrace{\pi^+(p_2) K^+(p_3)}^{K^{*0}} \quad (2.13b)$$

$\underbrace{\hspace{10em}}_{\rho^0}$
 $\underbrace{\hspace{10em}}_{K^{*0}}$

$$III : \quad K_1^0(1270/1400) \rightarrow \pi^0(p_1) \overbrace{\pi^-(p_2) K^+(p_3)}^{K^{*0}} \quad (2.13c)$$

$\underbrace{\hspace{10em}}_{\rho^-}$
 $\underbrace{\hspace{10em}}_{K^{*+}}$

$$IV : \quad K_1^0(1270/1400) \rightarrow \pi^+(p_1) \overbrace{\pi^-(p_2) K^0(p_3)}^{K^{*+}} \quad (2.13d)$$

$\underbrace{\hspace{10em}}_{\rho^0}$
 $\underbrace{\hspace{10em}}_{K^{*+}}$

Since the two K_1 resonances, $K_1(1270)$ and $K_1(1400)$, are rather close to each other and also relatively wide, the overlap between these two resonances may play a significant role in the polarization determination. On the other hand, the Belle collaboration [13] found no significant signal for $B \rightarrow K_1(1400) \gamma$ and set only the upper limit at 90% CL. Indeed, in [40, 41] it has been shown that such a suppression can be explained by taking into account the fact that these two states are a mixture of 1^3P_1 and 1^1P_1 states and by a reasonable choice of the mixing angle: our fitted value for the mixing angle gives a suppression of a factor of 40 in $B \rightarrow K_1(1400) \gamma$ mode with respect to the observed $B \rightarrow K_1(1270) \gamma$. Nevertheless, this issue must be kept in mind³.

²The case of the $B \rightarrow \phi K \gamma$ decay, first considered in [38] and revisited in [39], is different since there is no observed prominent ϕK resonance state and that the ϕ meson is very narrow.

³Although the Belle collaboration did not claim the clear observation of the $B \rightarrow K_1(1400) \gamma$ decay, one observes a non-negligible peak around 1.4 GeV/ c^2 in the $K \pi \pi$ invariant mass spectrum [42]

2.3.2 Derivation of the master formula

Helicity amplitude of $\bar{K}_1 \rightarrow P_1 P_2 P_3$ decay

The differential decay width of $\bar{K}_{1L,R}$ decay into three pseudoscalar mesons (P_1, P_2, P_3) can be described by the helicity amplitude, \mathcal{J}_μ , which we define as:

$$\mathcal{M}(\bar{K}_{1L,R} \rightarrow P_1 P_2 P_3) = \varepsilon_{K_{1L,R}}^\mu \mathcal{J}_\mu \quad (2.14)$$

Considering that \mathcal{J}_μ represents the decay amplitude of the K_1 decaying into three pseudoscalar mesons, we can parameterize it in terms of two functions $\mathcal{C}_{1,2}$:

$$\mathcal{J}_\mu = \mathcal{C}_1(s, s_{13}, s_{23}) p_{1\mu} - \mathcal{C}_2(s, s_{13}, s_{23}) p_{2\mu} \quad (2.15)$$

where we omitted to write explicitly the Dalitz and angular variable dependences of \mathcal{J}_μ . Here p_1 and p_2 denote the four-momenta of two pions defined in Eq. (2.13). Note the s -dependence of the coefficients, which means that in principle there could be some dependence on the off-shell p^2 of the K_1 . Nevertheless, this dependence is not important as soon as the integration is limited to the K_1 bump, especially for the ratio ω which is the relevant quantity in our method (see next section). The detailed expressions of $\mathcal{C}_{1,2}(s, s_{13}, s_{23})$ for given channels are derived later in this subsection but here we note that $\mathcal{C}_{1,2}(s, s_{13}, s_{23})$ can contain complex numbers.

Since the product of four-vectors is invariant under Lorentz transformations, the amplitude (2.14) is invariant under spacial rotation transformations. In this case it is convenient to express the \mathcal{J} -function in the K_1 -decay reference frame, which is rotated by (θ, ψ, ϕ) angles as shown in Fig. 2.2 (z' -axis is directed along the normal to the decay plane \vec{n} while the other rotated axes x' and y' are set to form an orthogonal basis). In this reference frame, \mathcal{J} , which is a linear combination of the p_1 and p_2 (Eq. (2.15)), has only two spacial x' - and y' -components which significantly simplifies the calculations. Performing three subsequent rotation transformations of the xyz -system of coordinates by angle θ around the y -axis, then by angle ψ around the z -axis and finally by angle ϕ around the new z' -axis (which coincides with the normal \vec{n}) one obtains

$$\vec{\mathcal{J}} = \begin{pmatrix} \cos \theta \cos \psi (\mathcal{J}'_x \cos \phi - \mathcal{J}'_y \sin \phi) - \sin \psi (\mathcal{J}'_x \sin \phi + \mathcal{J}'_y \cos \phi) \\ \cos \theta \sin \psi (\mathcal{J}'_x \cos \phi - \mathcal{J}'_y \sin \phi) + \cos \psi (\mathcal{J}'_x \sin \phi + \mathcal{J}'_y \cos \phi) \\ \sin \theta (-\mathcal{J}'_x \cos \phi + \mathcal{J}'_y \sin \phi) \end{pmatrix} \quad (2.16)$$

where vector $\vec{\mathcal{J}}' = (\mathcal{J}'_x, \mathcal{J}'_y, 0)$ is defined in the rotated $x'y'z'$ -system and is lying in the decay plane of $P_1 P_2 P_3$.

Using Eq. (2.16) and the definition of helicity in Eq. (1.25), we can rewrite the K_1 -

decay amplitude (2.14) in the K_1 reference frame as⁴

$$\begin{aligned} \mathcal{M}(\bar{K}_{1R,L} \rightarrow P_1 P_2 P_3) &= -\vec{\epsilon}_{K_{1R,L}} \cdot \vec{\mathcal{J}} \\ &= \frac{i}{\sqrt{2}} e^{\pm i\psi} [(\mathcal{J}'_x \sin \phi + \mathcal{J}'_y \cos \phi) \mp i \cos \theta (\mathcal{J}'_x \cos \phi - \mathcal{J}'_y \sin \phi)] \end{aligned} \quad (2.17)$$

Squaring the helicity amplitude (2.17) and integrating over ϕ one finds

$$\frac{1}{2\pi} \int_0^{2\pi} |\mathcal{M}(\bar{K}_{1R,L} \rightarrow P_1 P_2 P_3)|^2 d\phi = \frac{1}{4} \left[(1 + \cos^2 \theta) |\vec{\mathcal{J}}'|^2 \pm 2i \cos \theta (\mathcal{J}'_y \mathcal{J}'_{x*} - \mathcal{J}'_x \mathcal{J}'_{y*}) \right] \quad (2.18)$$

where $|\vec{\mathcal{J}}'|^2 = |\mathcal{J}'_x|^2 + |\mathcal{J}'_y|^2$. One can easily notice by writing explicitly by components that

$$i(\mathcal{J}'_y \mathcal{J}'_{x*} - \mathcal{J}'_x \mathcal{J}'_{y*}) = \text{Im}[\vec{n}' \cdot (\vec{\mathcal{J}}' \times \vec{\mathcal{J}}'^*)] \quad (2.19)$$

with $\vec{n}' = \vec{e}_{z'} = (0, 0, 1)$ in the $x'y'z'$ system of coordinates. It can be easily seen that the scalar and triple products are invariant under rotation transformations (it can be trivially demonstrated explicitly by using that fact that the rotation matrices are orthogonal). Therefore,

$$|\vec{\mathcal{J}}'|^2 = |\vec{\mathcal{J}}|^2, \quad \text{Im}[\vec{n}' \cdot (\vec{\mathcal{J}}' \times \vec{\mathcal{J}}'^*)] = \text{Im}[\vec{n} \cdot (\vec{\mathcal{J}} \times \vec{\mathcal{J}}^*)] \quad (2.20)$$

Thus, after the integration over ϕ one can easily find the decay distribution in the K_1 reference frame

$$\frac{d\Gamma(\bar{K}_{1R,L} \rightarrow P_1 P_2 P_3)}{ds ds_{13} ds_{23} d\cos \theta} \propto \frac{1}{4} |\vec{\mathcal{J}}|^2 (1 + \cos^2 \theta) \pm \frac{1}{2} \text{Im}[\vec{n} \cdot (\vec{\mathcal{J}} \times \vec{\mathcal{J}}^*)] \cos \theta \quad (2.21)$$

where $\vec{n} \equiv \frac{\vec{p}_1 \times \vec{p}_2}{|\vec{p}_1 \times \vec{p}_2|}$ so that:

$$|\vec{\mathcal{J}}|^2 = |\mathcal{C}_1|^2 |\vec{p}_1|^2 + |\mathcal{C}_2|^2 |\vec{p}_2|^2 - (\mathcal{C}_1 \mathcal{C}_2^* + \mathcal{C}_1^* \mathcal{C}_2) (\vec{p}_1 \cdot \vec{p}_2), \quad (2.22)$$

$$\vec{n} \cdot (\vec{\mathcal{J}} \times \vec{\mathcal{J}}^*) = -(\mathcal{C}_1 \mathcal{C}_2^* - \mathcal{C}_1^* \mathcal{C}_2) |\vec{p}_1 \times \vec{p}_2| \quad (2.23)$$

where

⁴One can notice that the same expression could also be obtained by defining the initial system of coordinates xyz by setting the decay plane in the xy -plane and defining the z -axis along the normal to the decay plane. In this case one should rotate the K_1 polarization vectors (2.4) by (θ, ψ, ϕ) angles.

$$\vec{p}_1 \cdot \vec{p}_2 = \frac{1}{2}(E_1 E_2 - (s_{12} - m_1^2 - m_2^2)), \quad (2.24)$$

$$|\vec{p}_1 \times \vec{p}_2| = \vec{p}_1 \cdot \vec{p}_2 \tan^{-1} \varphi, \quad (2.25)$$

$$E_i = \frac{s - s_{j3} + m_i^2}{2\sqrt{s}}, \quad (2.26)$$

$$\varphi = \cos^{-1} \left[\frac{\vec{p}_1 \cdot \vec{p}_2}{|\vec{p}_1| |\vec{p}_2|} \right] \quad (2.27)$$

Computation of \mathcal{J} -function in terms of quasi-two-body $K_1 \rightarrow V(\rightarrow P_i P_j) P_k$ couplings

Here we compute the \mathcal{J} function (2.15) in terms of the quasi-two-body couplings. Assuming that the decay of K_1 to three pseudoscalar mesons ($P_i P_j P_k$) proceeds via intermediate isobar V that subsequently decays to $P_i P_j$, these couplings are the two $K_1 \rightarrow V P_k$ form factors and one vector-pseudoscalar $V \rightarrow P_i P_j$ coupling.

The decay amplitudes for these decay channels (2.13) can be written as the sum of the amplitude with different intermediate vector meson channel:

$$\mathcal{M}(K_1 \rightarrow P_1 P_2 P_3) = \sum_V c_{ijk} \mathcal{M}_{(P_i P_j) P_k}^V \quad (2.28)$$

where $P_{1,2,3}$ represent the final state mesons carrying the momentum $p_{1,2,3}$ as assigned in Eq. (2.13) and V represents the vector meson resonance. The Clebsch-Gordan coefficients, c_{ijk} , for each intermediate channel are given as:

$$\mathcal{M}_I(K_1^+ \rightarrow \pi^0(p_1)\pi^+(p_2)K^0(p_3)) = \frac{\sqrt{2}}{3}\mathcal{M}_{(P_1 P_3) P_2}^{K^{*0}} - \frac{\sqrt{2}}{3}\mathcal{M}_{(P_2 P_3) P_1}^{K^{*+}} + \frac{1}{\sqrt{3}}\mathcal{M}_{(P_1 P_2) P_3}^{\rho^+} \quad (2.29a)$$

$$\mathcal{M}_{II}(K_1^+ \rightarrow \pi^-(p_1)\pi^+(p_2)K^+(p_3)) = -\frac{2}{3}\mathcal{M}_{(P_1 P_3) P_2}^{K^{*0}} - \frac{1}{\sqrt{6}}\mathcal{M}_{(P_1 P_2) P_3}^{\rho^0} \quad (2.29b)$$

$$\mathcal{M}_{III}(K_1^0 \rightarrow \pi^0(p_1)\pi^-(p_2)K^+(p_3)) = \frac{\sqrt{2}}{3}\mathcal{M}_{(P_1 P_3) P_2}^{K^{*+}} - \frac{\sqrt{2}}{3}\mathcal{M}_{(P_2 P_3) P_1}^{K^{*0}} + \frac{1}{\sqrt{3}}\mathcal{M}_{(P_1 P_2) P_3}^{\rho^-} \quad (2.29c)$$

$$\mathcal{M}_{IV}(K_1^0 \rightarrow \pi^+(p_1)\pi^-(p_2)K^0(p_3)) = -\frac{2}{3}\mathcal{M}_{(P_1 P_3) P_2}^{K^{*+}} - \frac{1}{\sqrt{6}}\mathcal{M}_{(P_1 P_2) P_3}^{\rho^0} \quad (2.29d)$$

For the computation of the quasi-two-body decay amplitude $\mathcal{M}_{(P_i P_j) P_k}^V$, we take into account the vector meson resonance width effect assuming the Breit-Wigner form, thus

$$\mathcal{M}_{(P_i P_j) P_k}^V \equiv \mathcal{M}(K_1 \rightarrow V P_k) \times \mathcal{M}(V \rightarrow P_i P_j) \times BW_V(s_{ij}) \quad (2.30)$$

The decay amplitude of the axial-vector K_1 to a vector (V) and a pseudoscalar (P_k) meson can be expressed in the following Lorentz invariant form:

$$\langle V(p_V, \varepsilon_V) P_k(p_k) | \Delta \mathcal{H}_{K_1} | K_1(p_{K_1}, \varepsilon_{K_1}) \rangle = \varepsilon_{K_1}^\mu T_{\mu\nu} \varepsilon_V^{\nu*} \quad (2.31)$$

where the hadronic tensor $T_{\mu\nu}$ can be parametrized in terms of two form factors f^V and h^V ,

$$T_{\mu\nu} = f^V g_{\mu\nu} + h^V p_{V\mu} p_{K_1\nu} \quad (2.32)$$

The amplitude of the subsequent decay V to two pseudoscalar mesons P_i and P_j can be parametrized in terms of one vector-pseudoscalar coupling $g_{VP_i P_j}$:

$$\langle P_i(p_i) P_j(p_j) | \Delta \mathcal{H}_V | V(p_V, \varepsilon^{(V)}) \rangle = g_{VP_i P_j} \varepsilon_V^\mu (p_i - p_j)_\mu \quad (2.33)$$

Using these form factors, we can obtain in the K_1 reference frame

$$\mathcal{M}_{(P_i P_j) P_k}^V = (\vec{p}_i \cdot \vec{\varepsilon}_{K_1}) a_{ij}^V + (\vec{p}_j \cdot \vec{\varepsilon}_{K_1}) b_{ij}^V \quad (2.34)$$

where

$$a_{ij}^V = g_{VP_i P_j} BW_V(s_{ij}) [f^V + h^V \sqrt{s}(E_i - E_j) - \Delta_{ij}] \quad (2.35a)$$

$$b_{ij}^V = g_{VP_i P_j} BW_V(s_{ij}) [-f^V + h^V \sqrt{s}(E_i - E_j) - \Delta_{ij}] \quad (2.35b)$$

with $\Delta_{ij} \equiv \frac{(m_i^2 - m_j^2)}{M_V^2} [f^V + h^V \sqrt{s}(E_i + E_j)]$.

Finally, we obtain the general $K_1 \rightarrow P_1 P_2 P_3$ amplitude as:

$$\begin{aligned} \mathcal{M}(K_1 \rightarrow P_1 P_2 P_3) &= c_{132} \mathcal{M}_{(P_1 P_3) P_2}^V + c_{231} \mathcal{M}_{(P_2 P_3) P_1}^V + c_{123} \mathcal{M}_{(P_1 P_2) P_3}^V \\ &\equiv \mathcal{C}_1 (\vec{p}_1 \cdot \vec{\varepsilon}_{K_1}) - \mathcal{C}_2 (\vec{p}_2 \cdot \vec{\varepsilon}_{K_1}) \end{aligned} \quad (2.36)$$

where

$$\mathcal{C}_1 = c_{132} (a_{13}^V - b_{13}^V) - c_{231} b_{23}^V + c_{123} a_{12}^V \quad (2.37a)$$

$$\mathcal{C}_2 = c_{132} b_{13}^V - c_{231} (a_{23}^V - b_{23}^V) - c_{123} b_{12}^V \quad (2.37b)$$

Thus, using Eqs. (2.36) and (2.37), the amplitudes (2.29) can be rewritten in the following form:

$$\mathcal{M}(K_{1L,R} \rightarrow K \pi \pi)_{A=I \sim IV} = \varepsilon_{K_{1L,R}}^\mu \mathcal{J}_\mu^A \quad (2.38a)$$

$$\mathcal{J}_\mu^A = \mathcal{C}_1^A(s, s_{13}, s_{23}) p_{1\mu} - \mathcal{C}_2^A(s, s_{13}, s_{23}) p_{2\mu} \quad (2.38b)$$

with

$$\mathcal{C}_1^{I,III} = \frac{\sqrt{2}}{3}(a_{13}^{K^*} - b_{13}^{K^*}) + \frac{\sqrt{2}}{3}b_{23}^{K^*} + \frac{1}{\sqrt{3}}a_{12}^\rho, \quad \mathcal{C}_1^{II,IV} = -\frac{2}{3}(a_{13}^{K^*} - b_{13}^{K^*}) - \frac{1}{\sqrt{6}}a_{12}^\rho \quad (2.39a)$$

$$\mathcal{C}_2^{I,III} = \frac{\sqrt{2}}{3}b_{13}^{K^*} + \frac{\sqrt{2}}{3}(a_{23}^{K^*} - b_{23}^{K^*}) - \frac{1}{\sqrt{3}}b_{12}^\rho, \quad \mathcal{C}_2^{II,IV} = -\frac{2}{3}b_{13}^{K^*} + \frac{1}{\sqrt{6}}b_{12}^\rho \quad (2.39b)$$

2.3.3 Hadronic parameters

The next step is to obtain the coupling constants and the form factors determining the above functions $\mathcal{C}_{1,2}$, i.e. the following hadronic parameters

$$g_{\rho\pi\pi}, \quad g_{K^*K\pi}, \quad f^V, \quad h^V \quad (2.40)$$

Noting that there are a total of four f^V and h^V ($V = \rho, K^*$) for each $K_1(1270)$ and $K_1(1400)$, we have ten free parameters in this decay mode. One may consider the relative phases between the form factors f^V and h^V , which increases the number of free parameter. However, these phases could actually be determined theoretically or experimentally.

Ideally, these parameters should be extracted from the same experimental data as the $B \rightarrow K_1\gamma$ decay. However, in practice, it is not realistic as it requires a huge number of data, which will not be achieved by this rare process. Therefore, it would be necessary to use other experimental data which provide information of the $K_1 \rightarrow K\pi\pi$ decay. In this section, we first present how to relate these experimental information to our hadronic parameters. In fact, it turns out that the currently available data is not sufficient to obtain all necessary information. Thus, in this thesis, we will use a theoretical model to complement them. It should also be noted that strictly speaking, to obtain these listed parameters from other experiments is not enough for the full model independent analysis, since the formulae derived in the previous subsection are based on certain assumptions such as the quasi-two-body decay, isobar model etc.

The VP_iP_j coupling constant $g_{VP_iP_j}$

The $g_{VP_iP_j}$ coupling can be extracted from the partial decay width of the vector mesons. These are well measured for $V = \rho, K^*$ so that we can obtain this coupling rather precisely. The partial decay width can be written as:

$$\Gamma(V \rightarrow P_iP_j) = \frac{g_{VP_iP_j}^2}{2\pi M_V^2} |\vec{p}|^3 \frac{1}{3} \quad (2.41)$$

where $|\vec{p}| = \sqrt{(M_V^2 - (m_i + m_j)^2)(M_V^2 - (m_i - m_j)^2)}/2M_V$. Then, using the experimental values of ρ and K^* widths, we find⁵

$$g_{\rho\pi\pi} = -(5.98 \pm 0.02), \quad g_{K^*K\pi} = (5.68 \pm 0.05) \quad (2.42)$$

⁵The relative sign of the couplings $g_{\rho\pi\pi}$ and $g_{K^*K\pi}$ is fixed by the 3P_0 quark-pair-creation model, so

The $K_1 \rightarrow VP_k$ form factors f_V and h_V

To describe the $K_1 \rightarrow VP_k$ decay, we used two independent form factors f_V and h_V in (2.31). On the other hand, the $K_1 \rightarrow VP_k$ can also be written in terms of the helicity amplitudes for the two possible $+z$ spin projection of K_1 and the vector meson, $(\lambda_{K_1}, \lambda_V) = (0, 0)$ and $(1, 1)$. These two amplitudes actually can be written in terms of common partial wave amplitudes. Thus, when we expand them up to $L = 2$, we can equivalently write these helicity amplitudes in terms of two partial wave amplitudes [44]:

$$\langle V(\vec{p}_V, \lambda_V) P(-\vec{p}_V) | \Delta \mathcal{H}_{K_1} | K_1(\vec{0}, \lambda_{K_1}) \rangle = (A_S^V + \sqrt{5} \langle 2, 0; 1, \lambda_V | 1, \lambda_V \rangle A_D^V) D_{\lambda_{K_1}, \lambda_V}^{1*}(\Omega_V) \quad (2.43)$$

where $A_{S,D}^V$ are the partial wave amplitudes. Then, these amplitudes can be experimentally extracted through the partial wave analysis of the $K_1 \rightarrow VP_k$ processes using:

$$\Gamma(K_1 \rightarrow VP_k)_{S\text{-wave}} = \frac{|\vec{p}_V|}{8\pi s_{K_1}} |A_S^V|^2 \quad (2.44a)$$

$$\Gamma(K_1 \rightarrow VP_k)_{D\text{-wave}} = \frac{|\vec{p}_V|}{8\pi s_{K_1}} |A_D^V|^2 \quad (2.44b)$$

Comparing Eq. (2.31) and (2.43), we can immediately find the relation between the two form factors and the partial wave amplitudes (f_V, h_V depend in general on s_{K_1} and s_V):

$$f_V = -A_S^V - \frac{1}{\sqrt{2}} A_D^V \quad (2.45a)$$

$$h_V = \frac{E_V}{\sqrt{s_{K_1}} |\vec{p}_V|^2} \left[\left(1 - \frac{E_V}{\sqrt{s_V}} \right) A_S^V + \left(1 + \frac{2E_V}{\sqrt{s_V}} \right) \frac{1}{\sqrt{2}} A_D^V \right] \quad (2.45b)$$

Partial wave analysis of the $K_1 \rightarrow VP_k$ process has indeed been performed by the ACCMOR collaboration [45] and very precious information related to K_1 meson has been extracted, which constitute the basis of the PDG entries. It is the currently available most extensive study of the $K\pi\pi$ channels, with full angular distributions analysis, determination of relative phases between all amplitudes. On the other hand, the interpretation of the ACCMOR data contains various problems in the theoretical point of view, or even empirically. We will come back to some of these issues later in the next chapter. In any case, we found that it is currently impossible to extract all the parameters from experimental data. Thus, we need the help of theoretical model inputs for this reason. In the following, we try to use the so-called 3P_0 model, which is an intuitive model describing the decay by the creation of a quark-antiquark pair.

that the relative sign of the total amplitudes of $K_1 \rightarrow K^* \pi \rightarrow K \pi \pi$ and $K_1 \rightarrow \rho K \rightarrow K \pi \pi$ is as predicted by the model (see Appendix D). This sign can be in principle verified by analysing the Dalitz plot of the recent data of the $B \rightarrow \psi K_1$ decay [43].

2.4 Determination of λ_γ in the DDLR method

In this section, we demonstrate how to determine the polarization parameter λ_γ from the experimental data using the maximum likelihood method. In particular, we introduce the DDLR method which was first applied in the τ polarization measurement at the ALEPH experiment [14].

2.4.1 The previous method of Gronau *et al.*

It is often thought that the polarization information can be obtained only from the angular distribution analysis. Such is the case in the method of Gronau *et al.* [11], where they proposed to measure the up-down asymmetry, defined as

$$\mathcal{A}_{up-down} = \frac{\int_0^1 d\cos\theta \frac{d\Gamma}{d\cos\theta} - \int_{-1}^0 d\cos\theta \frac{d\Gamma}{d\cos\theta}}{\int_{-1}^1 d\cos\theta \frac{d\Gamma}{d\cos\theta}} = \frac{3}{4}\lambda_\gamma \frac{\int ds_{13}ds_{23} \text{Im}[\vec{n} \cdot (\vec{\mathcal{J}} \times \vec{\mathcal{J}}^*)]}{\int ds_{13}ds_{23} |\vec{\mathcal{J}}|^2} \quad (2.46)$$

which is the asymmetry between the total number of the events with the photons emitted above and below the $K\pi\pi$ -plane in the K_1 reference frame, which is proportional to λ_γ . The main conclusions of the two papers of Gronau *et al.* are:

- In Ref. [12] Gronau *et al.* studied only the $B \rightarrow K_1(1400)\gamma$ decay. In Ref. [11] Gronau and Pirjol made a generalization of their method by combining the contributions from several overlapping resonances in a $K\pi\pi$ mass range near $1.4 \text{ GeV}/c^2$, $K_1(1400)$, $K_2^*(1430)$ and $K^*(1410)$. However they concluded that $K^*(1410)$ leads to no asymmetry, while the $K_2^*(1430)$ adds a relatively small contribution. Therefore, the dominance of the $K_1(1400)$ mode was assumed and the $K_1(1270)$ contribution was left aside.
- In particular, they focused on the $K_1(1400)$ decay modes involving one neutral pion. This was done in order to have two interfering $K^*\pi$ amplitudes related by the isospin symmetry.
- Since $\cos\theta$ changes the sign under the exchange of s_{13} and s_{23} , the up-down asymmetry integrated over the full Dalitz region vanishes (for the decay modes *I* and *III* (Eqs. (2.13a) and (2.13c)) the $\text{Im}[\vec{n} \cdot (\vec{\mathcal{J}} \times \vec{\mathcal{J}}^*)]$ function changes the sign under $s_{13} \leftrightarrow s_{23}$ and consequently, being integrated over the Dalitz plot, gives zero). In this case, in order to solve this problem, Gronau *et al.* proposed to define a new angle $\tilde{\theta}$ in the following way: $\cos\theta = \text{sgn}(s_{13} - s_{23}) \cos\tilde{\theta}$.
- Using the trick of the $\cos\theta$ redefinition, the up-down asymmetry was found to be [11]

$$\mathcal{A}_{up-down} \left(\begin{array}{l} B^+ \rightarrow (K^0\pi^+\pi^0)_{K_1(1400)}\gamma \\ B^0 \rightarrow (K^+\pi^-\pi^0)_{K_1(1400)}\gamma \end{array} \right) = (0.33 \pm 0.05)\lambda_\gamma \quad (2.47)$$

The corresponding asymmetry in the $K^+ \pi^- \pi^+$ and $K^0 \pi^+ \pi^-$ channels was found to be smaller since only one $K^* \pi$ intermediate state contributes and the dominant contribution to the asymmetry comes from the interference of S - and D -wave amplitudes⁶ [11]

$$\mathcal{A}_{up-down} \left(\begin{array}{l} B^+ \rightarrow (K^+ \pi^- \pi^+)_{K_1(1400)} \gamma \\ B^0 \rightarrow (K^0 \pi^+ \pi^-)_{K_1(1400)} \gamma \end{array} \right) \approx 0.07 \lambda_\gamma \quad (2.48)$$

Since one of the radiative B -decay modes involving K_1 was observed by the Belle collaboration [13], in this thesis we study the $B \rightarrow K_1(1270) \gamma$ decay instead of $B \rightarrow K_1(1400) \gamma$ as it was done by Gronau *et al.*.

Despite the study of the averaged over the Dalitz plot $\cos \theta$ -distribution in the $\mathcal{A}_{up-down}$ measurement method, the use of ω -distribution (which is introduced in the next subsection) does not require the trick of the redefinition of $\cos \theta$ in order to have a non-zero asymmetry. In addition, the DDLR method allows to combine all the possible $K \pi \pi$ charged states to be analysed together, what can significantly improve the sensitivity by increasing the event statistics.

2.4.2 Application of the DDLR method for the λ_γ determination

Usually experiment measures the differential decay distribution of the observed number of signal events depending on kinematic variables (angles, momenta, etc.) which is fitted with a theoretical distribution in order to determine the unknown theoretical parameters. As a simple illustration, consider the τ -polarization measurement in the two-body decay $\tau \rightarrow \pi \nu_\tau$. In the two-body decay the angular distribution of the pion momentum direction with respect to the τ helicity axis in the τ rest frame is studied. This angular distribution is described by the probability density function (PDF) of the signal event observation at the given $\cos \vartheta$, which is defined as a properly normalized differential branching ratio distribution

$$W_{\tau \rightarrow \pi \nu_\tau}(\vartheta) = \frac{1}{2}(1 + P_\tau \cos \vartheta) \quad (2.49)$$

where P_τ is the τ -polarization. In order to extract P_τ from experimental data we must fit the experimental $\cos \vartheta$ -distribution with our theoretical prediction using, for example, the method of least squares.

The method of least squares is a standard approach to the approximate solution of overdetermined systems, i.e. sets of equations in which there are more equations than unknowns. “Least squares” means that the overall solution minimizes the sum of the squares of the errors made in solving every single equation. The best fit in the least-squares

⁶As it was pointed out in [11], the following result can be changed by about 50% due to the correction of the $K \rho$ channel depending on the relative strong phase δ_ρ .

sense minimizes the sum of weighted squared residuals, a residual being the difference between the observed value and the fitted value provided by a model:

$$\chi^2(P_\tau) = \sum_{i=1}^{N^{\text{bins}}} \frac{(N_i^{\text{exp}} - N_i^{\text{th}})^2}{\sigma_{N_i^{\text{exp}}}^2} \quad (2.50)$$

where N_i^{exp} is the observed number of signal events in the i^{th} bin of the $\cos \vartheta$ -distribution histogram, while N_i^{th} is the expected number of events predicted by a model, i.e.

$$N_i^{\text{th}} \equiv N^{\text{th}}(\vartheta_i) = N^{\text{events}} \times W_{\tau \rightarrow \pi \nu_\tau}(\vartheta_i) \quad (2.51)$$

Thus, the value of P_τ that minimises the χ^2 function (2.50), gives us the best fitted τ -polarization parameter. Here one has to emphasize that the comparison of data and theoretical prediction requires the optimal binning of the histogram since an inappropriate choice of the bin width and the total number of bins can lead to a loss of sensitivity of the polarization measurement.

Now, if we take another example of the τ -decay, $\tau \rightarrow \rho \nu_\tau$. In this case, the PDF (i.e. the normalized decay distribution) has a much more complicated form including not only $\cos \vartheta$ as a kinematical variable but also another angle e.g. β (ϑ is the angle between the momentum of ρ and the τ -direction in the τ rest frame while β is the angle between the momentum of one of the pions and the ρ -direction in the ρ rest frame) and also the $\pi\pi$ invariant mass $m_{\pi\pi}$. In this case χ^2 would be

$$\chi^2(P_\tau) = \sum_{i=1}^{N_{\vartheta}^{\text{bins}}} \sum_{j=1}^{N_{\beta}^{\text{bins}}} \sum_{k=1}^{N_{m_{\pi\pi}}^{\text{bins}}} \frac{(N_{ijk}^{\text{exp}} - N_{ijk}^{\text{th}})^2}{\sigma_{N_{ijk}^{\text{exp}}}^2} \quad (2.52)$$

with $N_{ijk}^{\text{exp/th}}$ denoting the number of events that are in the $\{\vartheta_i, \beta_j, m_{\pi\pi k}\}$ point of the available discrete phase space,

$$N_{ijk}^{\text{th}} \equiv N^{\text{th}}(\vartheta_i, \beta_j, m_{\pi\pi k}) = N^{\text{events}} \times W_{\tau \rightarrow \rho \nu_\tau}(\vartheta_i, \beta_j, m_{\pi\pi k}) \quad (2.53)$$

One can see, that the addition of more observables (angles, invariant masses of the intermediate resonances, etc.) increases the sensitivity of the measurement due to the augmentation of the number of “equations” (i.e. number of terms in Eq. (2.52)), but, at the same time, it increases the complexity of the fit as well.

However, Davier *et al.* pointed out in [14] that such a complication of the multidimensional fit can be avoided in this particular case when the PDF depends on the polarization parameter P_τ *only linearly*. A new variable ω was introduced in this article, which can represent all the kinematical variables, thus allows to extract P_τ from a fit with this single variable. As we describe in the following, since our PDF also depends on the polarization parameter λ_γ linearly, the ω -method can be applied.

Now, we briefly introduce the basics of the DDLR method applied to determine the photon polarization parameter λ_γ in the $B \rightarrow K_1(1270)\gamma$ decay (for more details of the

general method see Appendix E). In the maximum likelihood method, knowing the λ_γ dependence of the PDF of the signal event observation at the given point of the phase space $\{s, s_{13}, s_{23}, \cos\theta\}$, which is defined as the properly normalized differential branching ratio distribution

$$W(s, s_{13}, s_{23}, \cos\theta) = \frac{1}{\Gamma} \frac{d\Gamma(B \rightarrow K_1(1270)\gamma \rightarrow K\pi\pi\gamma)}{ds ds_{13} ds_{23} d\cos\theta}, \quad (2.54)$$

the λ_γ closest to its true value can be obtained where the likelihood function (or equivalently, log-likelihood) given by the N sample of data takes its maximum value. In our case, the PDF, W , can be given as the decay width integrand normalized to unity (after multiplication by the modulus squared of the Breit-Wigner). Let us reiterate our statement that when one remains within the bump of the K_1 -resonance, the decay amplitude weakly depends on $s = p_{K_1}^2$, and one can set $s = M_{K_1}^2$ in Eq. (2.11), i.e. in the \mathcal{J} 's, which we assume hereafter.

Thus, using Eq. (2.11), the PDF for $B \rightarrow K_1\gamma \rightarrow (K\pi\pi)\gamma$ can be given as

$$W(s_{13}, s_{23}, \cos\theta) = f(s_{13}, s_{23}, \cos\theta) + \lambda_\gamma g(s_{13}, s_{23}, \cos\theta) \quad (2.55)$$

where

$$f(s_{13}, s_{23}, \cos\theta) = \frac{1}{4I} |\vec{\mathcal{J}}|^2 (1 + \cos^2\theta) \quad (2.56a)$$

$$g(s_{13}, s_{23}, \cos\theta) = \frac{1}{2I} \text{Im}[\vec{n} \cdot (\vec{\mathcal{J}} \times \vec{\mathcal{J}}^*)] \cos\theta \quad (2.56b)$$

$$I = \frac{2}{3} \int ds_{13} ds_{23} |\vec{\mathcal{J}}|^2 \quad (2.56c)$$

where f and g are normalised relatively to the measure $ds_{13} ds_{23} d\cos\theta$.

Then, similarly to Eq. (E.12) the likelihood function for the N events of data can be given as

$$\mathcal{L} = \prod_{i=1}^N [f(s_{13}^i, s_{23}^i, \cos\theta^i) + \lambda_\gamma g(s_{13}^i, s_{23}^i, \cos\theta^i)] \quad (2.57)$$

where i indicates the kinematic variable of each event. The true value of λ_γ should maximize this function, namely it should be the solution of the following equation:

$$\frac{\partial \mathcal{L}}{\partial \lambda_\gamma} = 0 \quad (2.58)$$

The next procedure to look for the value of λ_γ in our problem is usually to use the known distribution of f - and g -functions and fit the value of λ_γ so as to maximize the likelihood function. As has been shown in the example of $\tau \rightarrow \rho\nu \rightarrow (\pi\pi)\nu$, it should be noted that this is not a very simple task, especially since f and g in Eq. (2.56c) are very complicated functions. However, in [14], it is pointed out that when the PDF depends

on the parameter, which we are interested in, *only linearly*, one can reduce such a multi-dimensional fit to a one-dimensional one using a single variable ω which is defined as follows:

$$\omega(s_{13}, s_{23}, \cos \theta) = \frac{g(s_{13}, s_{23}, \cos \theta)}{f(s_{13}, s_{23}, \cos \theta)}. \quad (2.59)$$

which contains all information about the photon polarization.

Considering the fact that f , g and ω have very complicated dependences on these kinematic variables, the reduction to the one-dimensional fit achieved by using the variable ω is very efficient for the data analysis as shown in the following.

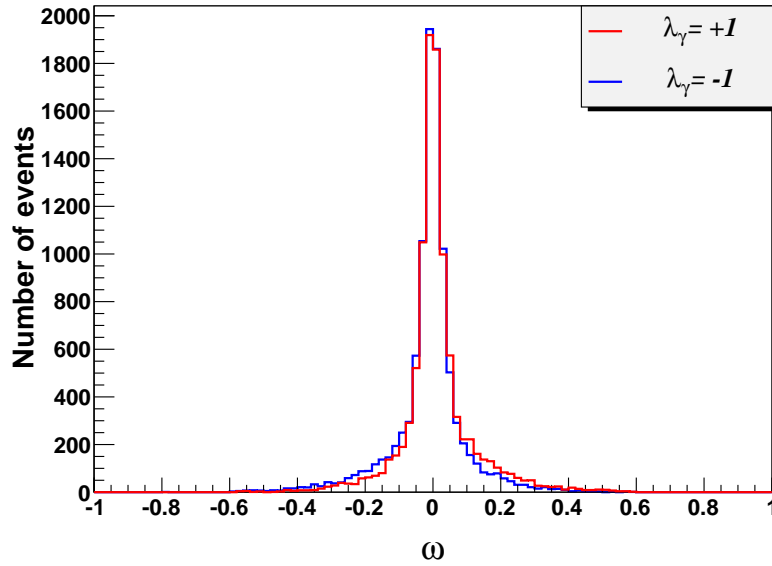


Figure 2.3: The simulated ω -distribution for $\lambda_\gamma = +1$ (red) and $\lambda_\gamma = -1$ (blue). The polarization parameter λ_γ can be determined from the difference between these two distributions (see the footnote 7 for more details).

Now we explain how to extract the value of λ_γ as well as its statistical error from a given ω -distribution. Since the use of the ω -variable reduces our fit to a one-dimensional one, λ_γ is obtained simply as a solution to the following equation:

$$\frac{\partial \ln \mathcal{L}}{\partial \lambda_\gamma} = N \left\langle \frac{\omega}{1 + \lambda_\gamma \omega} \right\rangle = 0. \quad (2.60)$$

where the averaged (integrated) quantity is defined in the standard way:

$$\langle X \rangle \equiv \frac{1}{N} \sum_{i=1}^N X_i \quad (2.61)$$

Of course, one could solve equation (2.60) by successive searches. However, we can provide an explicit expression for λ_γ . Although the ω -distribution is centered around zero (see Fig. 2.3) and consequently the approximate solution for λ_γ in terms of ω -moments (E.17) could be used, one sees that the normalised distribution in ω , $W'(\omega)$, can be written as

$$W'(\omega) = \varphi(\omega)(1 + \lambda_\gamma\omega) \quad (2.62)$$

where $\varphi(\omega)$ corresponds to the image of $f(s_{13}, s_{23}, \cos\theta)$ in the ω -space. In principle, it is a very complicated and unknown function with an analytical form that is very hard to derive. That is why we use a numerical MC method for the evaluation of $\varphi(\omega)$ in order to get the ω -distribution. However, $\varphi(\omega)$ turns out to be an even function of ω (for more details see Appendix E). Then, one can easily demonstrate by integration over the interval $-1 \leq \omega \leq 1$ that λ_γ can be expressed as ratios of odd over even momenta:

$$\lambda_\gamma = \frac{\langle \omega^{2n-1} \rangle}{\langle \omega^{2n} \rangle} \quad (n \geq 1) \quad (2.63)$$

Therefore, the expression (E.17) obtained by DDLR for small λ_γ seems exact. We verified the relation (2.63) by numerical calculation using MC simulation and found up to statistical error that indeed

$$\lambda_\gamma = \frac{\langle \omega \rangle}{\langle \omega^2 \rangle} = \frac{\langle \omega^3 \rangle}{\langle \omega^4 \rangle} = \dots \quad (2.64)$$

Using Eq. (E.15), one can also obtain the statistical error of the given value of λ_γ (2.63) as:

$$\sigma_{\lambda_\gamma}^2 = \frac{1}{N \langle \left(\frac{\omega}{1 + \lambda_\gamma \omega} \right)^2 \rangle}. \quad (2.65)$$

Thus, once the ω distribution is obtained experimentally, Eqs. (2.60) or (2.63) and (2.65) immediately provide the values of λ_γ and σ_{λ_γ} ⁷.

⁷In the real data, one must consider the systematic errors coming from detector effect etc. and perform a χ^2 -fit instead of using these simple formulae. There is one subtlety for that case. For each event, the photon should have the polarization either left- or right-handed. Thus, in MC, we produce the ω -distribution with purely left- and right-handed PDF. Then, the total ω -distribution of the experimental data is expected to be a linear combination of these two distribution with a ratio of ε :

$$N^{\text{exp}}(\omega) = \varepsilon N_R^{\text{MC}}(\omega) + (1 - \varepsilon) N_L^{\text{MC}}(\omega) \quad (2.66)$$

with $\varepsilon \equiv \frac{1 + \lambda_\gamma}{2}$. The N is the number of events in the experimental measurement. We show an example of the ω distribution of $\lambda_\gamma = -1$ (red) and $\lambda_\gamma = +1$ (blue) in Fig. 2.3. As seen in this equation, the λ_γ can be determined from the difference between these two distributions.

Chapter 3

Strong interaction decays of the K_1 -mesons

3.1 Overview of the previous K_1 -decay studies

3.1.1 Experimental overview

Here we summarise the experimental results of the axial vector K_1 -resonance study.

1. Two close in mass axial-vector mesons, $K_1(1270)$ and $K_1(1400)$, were disentangled in the experiments on the diffractive production of the $1^+(K\pi\pi)$ system in the $Kp \rightarrow K\pi\pi p$ reaction, first by the group at SLAC [46] and then by the ACCMOR collaboration in WA3 experiment at CERN [45]. They also observed separately: one $K_1(1270)$ in the strangeness-exchange reaction $\pi^- p \rightarrow \Lambda K\pi\pi$ [47] and the other $K_1(1400)$ in the charge-exchange reaction $K^- p \rightarrow \bar{K}^0 \pi^+ \pi^- n$ [48]. We rely mainly on the diffractive reactions which allow a more detailed study. The relative ratios of two dominant channels, $K^*\pi$ and $K\rho$, indicate that $K_1(1400)$ decouples from the $K\rho$, while the $K\rho$ decay mode of $K_1(1270)$ is dominant (see Table 3.1). This decay pattern suggests that the observed mass eigenstates, $K_1(1270)$ and $K_1(1400)$, are the mixtures of two strange axial-vector $SU(3)$ octet states $K_{1A}({}^3P_1)$ and $K_{1B}({}^1P_1)$.
 - In the experiment, carried out at SLAC by Carnegie *et al.* [46], the mixing angle was determined from the $SU(3)$ couplings to the $K^*\pi$ and $K\rho$ channels to be $\theta_{K_1} = (41 \pm 4)^\circ$. While the partial wave analysis of the WA3 experiment data, done by the ACCMOR collaboration (Daum *et al.* [45]), gives $\theta_{K_1} = (64 \pm 8)^\circ$ and $\theta_{K_1} = (54 \pm 4)^\circ$ for the low and high momentum transfer to the recoiling proton respectively.
 - In the work by Suzuki [49] two possible solutions for the K_1 mixing angle were found in order to explain the observed hierarchy in the K_1 -decays to $K^*\pi$ and $K\rho$: $\theta_{K_1} \approx 33^\circ$ or 57° .

2. The K_1 -resonances were also observed and studied in τ -decays by TPC/Two-gamma [50], ALEPH [51], OPAL [52] and CLEO [53] collaborations.
 - The results of the TPC/Two-gamma experiment [50] suggest that the decay proceeds mostly through $K_1(1400)$ (the corresponding measured branching ratios are $\mathcal{B}(\tau^- \rightarrow K_1(1270)^-\nu_\tau) = (0.41^{+0.41}_{-0.35})\%$ and $\mathcal{B}(\tau^- \rightarrow K_1(1400)^-\nu_\tau) = (0.76^{+0.40}_{-0.33})\%$), although their errors are too large to make a strong statement.
 - The latest measurements [51, 52, 53] show that the $K_1(1270)$ production is favoured over the $K_1(1400)$ production: $\mathcal{B}(\tau^- \rightarrow K_1(1270)^-\nu_\tau) = (4.7 \pm 1.1) \times 10^{-3}$ while $\mathcal{B}(\tau^- \rightarrow K_1(1400)^-\nu_\tau) = (1.7 \pm 2.6) \times 10^{-3}$ [37]. In the analysis, done by the CLEO collaboration [53], the K_1 mixing angle was determined from the measured ratio $\frac{\mathcal{B}(\tau \rightarrow K_1(1270)\nu_\tau)}{\mathcal{B}(\tau \rightarrow K_1(1400)\nu_\tau)}$: $\theta_{K_1} = (69 \pm 16 \pm 19)^\circ$ for $\delta = 0.18$ and $\theta_{K_1} = (49 \pm 16 \pm 19)^\circ$ for $\delta = -0.18$ where $|\delta| = (m_s - m_u)/\sqrt{2}(m_s + m_u) \approx 0.18$ is a phenomenological $SU(3)$ breaking parameter. This result is consistent with the calculation in [49].
3. Radiative B -decays involving the K_1 -mesons were also observed by the Belle collaboration [13]. The data indicate that $\mathcal{B}(B \rightarrow K_1(1270)\gamma) \gg \mathcal{B}(B \rightarrow K_1(1400)\gamma)$. At present moment the measurement of branching ratio $\mathcal{B}(B^+ \rightarrow K_1^+(1270)\gamma) = (4.3 \pm 0.9(\text{stat}) \pm 0.9(\text{syst})) \times 10^{-5}$ has large experimental uncertainty while no significant signal for $B^+ \rightarrow K_1^+(1400)\gamma$ was found and only an upper limit $\mathcal{B}(B^+ \rightarrow K_1^+(1400)\gamma) < 1.5 \times 10^{-5}$ at 90% CL was set.
4. Quite recently the Belle collaboration published a paper on $B \rightarrow J/\psi(\psi')K\pi\pi$ decays [43], which will be discussed in detail later.
5. In addition, the BABAR collaboration reported the measurement of the branching ratios of neutral and charged B -meson decays to final states containing a $K_1(1270)$ and $K_1(1400)$ meson and a charged pion: $\mathcal{B}(B^0 \rightarrow K_1(1270)^+\pi^- + B^0 \rightarrow K_1(1400)^+\pi^-) = 3.1^{+0.8}_{-0.7} \times 10^{-5}$ and $\mathcal{B}(B^+ \rightarrow K_1(1270)^0\pi^+ + B^+ \rightarrow K_1(1400)^0\pi^+) = 2.9^{+2.9}_{-1.7} \times 10^{-5}$ [54]. In order to parametrize the signal component for the production of the K_1 -resonances in B -decays, the K -matrix formalism, used in the analysis by Daum *et al.* in [45], was applied to the model description. Since only some parameters, used in the analysis of the ACCMOR collaboration, have been reported, the BABAR collaboration refitted the ACCMOR data in order to determine the parameters describing the diffractive production of the K_1 -mesons and their decays. One observes that some results are somewhat different. In particular, using the low t -data, the refitted value of the K_1 mixing angle turns out to be 72° compared to 64° from the ACCMOR fit.

3.1.2 Theoretical overview

1. A study of the strange axial-vector mesons was done in by Blundell, Godfrey and Phelps [55], who studied the properties of K_1 by combining the wave functions,

K_1	$M_{K_1}^{ACCMOR},$ GeV/ c^2	$\Gamma_{K_1}^{ACCMOR},$ MeV/ c^2	$\mathcal{B}(K^*\pi)_S$	$\mathcal{B}(K^*\pi)_D$	$\mathcal{B}(K\rho)_S$
$K_1(1270)$	1.27 ± 0.007	90 ± 8	0.13 ± 0.03	0.07 ± 0.006	0.39 ± 0.04
$K_1(1400)$	1.41 ± 0.025	165 ± 35	0.87 ± 0.05	0.03 ± 0.005	0.05 ± 0.04

Table 3.1: Fitted masses, total widths and partial branching ratios of $K_1(1^+)$ decays into vector-pseudoscalar states, measured by ACCMOR collaboration in the $Kp \rightarrow K\pi\pi p$ reaction for the low momentum transfer to the recoiling proton [45]. The total widths, defined by the ACCMOR collaboration, seem to be misleading for the calculation of partial widths as discussed later in the text.

inspired by the Godfrey-Isgur quark model, to describe the bound states and the flux-tube-breaking or 3P_0 models (which are in fact non-relativistic) to describe the decays.

- Using the TPC/Two-gamma results on the ratio $\frac{\mathcal{B}(\tau \rightarrow K_1(1270)\nu_\tau)}{\mathcal{B}(\tau \rightarrow K_1(1400)\nu_\tau)}$ and the quark model calculation of the K_1 decay constants to the decays $\tau \rightarrow K_1\nu_\tau$, the obtained constraint is $-35^\circ \lesssim \theta_{K_1} \lesssim 45^\circ$ at 68% CL, which is in agreement with [49]. Although the relative errors for the individual branching ratios are smaller than those of the ratio, using the branching ratios introduces additional uncertainties due to the errors associated with the poorly known K_1 wavefunctions, which makes the θ_{K_1} -extraction very model dependent.
 - The strong decays of the K_1 mesons to the final states $K^*\pi$ and $K\rho$ were studied as well in order to determine the mixing angle. A χ^2 fit of the experimental data on the partial decay widths $\Gamma(K_1(1270/1400) \rightarrow K^*\pi)$ and $\Gamma(K_1(1270/1400) \rightarrow K\rho)$ was used for the θ_{K_1} -determination.
 - Performing a χ^2 -fit with the predicted decay widths, calculated within the pseudo-scalar-meson-emission model, using simple harmonic oscillator wave functions with a single parameter $\beta = 0.40$ GeV, the fitted value of the mixing angle was obtained to be $\theta_{K_1} = (48 \pm 5)^\circ$.
 - The strong K_1 -decays were also calculated using both the flux-tube-breaking model and the 3P_0 model for several sets of meson wavefunctions. In all cases a second fit was performed by allowing both θ_{K_1} and the quark-pair-creation constant γ to vary, which reduces the χ^2 significantly. Using simple harmonic oscillator wave functions with $\beta = 0.40$ GeV, comparison of the predicted decay widths by the 3P_0 model to experimental results gives $\theta_{K_1} = (45 \pm 4)^\circ$, while the flux-tube-breaking model's prediction gives $\theta_{K_1} = (44 \pm 4)^\circ$. The last result for θ_{K_1} is slightly changed for the case of use of different set of the meson wave functions from Ref. [56]: $\theta_{K_1} = (51 \pm 3)^\circ$.
2. In addition, a detailed study of the $B \rightarrow K_1(1270)\gamma$ and $B \rightarrow K_1(1400)\gamma$ decays in the light-cone QCD sum rules approach was presented by Hatanaka and Yang

in [40].

- The sign ambiguity of the mixing angle is resolved by defining the signs of the decay constants $f_{K_{1A}}$ and $f_{K_{1B}}^\perp$.
- From the comparison of the theoretical calculation and the data for decays $B \rightarrow K_1\gamma$ and $\tau \rightarrow K_1\nu_\tau$, it was found that $\theta_{K_1} = -(34 \pm 13)^\circ$ is favoured within the conventions of Hatanaka and Yang. It is difficult to establish the relation with our own convention.
- The predicted branching ratios, $\mathcal{B}(B \rightarrow K_1(1400)\gamma)$ and $\mathcal{B}(B \rightarrow K_1(1270)\gamma)$, are in agreement with the Belle collaboration measurement within the errors.

3.2 Theoretical model

The need for a theoretical model

In principle, all the hadronic parameters (i.e. K_1 masses and partial decay widths, form factors and relative phases) can be determined from the fits of the experimental data. However, at present moment we are far from being able to perform this with the accuracy, required to determine the photon polarization λ_γ . We found that the up-down asymmetry and the ω -moments are sensitive to certain hadronic parameters which are hard to determine, e.g. to the relative phases of couplings or to the D -waves.

Up to now the most complete and accurate experimental analysis is the one by Daum *et al.*. However, as it is explained later in the next section, one discovers many difficulties in understanding and using the results of the ACCMOR analysis. Among them there are problems with conventions of the coupling signs, there is an incomplete report of the parameters of the fit and intrinsic difficulties with physical treatment. Other experiments, which have been mentioned above, give precious complementary information but they are not able to solve all the problems, all the more since they are less accurate. Due to the insufficient knowledge of hadronic parameters it becomes necessary to use the help of a theoretical model. Of course, there is no fundamental theoretical treatment of such processes. We have only at our disposal the phenomenological approach of the quark models. Indeed, in the case of decays, which is our concern, they include an essential approximation: they are non-relativistic. There is an inherent sizable uncertainty. Therefore, the quark model can not provide accurate predictions which are ultimately needed for the precise determination of λ_γ . It is a provisory step in the expectation of new systematic experimental studies which could provide a precise measurement of a whole set of hadronic parameters.

However, approximate as it is, the quark model can be very precious to check the consistency of the present data and to orient the future studies of K_1 -decays. Moreover, it allows to make an estimation of the sensitivity of λ_γ potential measurement methods.

3.2.1 The mixing of the kaon resonances

In the quark model there are two possible states for the orbitally excited axial-vector mesons: $J^{PC} = 1^{++}$ and $J^{PC} = 1^{+-}$, depending on different spin couplings of two constituent quarks. In the $SU(3)$ -limit these states can not mix, but since the s -quark is actually heavier than the u - and d -quarks, the observed $K_1(1270)$ and $K_1(1400)$ mesons are not pure 1^3P_1 or 1^1P_1 states. They are considered to be mixtures of non mass eigenstates K_{1A} and K_{1B} . Introducing a $K_{1A} - K_{1B}$ mixing angle θ_{K_1} , mass eigenstates can be defined in the following way [49]:¹

$$\begin{aligned} |K_1(1270)\rangle &= |K_{1A}\rangle \sin \theta_{K_1} + |K_{1B}\rangle \cos \theta_{K_1} \\ |K_1(1400)\rangle &= |K_{1A}\rangle \cos \theta_{K_1} - |K_{1B}\rangle \sin \theta_{K_1} \end{aligned} \quad (3.1)$$

Since all of $SU(3)$ operators can be expressed as combinations of isospin, U - and V -spin operators, if an operator describing the interaction is invariant under the $SU(3)$ -group transformations, it is also invariant under the isospin, U -spin and V -spin transformations [57]. However, it is sufficient to require the invariance only under the isospin and U -spin (or V -spin) transformations, since V -spin is dependent on the isospin and U -spin and the V -spin operators can be obtained from the U -spin operators by an isospin transformation (U -spin can be turned into V -spin via rotation by 120°).

Analogously to G -parity, one can define U - and V -parities: $G_U = C(-1)^U$ and $G_V = C(-1)^V$ respectively, where C is the charge-conjugation parity of the neutral non-strange members of the multiplet. The neutral and charged kaons in the octets are the eigenstates of U - and V -parities and always have U or $V = 1$ respectively.

In the $SU(3)$ -limit two kaons that belong to the octets of the same spin but opposite C -parity can not mix. To illustrate it, one can consider a matrix element of some arbitrary operator \mathcal{O} between two neutral kaons from different octets [58, 59]:

$$\langle K_A | \mathcal{O} | K_B \rangle = \langle K_A | G_U^{-1} G_U \mathcal{O} G_U^{-1} G_U | K_B \rangle = C_A C_B \langle K_A | G_U \mathcal{O} G_U^{-1} | K_B \rangle \quad (3.2)$$

If the \mathcal{O} operator is $SU(3)$ -invariant, i.e. $G_U \mathcal{O} G_U^{-1} = \mathcal{O}$, the matrix element of the transition $\langle K_A | \mathcal{O} | K_B \rangle = 0$ unless $C_A = C_B$.

Strong interactions can break the $SU(3)$ -symmetry and produce the mass splittings. It is experimentally confirmed that isospin is conserved in strong interactions. Hence,

¹To be able to compare with other mixing angle estimations, one has to be careful due to the different parametrizations that are used in the literature. For instance, in the analysis by Carnegie *et al.* [46] the parametrization is $|K_1(1270)\rangle = |K_{1A}\rangle \cos \theta_{K_1}^{(SLAC)} + |K_{1B}\rangle \sin \theta_{K_1}^{(SLAC)}$, $|K_1(1400)\rangle = -|K_{1A}\rangle \sin \theta_{K_1}^{(SLAC)} + |K_{1B}\rangle \cos \theta_{K_1}^{(SLAC)}$. To compare with the results made by Daum *et al.* [45], parametrization is written as follows: $|K_1(1270)\rangle = -|K_{1A}\rangle \sin \theta_{K_1}^{(ACCMOR)} + |K_{1B}\rangle \cos \theta_{K_1}^{(ACCMOR)}$, $|K_1(1400)\rangle = |K_{1A}\rangle \cos \theta_{K_1}^{(ACCMOR)} + |K_{1B}\rangle \sin \theta_{K_1}^{(ACCMOR)}$. Comparing the fitted effective couplings one can see that the coupling to K_{1B} has a different sign in these two definitions. Since one can measure only the absolute value of the amplitude, this sign changes nothing and hence it is possible to redefine the sign of this coupling in the paper by Daum *et al.*. After that one can easily establish the correspondence between these two forms of parametrization and the one we use in this paper: $\theta_{K_1} = \theta_{K_1}^{(ACCMOR)} = 90^\circ - \theta_{K_1}^{(SLAC)}$.

if the strong interaction operator breaks the $SU(3)$ -symmetry, U - and V -parities are not conserved anymore, even if G -parity is conserved. In this case $G_U \mathcal{O} G_U^{-1} \neq \mathcal{O}$ and consequently $\langle K_A | \mathcal{O} | K_B \rangle \neq 0$ and the mixing takes place.

3.2.2 3P_0 Quark-Pair-Creation Model

There are several additive quark models of strong vertices. All these models relate to the recoupling coefficients of unitary spin, quark spin and the quark orbital angular momenta, but differ in the dynamical description. One of the simplest additive quark model describing three-meson vertices is the naive quark-pair-creation model (QPCM) of Micu and of Carlitz and Kislinger [60, 61] and developed by Le Yaouanc *et al.* [62] and then extensively discussed by the group of N. Isgur in Canada [56, 63, 55, 64]. As in the usual additive quark models with spectator quarks, the quark-antiquark pair is “naively” created not from the ingoing quark lines but within the hadronic vacuum. The strong interactions vertices in the QPCM are expressed in terms of the explicit harmonic oscillator spacial $SU(6)$ wave functions (compared to the work by Micu [60], who just fitted the various spacial integrals using the measured decay widths, what does not allow to study the polarization effects) and a nonlocal vacuum quark-antiquark pair production matrix element, depending on the internal quark momenta (while Carlitz and Kislinger [61] neglected the internal momentum distributions). Contrary to the QPCM by Colglazier and Rosner [65], the 3P_0 structure of the created pair describes any decay process of any hadron, using one universal parameter. The model parameters are of the hadron itself and not the decay process as in [65], where the various extra couplings between the pair and the incoming meson depend on the nature of the hadron states and may be weighted by different arbitrary coefficients for different hadrons.

The naive QPCM has the advantage of making definite predictions for all hadronic vertices and moreover, contrary to the other works, it predicts the relative signs of the couplings. Another appealing feature of the model is that it consists only one phenomenological parameter (the quark-pair-creation constant), what allows a much more general description and relates the amplitudes of different processes. The main weakness of the QPCM is that it cannot take into account the symmetry breaking effecting on the hadron wave functions and that the emitted hadrons are considered to be non-relativistic. Thus one has to look for the decays that are not significantly sensitive to these effects.

Formalism

In the QPCM, instead of being produced from the gluon emission, the quark-antiquark pair $q\bar{q}$ (see Fig. 3.1) is created anywhere within the hadronic vacuum by an operator proportional to $(u\bar{u} + d\bar{d} + s\bar{s})\mathbf{S} \cdot \mathbf{p}$ where \mathbf{S} refers to spin 1 and \mathbf{p} is the relative momentum of the pair. It is combined with the initial quark-antiquark system $\bar{q}_2 q_1$ and produces the final state $B(q_1 \bar{q})C(q\bar{q}_2)$. The initial spectator quarks are supposed not to change their $SU(3)$ quantum numbers, nor their momentum and spin. In order to conserve the vacuum quantum numbers the pair must be created in the 3P_0 state due to $P = -(-1)^L$

and $C = (-1)^{L+S}$ parity conservation with 0-total momentum ($\vec{k}_3 + \vec{k}_4 = 0$) and to be a $SU(3)$ -singlet. Thus the matrix element of the quark-antiquark pair production from the vacuum is unambiguously constructed with the help of the spins and momenta of the quark and antiquark only [62]:

$$\langle \bar{q}q | \hat{T}_{vac} | 0 \rangle = \delta(\vec{k}_3 + \vec{k}_4) \gamma \sum_m (1, m; 1, -m | 0, 0) \mathcal{Y}_1^m(\vec{k}_3 - \vec{k}_4) \chi_1^{-m} \phi_0 \quad (3.3)$$

where γ is a phenomenological dimensionless pair-creation constant (which is determined from the measured partial decay widths and taken to be of the order of 3-5), χ_1^{-m} are the spin-triplet wave functions, $\phi_0 = \frac{1}{\sqrt{3}}(u\bar{u} + d\bar{d} + s\bar{s})$ is the $SU(3)$ -singlet and \mathcal{Y}_1^m represents the $L = 1$ angular momentum of the pair.

Taking the matrix element of the pair-creation operator between the $SU(6)$ harmonic-oscillator wave functions of hadrons, the matrix element for the decay $A \rightarrow B + C$ can be written as:

$$\langle BC | \hat{T} | A \rangle = \gamma \sum_m (1, m; 1, -m | 0, 0) \Phi_B \Phi_C \Phi_A^m \Phi_{vac}^{-m} I_m^{(ABC)} \quad (3.4)$$

where $\Phi = \chi_1^m \phi$ are the $SU(6)$ spin-flavour wave functions and $I_m^{(ABC)}$ are the spacial integrals dependent on the momentum of the final states, which are computed in Appendix D.

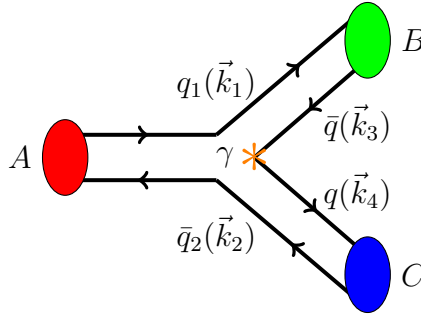


Figure 3.1: Three-meson vertex in the quark-pair-creation model.

Assuming A , B and C to be an axial vector, pseudoscalar and vector mesons respectively, the spin part of the matrix element can be written as

$$\begin{aligned} \chi_C \chi_B \chi_A \chi_{pair} &= \sum_{m_i} \left(\frac{1}{2}, m_1; \frac{1}{2}, m_3 | 0, 0 \right) \left(\frac{1}{2}, m_4; \frac{1}{2}, m_2 | 1, \lambda_C \right) \\ &\times \left(\frac{1}{2}, m_1; \frac{1}{2}, m_2 | S_A, m_{S_A} \right) (1, m_{L_A}; S_A, m_{S_A} | 1, \lambda_A) \left(\frac{1}{2}, m_4; \frac{1}{2}, m_3 | 1, -m \right) \end{aligned} \quad (3.5)$$

Consider for instance $K^{*0} \pi^+$ decay mode of K_1 -meson. After the summation over the spin projections the calculated helicity amplitudes for the K_{1A} (1^3P_1) and K_{1B} (1^1P_1)

will be (the definition of the helicity amplitudes and their relation with the partial wave amplitudes can be found in Appendix D):

$$\begin{aligned}\mathcal{M}_{00}^{10(A)} &= -\gamma \frac{I_1^{(K_1 K^* \pi)}}{3\sqrt{2}}, & \mathcal{M}_{10}^{11(A)} &= -\gamma \frac{I_1^{(K_1 K^* \pi)} - I_0^{(K_1 K^* \pi)}}{6\sqrt{2}} \\ \mathcal{M}_{00}^{10(B)} &= -\gamma \frac{I_0^{(K_1 K^* \pi)}}{6}, & \mathcal{M}_{10}^{11(B)} &= \gamma \frac{I_1^{(K_1 K^* \pi)}}{6}\end{aligned}\quad (3.6)$$

The corresponding amplitudes for the $K^+ \rho^0$ mode are obtained by multiplying the $K^{*0} \pi^+$ amplitudes by $1/\sqrt{2}$ and changing the sign of K_{1A} -part.

Taking into account the isospin factors for different charge states², the generalized amplitudes are summarized in Table 3.2. The functions S and D are defined as

$$S^{(ABC)} = \gamma \sqrt{\frac{3}{2}} \frac{2I_1^{(ABC)} - I_0^{(ABC)}}{18}, \quad D^{(ABC)} = \gamma \sqrt{\frac{3}{2}} \frac{I_1^{(ABC)} + I_0^{(ABC)}}{18} \quad (3.7)$$

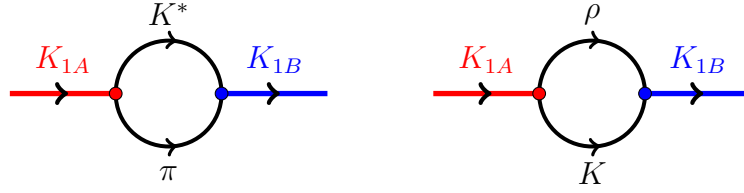
Decay mode	A_S	A_D
$K_{1B} \rightarrow K^* \pi$	$-S^{(K_1 K^* \pi)}$	$-\sqrt{2} D^{(K_1 K^* \pi)}$
$K_{1A} \rightarrow K^* \pi$	$\sqrt{2} S^{(K_1 K^* \pi)}$	$-D^{(K_1 K^* \pi)}$
$K_{1B} \rightarrow K \rho$	$S^{(K_1 K \rho)}$	$\sqrt{2} D^{(K_1 K \rho)}$
$K_{1A} \rightarrow K \rho$	$\sqrt{2} S^{(K_1 K \rho)}$	$-D^{(K_1 K \rho)}$

Table 3.2: Partial wave amplitudes of $K_{1A}(1^3P_1)$ and $K_{1B}(1^1P_1)$ decays into vector-pseudoscalar states, calculated within QPCM.

One has to point out that our treatment obeys the $SU(3)$ -symmetry. $SU(3)$ breaking effects are present only in two places: 1) we use the physical observed masses of hadrons; 2) we introduce mixing between the K_{1A} and K_{1B} states. This is indeed the effect of the symmetry breaking. It is induced, for instance, by spin-orbit forces with different s and u, d quark masses. And also the mixing is generated by the loops as depicted in Fig. 3.2. The $K^* \pi$ and $K \rho$ loop contributions cancel each other only if one sets $M_{K^*} = M_\rho$ and $m_\pi = m_K$, i.e. in the case of the exact $SU(3)$ -symmetry.

Then the decay amplitudes of K_1 into $K^* \pi$ or $K \rho$ final states can be expressed as functions of the pseudoscalar meson momentum in the K_1 reference frame and the mixing

²The amplitudes were calculated for $K_1^+ \rightarrow K^{*0} \pi^+$ and $K_1^+ \rightarrow K^+ \rho^0$. The amplitude of $K \rho$ must be divided over $\sqrt{2}$ due to isospin wave function of ρ^0 . To obtain the general amplitude which doesn't depend on the charge combination one has to divide over the isospin factor: $-\sqrt{2/3}$ for K^* and $\sqrt{1/3}$ for ρ since for the matching with the relativistic form factors the charge combination is not relevant. Finally one obtains the factor $\sqrt{3/2}$ in Eq. (3.7).

Figure 3.2: $K_{1A} - K_{1B}$ mixing via loop effects.

angle θ_{K_1} :

$$\begin{aligned}
 A_S(K_1(1270) \rightarrow K^*\pi/K\rho) &= S^{(K_1K^*\pi/K_1K\rho)}(\sqrt{2}\sin\theta_{K_1} \mp \cos\theta_{K_1}) \\
 A_D(K_1(1270) \rightarrow K^*\pi/K\rho) &= D^{(K_1K^*\pi/K_1K\rho)}(-\sin\theta_{K_1} \mp \sqrt{2}\cos\theta_{K_1}) \\
 A_S(K_1(1400) \rightarrow K^*\pi/K\rho) &= S^{(K_1K^*\pi/K_1K\rho)}(\sqrt{2}\cos\theta_{K_1} \pm \sin\theta_{K_1}) \\
 A_D(K_1(1400) \rightarrow K^*\pi/K\rho) &= D^{(K_1K^*\pi/K_1K\rho)}(-\cos\theta_{K_1} \pm \sqrt{2}\sin\theta_{K_1})
 \end{aligned} \tag{3.8}$$

Correspondingly, the partial decay widths can be determined by using amplitudes squared from the Eqs. (3.8) multiplied by the phase space factors:

$$\Gamma_{S/D}^{QPCM}(K_1 \rightarrow VP) = 8\pi^2 \frac{E_V E_P k_P}{M_{K_1}} |A_{S/D}(K_1 \rightarrow VP)|^2. \tag{3.9}$$

The choice of the wave functions

The unknown parameters of the model are the quark-pair-creation constant γ and the K_1 mixing angle, which we determine by fitting the experimental data on the K_1 -decays (see the next section). However, before proceeding to this determination, the model must be specified by the choice of the set of meson wave functions. In accordance with a fact that the 3P_0 model is a simple model, we will remain within the traditional $SU(6)$ approximation which describes rather well ordinary radiative decays (e.g. $\omega \rightarrow \pi\gamma$). This includes the $SU(3)$ -symmetry approximation which anyway is also present in the 3P_0 model through the fact that the quark-pair-creation constant is the same for all reactions. In this approach the effect of the $SU(3)$ breaking is taken into account only through the dependence of the decay momentum of the physical hadronic masses. For practical reasons, we choose a set of harmonic oscillator wave functions, which are known to give a reasonable approximation.

Here one has to stress that the harmonic oscillator radius of the meson wave function ($\psi(r) \propto \exp(-r^2/2R^2)$, for details see Appendix D) is not a free phenomenological parameter. In principle, it can be predicted by the quark-potential model describing the bound states of two quarks. To get a first and rough estimate we can use the following relation, obtained in the non-relativistic harmonic oscillator model for the energy shift

between the ground state and the first radial excitation:

$$\Delta E_1 = \frac{2}{m_q R^2} \quad (3.10)$$

with m_q being the quark mass, which can be standardly estimated from the magnetic moment of the proton: $\mu_p = \frac{e}{2m_q} = \frac{2.79}{2m_N}$. Whence $m_q \simeq 0.34 \text{ GeV}$ ³. ΔE_1 can be estimated from the energy of the $L = 1$ state of the order of (1.2-1.3) GeV and the weighted average energy of the ground state $(3m_\rho + m_\pi)/4 \simeq 0.6 \text{ GeV}$. Then the estimated radius is given by

$$R = \sqrt{\frac{2}{\Delta E_1 m_q}} \sim \sqrt{\frac{2}{(1.25 - 0.6) 0.34}} \simeq 3 \text{ GeV}^{-1} \quad (3.11)$$

On the other hand, it is obvious that this approximation of the Schroedinger equation with the harmonic oscillator potential is rather naive: the realistic potential is known to be of the form of linear (that describes confinement) plus Coulomb potential. One has also to notice that the application of the use of the non-relativistic character of the Schroedinger equation to the heavy-light systems is dubious. Therefore, one could take a value inspired by the well known model of Godfrey and Isgur. Of course, in the latter model the solutions are no longer the harmonic oscillator wave functions. However, such harmonic oscillator wave functions can represent a good approximation if the radius R is adjusted. For most $L = 0, 1$ states one finds in this model the typical value $R \sim 2.5 \text{ GeV}^{-1}$ [63]. For our predictions we therefore adopt a set of wave functions with a common harmonic oscillator radius having precisely this value,

$$R = 2.5 \text{ GeV}^{-1} \quad (3.12)$$

This is also one of the choices made by Blundell *et al.* [55]. We must warn that in this model pion and kaon have actually quite smaller radius ($\sim 1.4 \text{ GeV}^{-1}$ [63]) due to the strong spin-spin interaction force. We disregard this fact in the spirit of the $SU(6)$ approach. If we were adopting the low values for the Goldstone boson we would obtain unsatisfactory results. For example, using $R_\pi \simeq 1.4 \text{ GeV}^{-1}$, we can not reproduce correctly the D/S ratio in the $b_1 \rightarrow \omega\pi$ decay which is precisely measured.

3.2.3 The issue of the damping factor

In the end of the introduction of the theoretical model, we discuss the necessity of introducing an additional cut-off (or damping factor) in the coupling vertices, in addition to the natural one provided by the 3P_0 model. Generally speaking, there is need in the cut-off for calculations involving far off-shell particles. This appears in various circumstances:

³Note that this is the *phenomenological* mass in the quark models and not the physical constituent quark mass.

- In the calculation of λ_γ . Indeed, the interference of several channels needed to obtain a non-zero imaginary part of $\vec{n} \cdot (\vec{\mathcal{J}} \times \vec{\mathcal{J}}^*)$ (see Eq. (2.11)) requires a large off-shellness of the intermediate isobars.
- In the branching ratios, obtained by the integration over the large phase space for the production of $K\pi\pi$ (e.g. $B \rightarrow K\pi\pi\gamma$). This is especially important for the higher partial waves like D -waves.
- Another effect appears in the decay to one isobar and one stable particle: integrating over the mass of the isobar, the calculated partial width depends on the presence of the damping factor. The low end of the isobar mass spectrum corresponds indeed to large off-shell momenta.

The later effect is especially crucial for the transition rate of $K_1(1270) \rightarrow K\rho$, which is large, although it would be kinematically almost forbidden at the nominal values of the masses. A well-known and simple way to take the widths into account is by integrating over the off-shell “masses”, p^2 , with the weight of the Breit-Wigner’s. However, it is then found that the integrals will diverge for P - or D -waves, due to the k^{2l} factors, where k is the decay momentum, if the coefficients are taken to remain constant. Of course, the reactions will in general provide natural limits of integration: for instance, the spectrum studied by the ACCMOR collaboration stops at $M_{K\pi\pi} = 1.6 \text{ GeV}/c^2$, but even that cut would give exceedingly large P - or D -wave contributions. In fact, it seems that various indications hint at the necessity of a strong dynamical cut-off, or “damping factor”, affecting for instance the Breit-Wigner shape (e.g. accurate studies of $\Delta(1236)$ [66] or $K^*(890)$, see Ref. [48]), the prototype of which are the Blatt-Weisskopf factors. The need for it is also shown by calculations of hadronic loops in the 3P_0 model [67]. One obtains a natural damping factor through the Gaussian factors $e^{-\beta k^2}$:

$$A_S \propto (3 - \alpha k^2)e^{-\beta k^2}, \quad A_D \propto \alpha k^2 e^{-\beta k^2} \quad (3.13)$$

but one finds $\beta \sim 0.3 \text{ GeV}^{-2}$ which is too small. Following Ref. [67], we introduce the empirical Gaussian cutoff $\exp[-\beta'(k^2 - k_0^2)]$ with $\beta' \approx 3 \text{ GeV}^{-2}$, where k_0 is the decay momentum when all the particles are put on-shell:

$$A_S \propto (3 - \alpha k^2)e^{-\beta k^2} \times e^{-\beta'(k^2 - k_0^2)}, \quad A_D \propto \alpha k^2 e^{-\beta k^2} \times e^{-\beta'(k^2 - k_0^2)} \quad (3.14)$$

With this additional damping factor one finds that the integrated D/S -ratio becomes stable. The isobar (K^*/ρ) decay does not depend much on the damping factor.

3.3 How to compare the theoretical model computation with the experimental data?

Let us emphasize that the very extensive work of Daum *et al.* consists of two distinct steps:

- The first one is the partial wave analysis (PWA) where the $K\pi\pi$ three-body final state is decomposed into a sum of quasi-two-body “partial waves” ($K^*\pi$, $K\rho$, etc.) with various quantum numbers of the total spin and orbital momentum. In this first step there is no reference to any parent resonance like K_1 . This step corresponds to the fitted values of the quasi-two-body partial wave amplitudes plotted with the corresponding error bars in [45].
- The second step is the fit of the partial wave amplitudes, extracted on the previous step, within the K -matrix formalism in order to study the structure of the initial parent resonance and its properties (pole masses, couplings to various decay channels, etc.).

Let us stress that this two-step procedure is different from the modern Dalitz plot analyses where the isobar and parent resonances are included together in one unique formula of the total amplitude. In that case the total amplitude is written as a product of the parent resonance decay amplitude and the amplitude of the subsequent decay of the isobar taking into account the width effects of the unstable resonances by the Breit-Wigner forms.

In the following we do not question the first step; we rather indicate various difficulties which we have encountered in trying to use the K -matrix parameters from the analysis of Daum *et al.*. In the following subsection, we first recall the general K -matrix formalism.

3.3.1 The K -matrix formalism

In order to extract our theoretical parameters, γ and θ_{K_1} , we need the experimental partial widths. We also need them to verify our prediction of the model. And the question is: how to define a partial width? Resonances are often parametrized in terms of the Breit-Wigner form

$$BW_r^{(NR)}(m) \propto \frac{1}{m_r - m - i\frac{\Gamma_r}{2}}, \quad \text{or} \quad BW_r^{(R)}(m) \propto \frac{1}{m_r^2 - m^2 - im_r\Gamma_r} \quad (3.15)$$

in the non-relativistic and relativistic cases respectively. Resonance width, in principle, depends on energy, $\Gamma_r(m)$. This approximation assumes an isolated resonance with a single measured decay. If there is more than one resonance in the same partial wave which strongly overlap, an elegant way that provides the unitarity of the S -matrix⁴ is to use the K -matrix formalism for the two-body decays of the resonance states (for more details see Appendix C).

⁴Note that in the case of two overlapping resonances the Breit-Wigner parametrization of the amplitude satisfies the unitarity condition of the S -matrix only with the complex couplings satisfying certain condition. As we demonstrate later, these complex couplings can be obtained from the real K -matrix couplings by a complex rotation.

From the unitarity of the S -matrix

$$S \equiv 1 + 2i\rho^{\frac{1}{2}}T\rho^{\frac{1}{2}} \quad (3.16)$$

one gets

$$T - T^\dagger = 2iT^\dagger\rho T = 2iT\rho T^\dagger \quad (3.17)$$

where the diagonal matrix $\rho_{ij}(m)$ is the phase space factor which is discussed in detail later in this section. In terms of the inverse operators Eq. (3.17) can be rewritten as

$$(T^\dagger)^{-1} - T^{-1} = 2i\rho \quad (3.18)$$

One can further transform this expression into

$$(T^{-1} + i\rho)^\dagger = T^{-1} + i\rho \quad (3.19)$$

Using the definition of the K -matrix

$$K^{-1} \equiv T^{-1} + i\rho \quad (3.20)$$

one can easily find from Eq. (3.19), (3.20) that the K -operator is Hermitian, i.e.

$$K = K^\dagger \quad (3.21)$$

From the time reversal invariance of S and T it follows that K must be symmetric, i.e. *the K -matrix can be chosen to be real and symmetric*. Resonances should appear as a sum of poles in the K -matrix. In the approximation of resonance dominance one gets therefore

$$K_{ij} = \sum_{a'} \frac{f_{a'i}f_{a'j}}{m_{a'} - m} \quad (3.22)$$

where the sum on a' goes over the number of poles with masses $m_{a'}$. In the common approximation in the resonance theory, the couplings $f_{a'i}$ are taken to be real.

The partial and total K -matrix widths can be defined as

$$\Gamma_{a'i}(m) = 2f_{a'i}^2\rho_{ii}(m) \quad (3.23a)$$

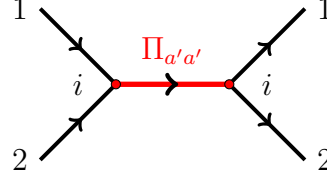
$$\Gamma_{a'}(m) = \sum_i \Gamma_{a'i}(m) \quad (3.23b)$$

Note that the K -matrix width does not need to be identical with the width which is observed in experiment nor with the width of the T -matrix pole in the complex energy plane.

For the illustration, we give two simple examples.

- *One resonance decaying to one channel*

Consider a resonance a' that couples to one channel i :



Using the definition (3.22), the K -matrix for the elastic scattering is given by

$$K = \frac{f_{a'1}^2}{m_{a'} - m} \quad (3.24)$$

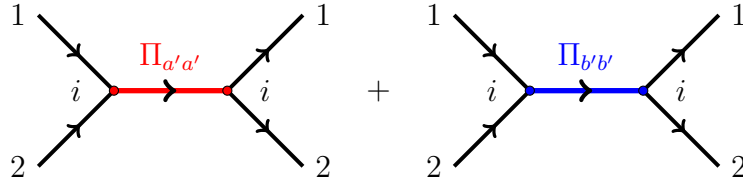
One can easily obtain the transition amplitude

$$T = \frac{f_{a'i}^2}{m_{a'} - m - if_{a'i}\rho_{ii}(m)} = \frac{f_{a'i}^2}{m_{a'} - m - i\frac{\Gamma_{a'}(m)}{2}} \quad (3.25)$$

which is equivalent to the non-relativistic Breit-Wigner parametrization of Eq. (3.15).

- *Two resonances decaying to one channel*

Consider again an elastic scattering at mass m , but suppose that there exist two resonances with masses $m_{a'}$ and $m_{b'}$ coupling to channel i :



In this case the K -matrix is

$$K = \frac{f_{a'i}^2}{m_{a'} - m} + \frac{f_{b'i}^2}{m_{b'} - m} \quad (3.26)$$

Thus, the transition amplitude is given by

$$T = \frac{f_{a'i}^2}{m_{a'} - m - i\frac{\Gamma_{a'}(m)}{2} - i\frac{\Gamma_{b'}(m)}{2} \frac{m_{a'} - m}{m_{b'} - m}} + \frac{f_{b'i}^2}{m_{b'} - m - i\frac{\Gamma_{b'}(m)}{2} - i\frac{\Gamma_{a'}(m)}{2} \frac{m_{b'} - m}{m_{a'} - m}} \quad (3.27)$$

If $m_{a'}$ and $m_{b'}$ are quite far away from each other relative to the widths, then the dominating contribution is either from the first or the second resonance depending

on whether m is near $m_{a'}$ or $m_{b'}$. If it is so, then the amplitude is given merely by the sum of two Breit-Wigner forms:

$$T \simeq \frac{f_{a'i}^2}{m_{a'} - m - i\frac{\Gamma_{a'}(m)}{2}} + \frac{f_{b'i}^2}{m_{b'} - m - i\frac{\Gamma_{b'}(m)}{2}} \quad (3.28)$$

In the other case, when two resonances are sufficiently close to each other or if they have rather large widths, the approximation (3.28) is no longer valid, however one can still write T as a sum of two Breit-Wigners (see Appendix C) but using different masses and couplings.

Then, as we show in the Appendix C, one should identify the K -matrix couplings with the ones predicted by the 3P_0 model taking into account the mixing effect. To establish the relation between the definitions in these two formalisms, we identify the 3P_0 partial widths $\Gamma_{K_1i}^{QPCM}(M_{peak})$ with

$$\Gamma_{K_1i} = 2f_{K_1i}^2 \text{Re}[\rho_{ii}(M_{peak})] \quad (3.29)$$

where ρ_{ij} and f_{K_1i} are the phase space (we use the real part of the phase space since ρ_{ij} is defined as a complex quantity as will be explained later) and the K -matrix couplings in the formalism of Daum *et al.* (see Appendix C where it is explained in detail how to embed the quark model into the K -matrix formalism).

Indeed, the main experiments on the K_1 -decays [45, 46] were analysed with the same K -matrix formalism developed by Bowler *et al.* [68] and obtained very similar results. We use in our analysis the parameters of the analysis done by Daum *et al.* (ACCMOR experiment) which seems to be the most detailed. On the other hand, there are certain physical parameters of the fit which are not tabulated in this paper. Then we also use, where necessary, the results of the K -matrix re-analysis of the ACCMOR data by the BABAR collaboration [54].

Now, Eq. (3.9) is valid only for the narrow isobar. If we have to take into account the effect of the finite width of the isobar, we have to integrate the quasi-two-body phase space over the Breit-Wigner of the isobar. One has to underline, that in this approach we do not have to integrate over the Breit-Wigner of the K_1 -resonance unlike what is done, for instance, in Ref. [63]. We indeed calculate the width at the peak. On the contrary, if we would like to compare with the results of the Belle collaboration analysis [43], this approach must be changed and we would have to integrate over the whole three-body phase space of $K\pi\pi$.

3.3.2 Observed problems in the K -matrix analysis

We found several problems in using the experimental analysis:

- **Absence of the $K\pi\pi$ non-resonant contribution in the K -matrix.**

We note that the K -matrix of Daum *et al.* is composed only of two resonance poles. There is no non-resonant contribution which is usually parametrized as polynomial in terms of m in the K -matrix parametrization. This implies the strong assumption that the quasi-two-body scattering of vector-scalar mesons ($K^*\pi$ and $K\rho$) passes only through the K_1 resonant intermediate states.

- **D -wave amplitudes issue.**

The results of the ACCMOR analysis show that the D -wave in $K_1(1270) \rightarrow K^*\pi$ depends strongly on the production transfer t in the $Kp \rightarrow K\pi\pi p$ reaction. This fact may escape the attention of PDG reader, because it averages between two sets of data (low t , high t). As for the D -wave amplitude in the $K\rho$ channel, there is no information; only branching ratios are quoted in the paper but not the K -matrix couplings and their phases which are crucial for our study.

- **The problem of correct definition of the total width**

When the mass of the resonance at the peak is close to a decay threshold, different definitions of the resonance width are no longer equivalent. Such possible definitions are the width at the peak $\Gamma(M_{peak})$, the width at the S -matrix pole, and finally the full width if measured at one-half the maximum height (FWHH) of the Breit-Wigner distribution defined as

$$\Gamma_{K_1}^{FWHH} \equiv m_2 - m_1, \quad (3.30)$$

where m_1 and m_2 are defined as two solutions in m of the equation

$$\frac{f_{a'(b')1}^2 \rho_{11}(m)}{m_{a'(b')} - m - i\Gamma_{a'(b')}(m)} = \frac{1}{2} \frac{f_{a'(b')1}^2 \rho_{11}(M_{peak})}{m_{a'(b')} - M_{peak} - i\Gamma_{a'(b')}(M_{peak})} \quad (3.31)$$

using the $K^*\pi$ channel (labelled as channel 1).

The last two widths are found to be smaller than the first one. That is why the $K_1(1270)$ width, $\Gamma_{K_1(1270)} = (90 \pm 8) \text{ MeV}/c^2$ [45], which is assumed to be defined as the full width if measured at one-half the maximum height of the Breit-Wigner distribution of K_1 , is less by a factor 1.5-2 than the total width at the peak (see Table 3.3) which is computed using the K -matrix couplings and summing over all possible intermediate channels, i.e.

$$\Gamma_{K_1}^{peak} \equiv 2 \sum_i f_{K_1 i}^2 \text{Re}[\rho_{ii}(M_{peak})] \quad (3.32)$$

We find, indeed, for the later to be of the order of $200 \text{ MeV}/c^2$ with the inclusion of the $\kappa\pi$ channel (see Table 3.3). As a consequence, one observes a large discrepancy between the two possible definitions of the partial width that can be extracted from data of the ACCMOR collaboration: the partial width, defined in a “standard” way as $\Gamma(K_1(1270) \rightarrow K\rho) = \Gamma_{K_1} \times \mathcal{B}(K_1(1270) \rightarrow K\rho)$, is less by a factor 2-3

compared to the partial width at the peak, defined from the K -matrix couplings (see Table 3.4). The total width, defined by ACCMOR collaboration, seems therefore to be misleading. And, indeed, previous theoretical analyses (for instance, in Ref. [55]) unduely used for experimental partial widths the product of branching ratios with this total width.

K_1	$\Gamma_{K_1}^{ACCMOR}$, MeV/ c^2	$\Gamma_{K_1}^{peak}$, MeV/ c^2	$\Gamma_{K_1}^{FWHH}$, MeV/ c^2
$K_1(1270)$	90 ± 8	~ 190	~ 80
$K_1(1400)$	165 ± 35	~ 230	~ 230

Table 3.3: Experimental total decay widths, calculated using the fitted parameters from Ref. [45]. In our opinion, only the widths calculated at the peak must be used to compute partial widths from the branching ratios. Note that the D -waves are not included in the $\Gamma_{K_1}^{peak}$ estimation.

Decay channel i	$\Gamma_{K_1 i} = \mathcal{B}_{K_1 i} \times \Gamma_{K_1}^{ACCMOR}$, MeV/ c^2	$\Gamma_{K_1 i}^{peak} = 2f_{K_1 i}^2 Re\rho_{ii}$, MeV/ c^2
$K_1(1270) \rightarrow (K^*\pi)_S$	12 ± 3	28 ± 26
$K_1(1270) \rightarrow (K\rho)_S$	41 ± 10	122 ± 28
$K_1(1400) \rightarrow (K^*\pi)_S$	162 ± 13	211 ± 59
$K_1(1400) \rightarrow (K\rho)_S$	2 ± 2	20 ± 25

Table 3.4: Experimental partial decay widths, calculated using the fitted parameters from Ref. [45]. As is is underlined before, only the values from the last column must be used.

- **The problem of the phase space, ρ_{ij}**

In the expression of the T -matrix in the K -matrix formalism the phase space factor ρ_{ij} is defined as

$$\rho_{ij}(m) = \frac{2k_i(m)}{m} \delta_{ij} \quad (3.33)$$

Naively, k_i , is the break-up momentum for the two-body decay channel i . But, in fact, Bowler *et al.* used for k_i a particular formulation, proposed by Nauenberg and Pais [69], which tries to take into account two important effects:

- The requirement of the analiticity of the amplitude. The simplest way to satisfy it is the analytic continuation of the phase space through the threshold:

$$\rho_{ij}(m) = \begin{cases} \frac{2k_i(m)}{m} \delta_{ij}, & \text{above threshold} \\ \frac{2i|k_i(m)|}{m} \delta_{ij}, & \text{below threshold} \end{cases} \quad (3.34)$$

It is the basic idea of the so called “Flatte model” which has been used to analyse the $a_0(980)$ decay into $\eta\pi$ and $K\bar{K}$ states, the resonance being very

close to the $K\bar{K}$ decay threshold. Similarly, this effect is also present in the $K_1(1270)$ decays into $K\rho$ and $K^*\pi$ channels with the resonance being at the threshold of $K\rho$. This is not so relevant for the $K_1(1400)$ decays where the resonance is far above the thresholds.

- The effect of the isobar width. The peculiarity of the $K_1(1270)$ with respect to $a_0(980)$ case is that the two-body final state includes one unstable particle, the isobar V ($V = \rho$ or K^*). In order to take into account the width of the isobar, it is logical to integrate the three-body phase space over the Breit-Wigner of the isobar:

$$k_i(m) = \int_{m_V^{min}}^{\infty} k_i(m, m_V) \frac{\Gamma_V/2\pi}{(M_V - m_V)^2 + \frac{\Gamma_V^2}{4}} dm_V \quad (3.35)$$

where $k_i(m, m_V)$ has its non-relativistic expression⁵

$$k_i(m, m_V) = \sqrt{\frac{2m_V m_P}{m_V + m_P} (m - m_V - m_P)} \quad (3.36)$$

The infinite upper limit in Eq. (3.35) corresponds to the analytical continuation of k_i below the threshold for $m_V > m - m_P$.

As an approximation to this integral, Nauenberg and Pais proposed to use the complex mass of the isobar, $M_V \rightarrow M_V - i\Gamma_V/2$, in the expression of the momentum $k_i(m, m_V)$. These two prescriptions lead to a complex phase space, defined as

$$\rho_{ij}(m) = \frac{2k_i(m)}{m} \delta_{ij} = \frac{2}{m} \sqrt{\frac{2M_V m_P}{M_V + m_P} \left(m - M_V - m_P + i\frac{\Gamma_V}{2} \right)} \delta_{ij} \quad (3.37)$$

where P ($P = K$ or π) is the final state pseudoscalar meson in the quasi-two-body decay. According to us this prescription of using a complex mass is not satisfactory for the ρ and K^* , especially for $K_1(1270) \rightarrow K\rho$. Indeed, we found by direct integration of Eq. (3.35) that the results are quite different from the ones obtained using Eq. (3.37), especially the real part of $\rho_{ij}(m)$ which corresponds to the real phase space in the $K_1(1270) \rightarrow K\rho$ case (see Fig. 3.3). The same observation was formulated by Frazer and Hendry [70] when the paper of Nauenberg and Pais was published. They pointed out that this approximation is valid only for the very narrow resonances. The failure of this approach is very worrying since it is basic for the whole analysis.

• The problem of the P - and D -waves

⁵For the relativistic phase space Eq. (3.20) no longer defines a real K -matrix in the physical region. The reason is that the relativistic momentum does not remain imaginary below the threshold due to an additional complex branch point $\propto \sqrt{m^2 - (m_V - m_P)^2}$. Therefore Nauenberg and Pais Ref. [69] restricted to non-relativistic case.

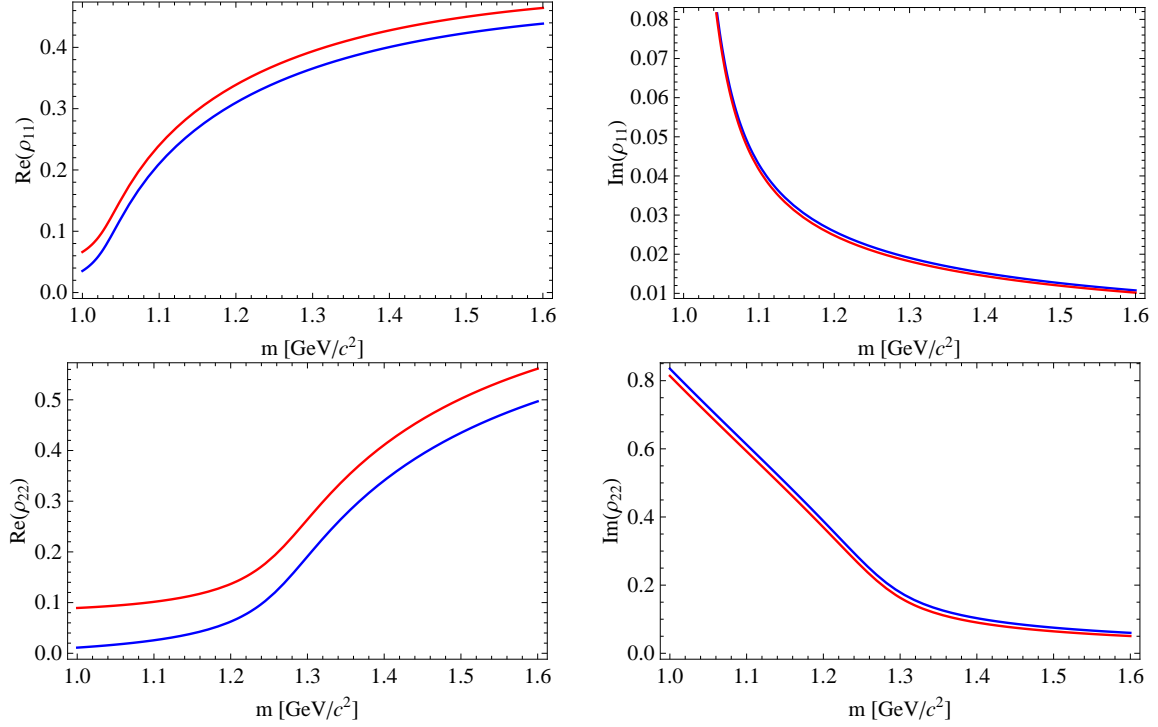


Figure 3.3: Dependence of the phase space factor ρ_{ij} on the mass of the decaying resonance m for the $K^*\pi$ (top) and $K\rho$ (bottom) channels. For comparison, ρ_{ij} is calculated using the proper analytic continuation, Eq. (3.35), (blue) and the approximation of Nauenberg and Pais, Eq. (3.37), (red). The difference between two approaches for $Re(\rho_{22})$ turns out to be significant for the $K\rho$ channel.

In addition, the prescription of Nauenberg and Pais has not been established for the P - and D -waves. We do not know what has been done exactly by Daum *et al.* to treat these waves. On the other hand, such waves are to be included in the analysis, especially the $\kappa\pi$ in the P -wave is very important. Since we are not able to redo the analysis by Daum *et al.* we use the couplings to $K_0^*(1430)\pi$ channel refitted by BABAR collaboration [54]. They include a centrifugal barrier factor depending on the complex momentum which is defined by Eq. (3.37)⁶. However, there is a new following problem here. The approximation of BABAR for the centrifugal barrier factor is not an approximation to the integral

$$\int_{m_V^{min}}^{\infty} k_i(m, m_V) \left[\frac{k_i^2(m, m_V) \tilde{R}^2}{1 + k_i^2(m, m_V) \tilde{R}^2} \right] \frac{\Gamma_V/2\pi}{(M_V - m_V)^2 + \frac{\Gamma_V^2}{4}} dm_V \quad (3.38)$$

which gives a positive real part while the approximation gives a negative one. This contradiction can be masked by the normalization of the centrifugal barrier factor

⁶According to private communications.

at the peak. Although, this is obviously not a satisfactory solution.

- **The diagonalization of the mass matrix and corresponding rotation of the K -matrix couplings**

In several cases we have to deal not with the K -matrix couplings but with Breit-Wigner parametrization of the intermediate resonances. This is the case, for example, in our calculation of the \mathcal{J} -function (2.15). This is also the case of the Dalitz plot analyses such as the one of the Belle collaboration [43]. Then the relevant couplings are slightly different from those of the K -matrix. They are obtained from the latter by a complex rotation. Indeed, to pass to the physical states we have to diagonalize the mass matrix of the states in the K -matrix formalism (see Appendix C). This diagonalization can be performed by a complex orthogonal matrix. This rotation is complex because of the non-diagonal elements of the imaginary part of the mass matrix. The complex rotation angle (which depends on the energy) has both real and imaginary parts which are found to be of the order 10° (this result was obtained by explicit diagonalization of the mass matrix). As a consequence, this rotation affects the couplings: the rotation makes the couplings of the Breit-Wigner somewhat different from the ones of the real K -matrix. The magnitudes of the new couplings are different and phases appear. We found that the largest couplings (i.e. considering the dominant decay channels, $K_1(1270) \rightarrow K\rho$ and $K_1(1400) \rightarrow K^*\pi$) are slightly affected and acquire small phases. On the other hand for the smallest couplings ($K_1(1270) \rightarrow K^*\pi$ and $K_1(1400) \rightarrow K\rho$) the rotation effects are more important. In practical calculations of λ_γ for the present moment we have neglected these effects so that we use directly the couplings obtained from the 3P_0 model.

- **Relative signs and phases**

It appears that the phases of the amplitudes, deduced from the K -matrix are not exactly what is observed: this is a phenomenon of so-called “off-set” phases. The $K\rho$ channel was found to have an additional unexplained phase of 30° [45] relative to the $(K^*\pi)_S$ which was set as a reference one. For the $\kappa\pi$ channel the discrepancy reaches 90° .

3.4 Numerical results

Let us summarize our final prescriptions we use for the calculation of the partial widths and for the further extraction of our theoretical model parameters from the experimental measurements. Our basic approach is to use *partial widths at the peak* on both, theoretical and experimental, sides. We abandon the idea of using the branching fractions and the total K_1 -widths for the comparison with our predictions.

1. For the theoretical prediction, in order to take into account the isobar width effects in our theoretical prediction of the partial widths $\Gamma_{K_1 i}^{QPCM}$, the amplitudes (3.8)

squared are integrated over the invariant mass of the isobar:

$$\Gamma_{K_1 i}^{QPCM} = 8\pi^2 \int_{m_V^{min}}^{M_{K_1} - m_P} \frac{E_V E_P k_P}{M_{K_1}} |A_i(K_1 \rightarrow VP)|^2 \frac{\Gamma_V/2\pi}{(M_V - m_V)^2 + \frac{\Gamma_V^2}{4}} dm_V \quad (3.39)$$

Note that since we consider the widths at the peak there is no integration over the K_1 invariant mass unlike what is done in several theoretical papers (e.g. see Ref. [63]). Moreover, one can notice that the integration over the mass of the isobar is one within the correct physical region restricted by the corresponding physical bound of the two-body decay (i.e. we use the real phase space).

2. For the experimental input, we make the simple assumption that the partial widths, calculated from the K -matrix couplings at the peak according to Eq. (3.40), are correct, although the complex phase space *à la* Nauenberg and Pais (3.37) might be not correct (i.e. what we measure by fitting data, is always the combination like $f_{a'(b')i}^2 \times \rho_{ij}(m)$ which are assumed to be extracted correctly). Therefore, we use the K -matrix couplings and the real part of the complex phase space *à la* Nauenberg and Pais in order to extract the experimental values of the partial widths

$$\Gamma_{K_1 i}^{peak} = 2f_{a'(b')i}^2 \text{Re}[\rho_{ij}(M_{peak})] \quad (3.40)$$

3. We calculate this partial width according to Eq. (3.23) also for the P ($L = 1$) and D -waves ($L = 2$), assuming that the K -matrix couplings f contain the barrier factors $B_i^L(m)$ that are properly normalized at the peak:

$$f_{a(b)i}(m) \Big|_{P,D\text{-waves}} = f_{a(b)i} \frac{B_i^L(m)}{B_i^L(M_{peak})} \quad (3.41)$$

$$B_i^L(m) = \left[\frac{k_i^2(m) \tilde{R}^2}{1 + k_i^2(m) \tilde{R}^2} \right]^{L/2}$$

where $\tilde{R}^2 = 25 \text{ GeV}^{-2}$ [54]. This assumption seems to be correct since it leads to the calculated branching ratios that are very close to the ones announced in the paper by Daum *et al.*. In any case we avoid as much as possible to rely on the experimental data on $K_1(1270) \rightarrow K\rho$ and the D -wave of $K_1(1270) \rightarrow K^*\pi$ and we trust our theoretical prediction.

3.4.1 Fit of parameters γ and θ_{K_1}

In order to extract our phenomenological parameters, the quark-pair-creation constant γ and K_1 mixing angle, we do a fit using the method of least squares. As an experimental input we use the partial widths (namely, $\Gamma_{K_1 i}^{peak}$ from Table 3.4) only of the following

processes: $K_1(1270) \rightarrow (K^*\pi)_S$, $K_1(1400) \rightarrow (K^*\pi)_S$, $K_1(1400) \rightarrow (K\rho)_S$, which are assumed to be Gaussian distributed with mean $\Gamma_{K_1 i}^{QPCM}(\gamma, \theta_{K_1})$ and known variance $\sigma_{\Gamma_{K_1 i}^{peak}}$. The D -waves are not taken into account in our fit. Moreover, the dominant channel $K_1(1270) \rightarrow K\rho$ due to the dangerous threshold and phase space effects is avoided since the narrow width approximation can be incorrect for the decays near the threshold and here the width effects can play a significant role.

Then, the likelihood function is constructed as a sum of squares

$$\chi^2(\gamma, \theta_{K_1}) = -2 \ln L(\gamma, \theta_{K_1}) = \sum_{i=1}^3 \frac{(\Gamma_{K_1 i}^{peak} - \Gamma_{K_1 i}^{QPCM}(\gamma, \theta_{K_1}))^2}{\sigma_{\Gamma_{K_1 i}^{peak}}^2} \quad (3.42)$$

In order to find the unknown parameter θ_{K_1} the function χ^2 is minimized, or equivalently the likelihood function $L(\theta_{K_1})$ is maximized. The minimization of the χ^2 gives the minimal value $\chi_{\min}^2 = 0.61$ and the estimators $\hat{\gamma} = 4.0$ and $\hat{\theta}_{K_1} = 59^\circ$.

The covariance matrix for the estimators $\mathcal{V}_{ij} = \text{cov}[\hat{\xi}_i, \hat{\xi}_j]$ can be found from

$$(\mathcal{V}^{-1})_{ij} = \frac{1}{2} \frac{\partial^2 \chi^2}{\partial \xi_i \partial \xi_j} \bigg|_{\xi=\hat{\xi}} \quad (3.43)$$

Thus one obtains

$$\text{cov}[\hat{\gamma}, \hat{\theta}_{K_1}] = \begin{pmatrix} \sigma_{\hat{\gamma}}^2 & C_{\gamma\theta_{K_1}} \\ C_{\gamma\theta_{K_1}} & \sigma_{\hat{\theta}_{K_1}}^2 \end{pmatrix} = \begin{pmatrix} 0.29 & 0.99 \\ 0.99 & 107.0 \end{pmatrix} \quad (3.44)$$

where the diagonal elements give the variances $\sigma_{\hat{\gamma}}^2$ and $\sigma_{\hat{\theta}_{K_1}}^2$. Finally, one finds the fitted values of the quark-pair-creation constant and K_1 mixing angle:

$$\gamma \simeq 4.0 \pm 0.5, \quad \theta_{K_1} \simeq (59 \pm 10)^\circ \quad (3.45)$$

Taking for granted that our theory is correct, one is now interested in the quality of the agreement between data and various realizations of the theory, determined by the set of parameters, namely $\{\gamma, \theta_{K_1}\}$. For metrological purposes one should attempt to estimate as best as possible the complete set of parameters $\{\gamma, \theta_{K_1}\}$. In this case we use the offset-corrected χ^2 [71]:

$$\Delta\chi^2(\gamma, \theta_{K_1}) = \chi^2(\gamma, \theta_{K_1}) - \chi_{\min}^2 \quad (3.46)$$

where χ_{\min}^2 is the absolute minimum value of the χ^2 function of Eq. (3.42) which is obtained when letting our model parameters free to vary. The minimum value of $\Delta\chi^2$ is zero by construction. Here one has to notice, that this absolute minimum does not correspond to a unique choice of the model parameters. This is due to the fact that the theoretical predictions used in the analysis are affected by important theoretical systematical errors. Since these systematics are restricted in the allowed regions there is always a multi-dimensional degeneracy for any value of χ^2 . However, since in our analysis there are

only two model parameters, our predictions for $\{\gamma, \theta_{K_1}\}$ are not affected by any other theoretical predictions.

A necessary condition is that the confidence level (CL) constructed from $\Delta\chi^2(\gamma, \theta_{K_1})$ provides correct coverage is that the CL interval⁷ for $\{\gamma, \theta_{K_1}\}$ covers the true parameter value with a frequency 1-CL if the measurements were repeated many times. The corresponding CL intervals for the confidence level of CL=68% are shown in Fig. 3.4.

3.4.2 Model predictions for partial widths

Now, we can make systematic predictions for various processes. First, it is very useful to check our result for the quark-pair-creation constant γ prediction with the much better studied $b_1 \rightarrow (\omega\pi)_S$ and $b_1 \rightarrow (\omega\pi)_D$ decays⁸ which depend only on γ . One can see from Fig. 3.5 that our estimation for γ , determined from the K_1 -decays (3.45), is in a good agreement with the one extracted from the $b_1 \rightarrow \omega\pi$ decay. Moreover, the extracted D/S ratio of the partial amplitudes is very well predicted and coincides with the measured value including the sign: $(A_D/A_S)_{QPCM} \simeq 0.28$ while the experiment gives $(A_D/A_S)_{\text{exp}} = 0.277 \pm 0.027$ [37]. Note that the Belle collaboration omits the D -waves in the $B \rightarrow J/\psi K_1$ analysis.

To summarize, we give in Table 3.5 our predictions for the S -wave partial widths of the strong interaction decays of the K_1 -mesons, using the fitted values of γ and θ_{K_1} . One can see that the agreement is satisfactory except for the $K_1(1270) \rightarrow K\rho$ channel. This is not unexpected in view of the difficulties of the experimental treatment as explained in the previous section.

Decay channel i	$\Gamma_{K_1 i}^{QPCM}$, MeV/ c^2	$\Gamma_{K_1 i}^{peak}$, MeV/ c^2
$K_1(1270) \rightarrow (K^*\pi)_S$	31	28 ± 26
$K_1(1270) \rightarrow (K\rho)_S$	61	122 ± 28
$K_1(1400) \rightarrow (K^*\pi)_S$	209	211 ± 59
$K_1(1400) \rightarrow (K\rho)_S$	1	20 ± 25

Table 3.5: Theoretical predictions for the partial decay widths, calculated using the fitted parameters $\gamma = 4.0$ and $\theta_{K_1} = 59^\circ$ and compared to the experimental partial values of widths at the peak (see Table 3.4).

As for the D -waves in the K_1 -decays, our impression is that they are poorly determined experimentally. Our prediction ($\Gamma(K_1(1270) \rightarrow (K^*\pi)_D) \simeq 3$ MeV/ c^2) lies below the experimental numbers: the couplings for the D -waves are not given in the paper by Daum

⁷In statistics, a confidence level interval is a particular kind of interval estimate of a fitted parameter and is used to indicate the reliability of an estimate. It is an observed interval (i.e. it is calculated from the observations), in principle different from sample to sample, that frequently includes the parameter of interest, if the experiment is repeated. How frequently the observed interval contains the parameter is determined by the confidence level.

⁸One has to point out that the branching ratio of $b_1 \rightarrow \omega\pi$ has not been measured precisely. However, the $\omega\pi$ is considered to be the dominant decay mode [37], so that we assume $\mathcal{B}(b_1 \rightarrow \omega\pi) \simeq 100\%$.

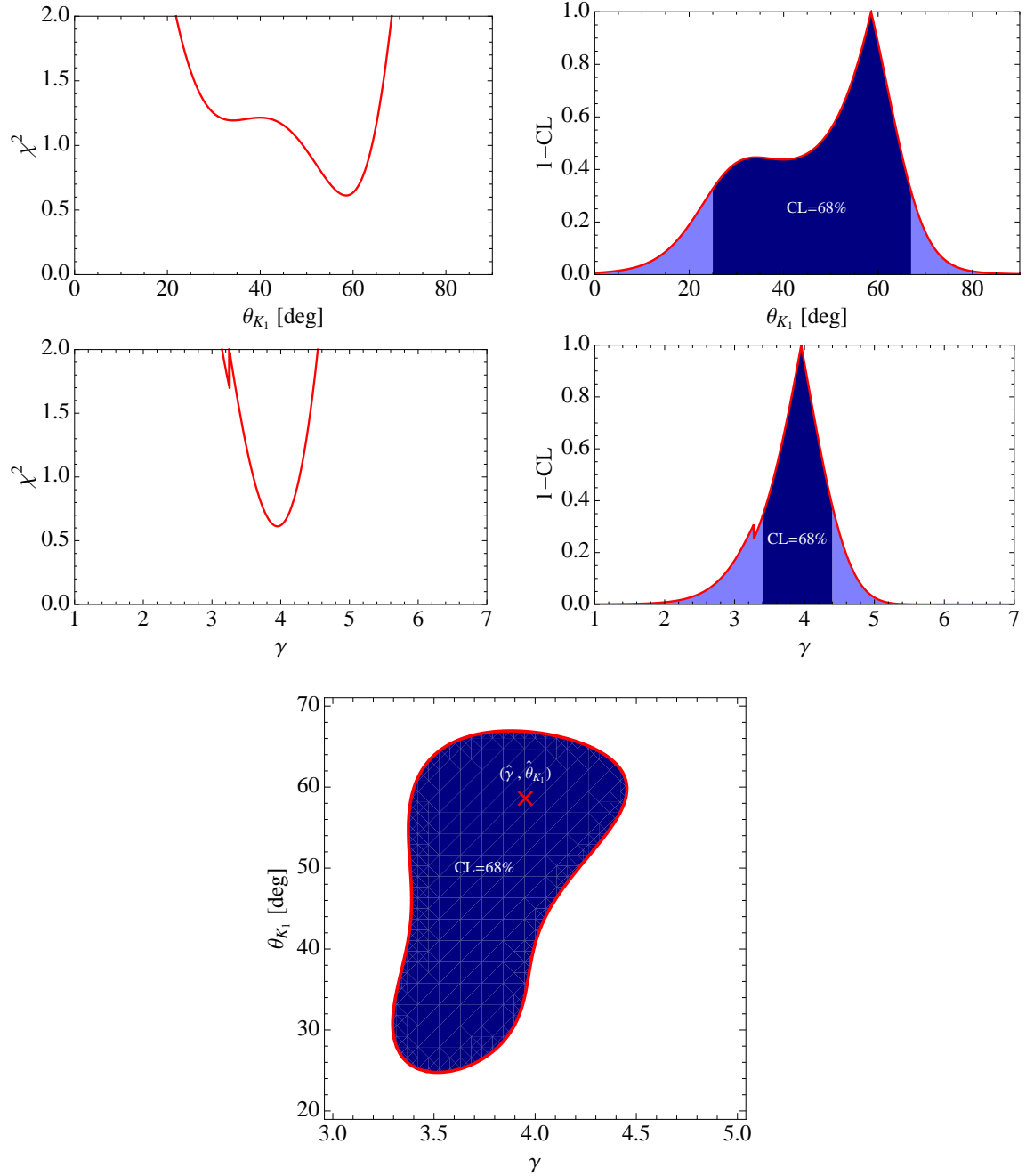


Figure 3.4: χ^2 distributions for the fitted parameters, K_1 mixing angle θ_{K_1} and quark-pair-creation constant γ (left), with the confidence level intervals that determine how frequently the observed interval contains the parameters (right).

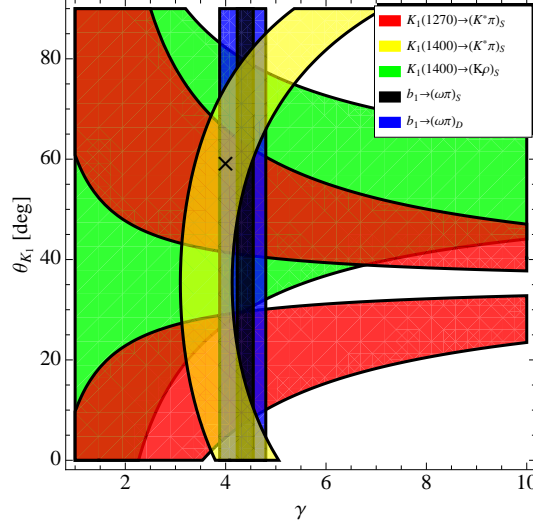


Figure 3.5: QPCM constraints for the quark-pair-creation constant γ and the K_1 mixing angle θ_{K_1} obtained from the fitted partial decay widths at the peak, calculated using the K -matrix couplings (Table 3.4). The cross indicates the optimal values of γ and θ_{K_1} extracted from the fit.

et al.. Tentatively they were re-fitted by the BABAR collaboration [54] from which we deduce the partial width $\Gamma(K_1(1270) \rightarrow (K^*\pi)_D) = (34 \pm 3) \text{ MeV}/c^2$. Here one has to notice that the errors of the re-fitted parameters are surprisingly small as the ones obtained by Daum *et al.*.

3.4.3 Prediction of signs of decay amplitudes and the “off-set” phase issue

Let us recall that our goal is to calculate the \mathcal{J} -function (2.15) which describes the three-body $K_1 \rightarrow K\pi\pi$ decay. Let us stress that the ω^n moments, used for the determination of the photon polarization parameter λ_γ , include the expression $\text{Im}[\vec{n} \cdot (\vec{\mathcal{J}} \times \vec{\mathcal{J}}^*)]$ which depends crucially on the relative phases of the couplings (2.42) and form factors (2.45). These quantities are directly related to the two-body decay amplitudes, calculated by using the quark model. The phases of these amplitudes do not make sense by themselves but only in the product of two amplitudes of the subsequent processes which describe the final three-body decay $K_1 \rightarrow K\pi\pi$. We define the relative phases for two $K_1 \rightarrow K\pi\pi$ amplitudes of various partial waves via different intermediate isobar states (i.e. $(K^*\pi)_S$, $(K^*\pi)_D$, $(K\rho)_S$). Standardly, the reference partial wave is chosen to be the S -wave of $K^*\pi$. For instance, the relative phase of the $K_1 \rightarrow K\rho \rightarrow K\pi\pi$ channel is defined as

$$\delta_\rho \equiv \arg \left[\frac{A_S(K_1 \rightarrow K\rho) \times A_P(\rho \rightarrow \pi\pi)}{A_S(K_1 \rightarrow K^*\pi) \times A_P(K^* \rightarrow K\pi)} \right] \quad (3.47)$$

One has to note, that the total relative phase which is contained in the \mathcal{J} -function contains

of course complex the phase of the denominator of Breit-Wigner of the isobar. For the conventions necessary to define δ_ρ we refer to Appendix D.

δ_ρ is independent of the conventional phase factors of the meson states (e.g. meson wave functions). In the 3P_0 model each decay amplitude is real with suitable conventions of the wave functions and by factorization of spherical harmonics. Then in the quark model δ_ρ is *real*. This is due to specific properties of the transition operator.

Sign of the D/S ratio

The simplest prediction is the one concerning the D/S ratio in the $b_1 \rightarrow \omega\pi$ and $a_1 \rightarrow \rho\pi$ decays. Indeed, this sign depends only on the well known standard conventions. It is then striking that all the signs are correctly predicted by the model. In the case of b_1 and a_1 these signs are well measured and given in PDG. For the $K_1 \rightarrow K^*\pi$ channel the signs are not given by Daum *et al.* in [45]. However, we can read the relative phase for $K_1(1270)$ from Fig. (13) in Ref. [45] which is positive ($f_{b5}/f_{b1} > 0$), while for $K_1(1400)$ we have to rely on the analysis of BABAR because it is not possible to fix it from the figure since the D -wave is too weak overwhelmed compared to the D -wave of $K_1(1270)$ ($f_{a5}/f_{a1} < 0$).

In the paper of Gronau *et al.* [11, 12] the D/S phase for $K^*\pi$ is given as $\delta_{D/S} = (260 \pm 20)^\circ$. We believe that the authors were misled by incorrect interpretation of Fig. (13) (bottom-right) in [45]: the plotted phase indeed peaks at 260° at $M_{K\pi\pi} \approx 1.4 \text{ GeV}/c^2$. But this is not the phase we are looking for since it contains the phase from the Breit-Wigner of $K_1(1270)$ which is dominating over the $K_1(1400)$ contribution and gives an additional phase of approximately 90° . Hence, the phase we are interested in must be read as $\delta_{D/S} \approx (260 - 90)^\circ \sim 180^\circ$. We must stress the following subtle point: the plotted phase is the difference of the phases of the D -wave strongly dominated by $K_1(1270)$ and the one of the S -wave which includes large contributions of both resonances. As a consequence, paradoxically, there appears a bump in the D -wave phase diagram, peaked at $M_{K\pi\pi} \sim (1.3 - 1.4) \text{ GeV}/c^2$ which is essentially determined by the tail of the Breit-Wigner of $K_1(1270)$. We checked this conclusion by explicit calculation of the amplitudes using the K -matrix couplings (see Fig. 3.6).

Relative sign of the $K\rho/K^*\pi$ couplings.

We study the real phase (i.e. the relative sign) of the $K_1(1270) \rightarrow K^*\pi$ and $K_1(1270) \rightarrow K\rho$ amplitudes, which plays important role in the λ_γ determination using the ω -method (due to the strong dependence on the phase of the interference term $\text{Im}[\vec{n} \cdot (\vec{\mathcal{J}} \times \vec{\mathcal{J}}^*)]$). Indeed, the odd moments of ω change their sign if one changes the relative sign between the $K_1^+ \rightarrow K^+\rho^0 \rightarrow K^+\pi^-\pi^+$ and $K_1^+ \rightarrow K^{0*}\pi^+ \rightarrow K^+\pi^-\pi^+$ amplitudes. One has to notice that in this case this phase can be hardly extracted from the K -matrix analysis by Daum *et al.* due to some unknown conventions (in particular, the order of particles that is significant for the determination of the couplings signs). We then rely on the recent analysis by the Belle collaboration of the $B \rightarrow J/\psi(\psi')K\pi\pi$ decay which gives more explicit explanation of the conventions.

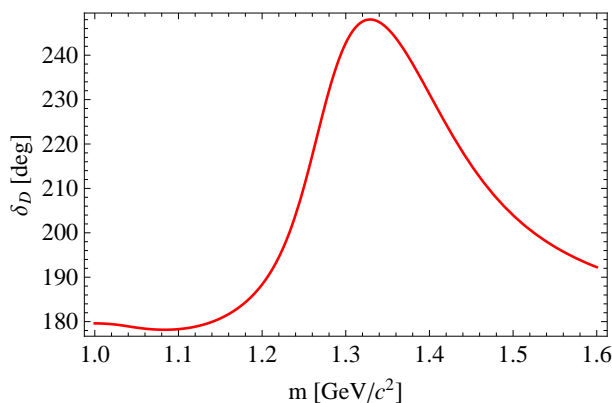


Figure 3.6: The D -wave phase relative to the S -wave of $K^*\pi$, calculated using the K -matrix couplings. One can see a bump at $M_{K\pi\pi} \sim (1.3 - 1.4) \text{ GeV}/c^2$.

Here we summarise what is new in the Belle $B \rightarrow J/\psi(\psi')K\pi\pi$ paper [43]. First we will list up the general conclusions of this paper and then, discuss some details of the Dalitz plot shown in this paper, which provides important information to our work.

General conclusions of the study of $B \rightarrow J/\psi K\pi\pi$ by the Belle collaboration

This paper, in principle, focuses on the measurement of the branching ratios of $B^+ \rightarrow J/\psi K^+\pi^+\pi^-$ and $B^+ \rightarrow \psi' K^+\pi^+\pi^-$. Since the $K\pi\pi$ final state comes from various resonances, K_{res} , this analysis provides information of the $K_{\text{res}} \rightarrow K\pi\pi$ strong decays. Since the $K_{\text{res}} = K_1(1270)$ turned out to be a prominent component (for both J/ψ and ψ'), some detailed study of $K_1(1270) \rightarrow K\pi\pi$ has been done:

- The Dalitz plot for the three-body decays is shown. We discuss more details on this later.
- The intermediated two-body decay branching ratios have been re-determined (see Table 3.6). The branching ratios for the dominant decay modes, $K_1(1270) \rightarrow K\rho$ and $K_1(1270) \rightarrow K^*\pi$, are found to be slightly different from the previous measurements (PDG), although they are still in accordance within several standard deviations. On the other hand, the $K_1(1270) \rightarrow K_0^*(1430)\pi$ channel, which was supposed to have a large branching fraction ($\mathcal{B}(K_1(1270) \rightarrow K_0^*(1430)\pi) = (28 \pm 4)\%$) according to the previous measurements [45, 37], was found to have a significantly smaller contribution of the order of 2% (see Table 3.6).
- In addition, by floating the mass and width of the $K_1(1270)$ in an additional fit of the $B^+ \rightarrow J/\psi K^+\pi^+\pi^-$ data, a smaller mass of $(1248.1 \pm 3.3(\text{stat}) \pm 1.4(\text{syst})) \text{ MeV}/c^2$ and larger width $(119.5 \pm 5.2(\text{stat}) \pm 6.7(\text{syst})) \text{ MeV}/c^2$ were measured for the $K_1(1270)$. Of course, there is a correlation between the fact that the “scalar+ π ” component becomes much smaller and the fact that the $K^*\pi$ and $K\rho$ contributions become larger (see Table 3.6).

Decay mode	PDG (%)	Fit 1 (%)	Fit 2 (%)
$K\rho$	42 ± 6	57.3 ± 3.5	58.4 ± 4.3
$K^*\pi$	16 ± 5	26.0 ± 2.1	17.1 ± 2.3
$K_0^*(1430)\pi$	28 ± 4	1.90 ± 0.66	2.01 ± 0.64

Table 3.6: The fitted branching ratios of the K_1 -decays measured by the Belle collaboration in the analysis of $B \rightarrow J/\psi K\pi\pi$ decay [43].

Here we want to draw attention of the reader to the conceptual difficulties raised by the definition of the $K_1(1270)$ -width. In the Fit 1 the K_1 width is the one given by PDG while in the Fit 2 the width was treated as a free parameter. Due to the threshold effect one should not expect that the width measured by the Belle collaboration from the Breit-Wigner denominator at the peak should coincide with the one defined by PDG, although it should be much larger. One observes that the floated width is larger than the PDG value but it is still much smaller than $200 \text{ MeV}/c^2$ as we would expect from the calculation using the K -matrix formalism (see Table 3.3).

One has to point out that the D -waves are not taken into account in the master formula of Belle. On the other hand, we found from the theoretical study that the D -wave of $K^*\pi$ can have a small but non-negligible effect. In principle, there are two bumps due the presence of the D -wave, but it is found that the one located in the intersection region of the $M_{K\pi} \sim M_{K^*}$ and $M_{\pi\pi} \sim M_\rho$ on the Dalitz plot is masked by the dominating peak of ρ . Using a Monte-Carlo simulation, we observed a second small but non-negligible bump at low $M_{\pi\pi}$ (see Fig. 3.7 in the center).

Dalitz analysis

In [43], the Dalitz plots for $K_1(1270) \rightarrow K\pi\pi$ is shown in the three variable planes, $M^2(K^+\pi^+\pi^-)$, $M^2(K^+\pi^-)$ and $M^2(\pi^+\pi^-)$. On the Dalitz plot in the $M^2(K\pi) - M^2(\pi\pi)$ plane, a strong interference effect between $K_1 \rightarrow K^*\pi$ and $K_1(1270) \rightarrow K\rho$ is observed (see Fig. 3.7). In particular, it is pointed out that the weakening of the $K\rho$ in the region of $M(K\pi) > M_{K^*(892)}$ is originated from the interference of the $K\rho$ and $K^*\pi$ amplitudes. Here we will attempt to study the real phase (in another word, the relative sign) of the $K_1 \rightarrow K^*\pi$ and $K_1(1270) \rightarrow K\rho$ amplitudes using this Dalitz plot. Indeed, as we will see later-on, this information of the phase has an important consequence on our λ_γ determination.

Determining the relative sign of the $K\rho/K^*\pi$ amplitudes

In this section, we demonstrate how the relative phase between the $K\rho/K^*\pi$ amplitudes can be determined from the Dalitz plot.

In [43], the full amplitude of K_1 three-body decays is defined as

$$|\mathcal{M}(s_{K_1}, s_{K^*}, s_\rho)|^2 = |a_{K^*}A_{K^*}(s_{K_1}, s_{K^*}) + a_\rho A_\rho(s_{K_1}, s_\rho)|^2 \quad (3.48)$$

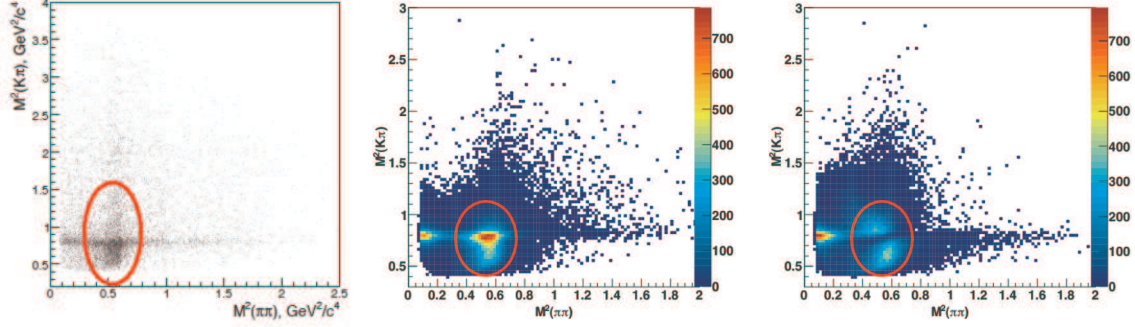


Figure 3.7: Dalitz plots of $B^+ \rightarrow K_1^+(1270)\gamma \rightarrow K^+\pi^-\pi^+\gamma$, measured by the Belle collaboration [43] (left) and MC simulated for the “off-set” phase equal to 0 (center) and π (right) of the $K\rho$ channel relative to $(K^*\pi)_S$. The “correct” phase $\delta_\rho = 0$ corresponds to our quark model prediction.

where the coefficients $a_{K^*,\rho}$ represent the strong decay of $K_1 \rightarrow K\pi\pi$ through K^*, ρ intermediate states. The amplitudes $A_{K^*,\rho}$ are defined as⁹

$$A_V(s_{K_1}, s_V) = \frac{\sqrt{M_{K_1}\Gamma_{K_1}}}{M_{K_1}^2 - s - iM_{K_1}\Gamma_{K_1}} \times \frac{\sqrt{M_V\Gamma_V}}{M_V^2 - s_V - iM_V\Gamma_V} \times \sqrt{1 + \frac{\vec{p}_i^2}{s_{K_1}} \cos^2 \theta_{ik}} \quad (3.49)$$

where p_i is the breakup momentum of P_i or V in the K_1 reference frame and θ_{ik} is the angle between the momenta of P_i and P_k in the V reference frame, which can be expressed in terms of s_{K_1}, s_{ij}, s_{ik} .

Compared to the obtained Dalitz plot, we can determine the coefficients $a_{K^*,\rho}$ including the relative phase between them. The obtained result by the Belle collaboration yields [43]:

$$|a_{K^*}| = 0.962 \pm 0.058 \pm 0.176, \quad |a_\rho| = 1.813 \pm 0.090 \pm 0.243$$

$$\delta_\rho \equiv \arg(a_\rho/a_{K^*}) = -(43.8 \pm 4.0 \pm 7.3)^\circ \quad (3.50)$$

Formula (3.48) can be written in the following general form factorizing out the phase:

$$|\mathcal{M}(s_{K_1}, s_{K^*}, s_\rho)|^2 = c_0(s_{K_1}, s_{K^*}, s_\rho) + c_1(s_{K_1}, s_{K^*}, s_\rho) \cos \delta_\rho + c_2(s_{K_1}, s_{K^*}, s_\rho) \sin \delta_\rho \quad (3.51)$$

where $c_i(s, s_{K\pi}, s_{\pi\pi})$ are the known functions, expressed in terms of various combinations of the real and imaginary parts of $|a_{K^*}|A_{K^*}(s_{K_1}, s_{K^*})$ and $|a_\rho|A_\rho(s_{K_1}, s_\rho)$. So, in order to establish the correspondence between our parametrization of $|\mathcal{M}|^2$ ($|\vec{\mathcal{J}}|^2$ in our case) one

⁹One has to notice that the D -wave amplitude is not taken into account in the following parametrization and that the last factor in Eq. (3.49) corresponds to the S -wave.

can compare the relative signs of the $\cos \delta_\rho$ and $\sin \delta_\rho$ coefficients, $c_{1,2}$, on the Dalitz plot. Direct numerical calculation shows that

$$\text{sign}(c_1^{\text{model}}) = \text{sign}(c_1^{\text{Belle}}), \quad \text{sign}(c_2^{\text{model}}) = -\text{sign}(c_2^{\text{Belle}}) \quad (3.52)$$

The issue of the complex phase

In principle, the QPCM predicts real $K_1 \rightarrow VP$ amplitudes, without any complex phases. This should correspond to the K -matrix couplings. The complex rotation of the K -matrix states to the physical states should introduce complex phases but we found by explicit calculation (see Appendix C) that the imaginary part of the rotation angle is small:

$$\varphi_{a' \rightarrow a^{ph}} \simeq 10^\circ \quad (3.53)$$

However, the Belle collaboration measured a sizeably larger imaginary relative phase (i.e. Eq. (3.50)) of $\delta_\rho \simeq -44^\circ$. We recall also that Daum *et al.* measured a non-zero phase of the order of 30° . Similar value was found in the reanalysis of the ACCMOR data by the BABAR collaboration: $\delta_\rho = -31^\circ$ [54].

There is no explanation of this complex phase in a definite theoretical model: neither in the 3P_0 quark model nor in the most general quasi-two-body K -matrix approach. Indeed, the “off-set” phase which is introduced in the analysis by Daum *et al.* depends only on the decay channel and is the same for the lower and upper resonances. The general production amplitude for each channel in the reaction $K^-p \rightarrow (K^- \pi^+ \pi^-)p$ is written as [45, 54]

$$F_i = e^{i\delta_i} \sum_j (1 - iK\rho)_{ij}^{-1} P_j \quad (3.54)$$

where the factor $(1 - iK)^{-1}$ represents the propagation and the decay of the K_1 -resonance. The last factor P_j describes the resonance production which can be in principle complex (indeed, one finds in [45] that there is a non-zero relative phase between the production couplings of two K_1 -resonances). From Eq. (3.54) it is obvious the “off-set” phase δ_i can not be ascribed to either the resonance decay or production amplitude.

This puzzling situation must not be ignored and has to be studied more carefully. In the present, we use the model prediction for the \mathcal{J} -function as it is with pure real couplings. On the other hand, to adopt pragmatic attitude we explore the effect of introducing this additional “off-set” phase $\delta_\rho = -\delta_\rho^{\text{Belle}}$ in the calculation of the \mathcal{J} -function and the estimation of the theoretical uncertainty of λ_γ .

3.4.4 The issue of the $\kappa\pi$ channel

The PDG assigns a large branching ratio $\mathcal{B}(K_1(1270) \rightarrow K_0^*(1430)\pi) = (28 \pm 4)\%$. It is extracted as all the branching ratios, from the ACCMOR data and analysis. However, this interpretation is dubious. The original ACCMOR measurement shows indeed a clear, strongly coupled peak in the “scalar + π ” channel around the mass $M_{K\pi\pi} \sim 1270 \text{ MeV}/c^2$.

However, it is not at all claimed that the scalar is $K_0^*(1430)$; it is treated as a lower and much broader scalar meson ($M \simeq 1.25 \text{ GeV}/c^2$, $\Gamma \simeq 600 \text{ MeV}/c^2$); or could be a continuum $(K\pi)_{S\text{-wave}}$ according to [72].

The $K_0^*(1430)$ meson is the scalar orbitally excited state of kaon which has the mass $M_{K_0^*(1430)} = (1425 \pm 50) \text{ MeV}/c^2$ and width $\Gamma_{K_0^*(1430)} = (270 \pm 80) \text{ MeV}/c^2$ [37]. According to quark models, the constituent quarks are in the 3P_0 state. In order to estimate the $K_0^*(1430)\pi$ contribution we use QPCM to calculate the P -wave amplitude for the decays $K_1(1270) \rightarrow K_0^*(1430)\pi$. One can see from Fig. 3.8 that $A_P(K_1(1270) \rightarrow K_0^*(1430)\pi)$ is strongly suppressed compared to $A_S(K_1(1270) \rightarrow K^*\pi)$. Moreover, there is also a suppression due to the phase space. Finally, after the integration over the phase space for $\sqrt{s_{K\pi}}$ within the allowed physical range $[m_K + m_\pi; M_{K_1(1270)} - m_\pi]$, we predict that

$$\frac{\mathcal{B}(K_1(1270) \rightarrow K_0^*(1430)\pi)}{\mathcal{B}(K_1(1270) \rightarrow K^*(892)\pi)} < 0.01\% \quad (3.55)$$

in blatant contradiction with the PDG entry.

What is most striking is that indeed, the Belle collaboration finds $\mathcal{B}(K_1(1270) \rightarrow K_0^*(1430)\pi) \simeq 2\%$ (see Table 3.6); it is very small as we predict. They did not find any other “lower scalar+ π ” component in the K_1 -decay: the \mathcal{B} missing with respect to ACCMOR seems to be filled by an enlargement of $K\rho$. Therefore, in our analysis, we do not include the $K_1(1270) \rightarrow K_0^*(1430)\pi$ channel. Neither do we include any other possible scalar in the presented results. However, to take into account the contrary conclusions of ACCMOR, we keep in mind the possibility that there is some significant portion of the branching ratio carried by a very wide scalar meson, different from the $K_0^*(1430)$, such as the low lying state $K_0^*(800)$ (also called κ) [73]. Note that such state is most probably not a $q\bar{q}$ state and therefore the decay into $\kappa\pi$ can not be estimated within our theoretical model. Such contribution has not been tested explicitly in the analysis by the Belle collaboration.

Let us mention two other relevant facts: on the one hand the non-strange counter part of $\kappa(800)$, σ , is found with sizable branching ratio in the decay of $a_1(1260)$ in the $\sigma\pi$ state. On the other hand it is surprising, as noticed by Daum *et al.*, that there is no $\kappa\pi$ channel in the $K_1(1400)$ decay.

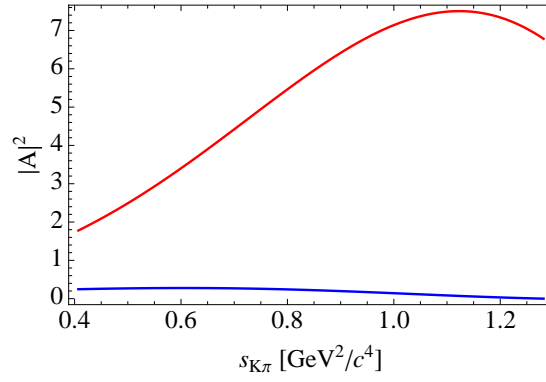


Figure 3.8: $|A_S(K_1(1270) \rightarrow K^*\pi)|^2$ (red) and $|A_P(K_1(1270) \rightarrow K_0^*(1430)\pi)|^2$ (blue) for $s_{K_1} = M_{K_1(1270)}^2$. The K_1 mixing angle θ_{K_1} is taken to be 60° .

Chapter 4

Sensitivity studies of the polarization measurement with $B \rightarrow K_1(1270)\gamma$ in the DDLR method

In this chapter, we perform a Monte Carlo simulation in order to estimate the sensitivity of the future experiments to the polarization parameter λ_γ using the DDLR method.

4.1 Statistical error on the polarization parameter

Our target is to experimentally justify or falsify the left-handed nature of the SM, e.g. $|\lambda_\gamma| \simeq 1$. However, since the measured value is always accompanied by the experimental errors, the test of the SM can be achieved only in terms of probability. In this section, we will investigate at which extent the polarization parameter can be determined in the future measurements by SuperB and LHCb¹.

As described in Section 2.4.2, in the DDLR method, once experimental data is obtained, we compute the ω -value for each event (inputting the kinematical variables of the event into Eq. (2.59)), which immediately gives the best fitted value of λ_γ through Eq. (2.64):

$$\lambda_\gamma^{\text{obs}} = \frac{\langle \omega \rangle}{\langle \omega^2 \rangle} \quad (4.1)$$

Then, using this $\lambda_\gamma^{\text{obs}}$ value, Eq. (2.65) readily gives the experimental error to the λ_γ :

$$\sigma_{\lambda_\gamma^{\text{obs}}}^{-2} = N \left\langle \left(\frac{\omega}{1 + \lambda_\gamma^{\text{obs}} \omega} \right)^2 \right\rangle \quad (4.2)$$

In the following, we attempt to obtain the σ_{λ_γ} value by assuming the SM, i.e. we generate “fake” data by using $\lambda_\gamma = 1$ ($N = 10^3$ and $N = 10^4$ events as an example) and

¹Throughout this section, we assume “ideal” situation, i.e. detector and background effects are not taken into account. Thus, the experimental error contains only the statistical ones.

follow the procedure described above (see also the flow chart in Fig. 4.1).

In order to generate the events as well as to compute the ω distribution, we use the input hadronic parameters as given in Chapter 3, taking into account the form factor momentum transfer dependence. These parameters include the experimentally measured isobar widths, the 3P_0 model parameters (the meson wave function radii, the quark-pair-creation constant, damping factor) and the phenomenological K_1 mixing angle.

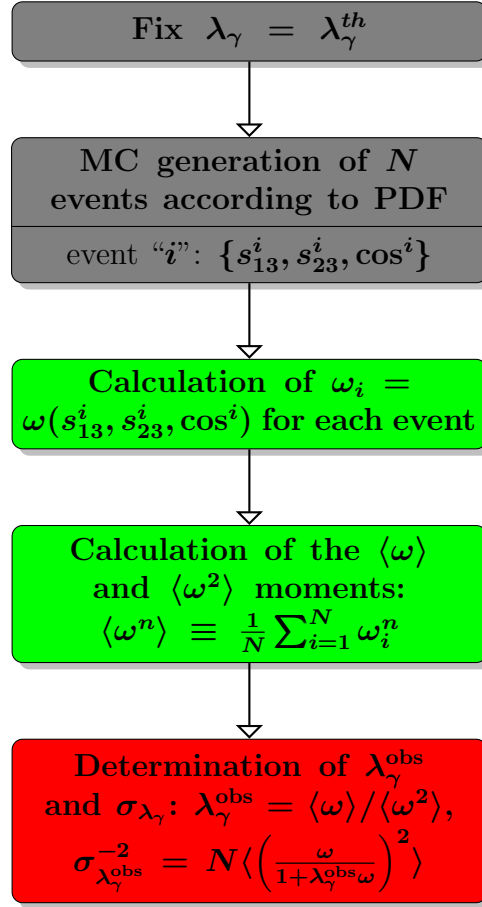


Figure 4.1: MC generation and λ_γ error determination procedure.

In Table 4.1, we present our result in the case of the SM, i.e. $\lambda_\gamma = 1$. One can see from the table, that for 10^4 events the error on λ_γ is smaller than 0.1. We found that the errors do not change much for different values of λ_γ . We found that the ω distributions for the $K^+\pi^+\pi^-$ and $K^0\pi^+\pi^-$, and $K^0\pi^+\pi^0$ and $K^+\pi^-\pi^0$ are the same. Then, it should be pointed out an advantage of using the ω -variable: all the channels corresponding to the same PDF can be merged altogether. That means that one can compute ω -variable for each event and build a single histogram, which can increase the statistical significance.

In the above, we use the full decay distribution, not only on the information of the angular part but also the information of the invariant mass of the hadronic system. In the original DDLR paper [14], it was pointed out that using an average decay distribution

in place of a full decay distribution for each set of invariant masses results in a decrease of the sensitivity. In order to test this, we also produce the ω' -distribution including only the $\cos\theta$ -dependence, i.e. integrated over the Dalitz plot

$$\omega'(\cos\theta) = \frac{\langle \text{Im}[\vec{n} \cdot (\vec{\mathcal{J}} \times \vec{\mathcal{J}}^*)] \rangle}{\langle |\vec{\mathcal{J}}|^2 \rangle} \frac{2 \cos\theta}{1 + \cos^2\theta} \quad (4.3)$$

where

$$\begin{aligned} \langle |\vec{\mathcal{J}}|^2 \rangle &= \int |\vec{\mathcal{J}}|^2 ds_{13} ds_{23} \\ \langle \text{Im}[\vec{n} \cdot (\vec{\mathcal{J}} \times \vec{\mathcal{J}}^*)] \rangle &= \int \text{Im}[\vec{n} \cdot (\vec{\mathcal{J}} \times \vec{\mathcal{J}}^*)] ds_{13} ds_{23} \end{aligned} \quad (4.4)$$

and compute σ_{λ_γ} . We found that the inclusion of the full Dalitz information can indeed improve the sensitivity by typically a factor of two comparing to the angular fit. The use of the ω' is equivalent to the up-down asymmetry method of Gronau *et al.*. We confirmed this fact by comparison of the corresponding statistical errors which turn out to be practically the same. The comparison of the statistical errors of two methods, DDLR and the one by Gronau *et al.*, depending on the annual yield of signal events is presented in Fig. 4.2.

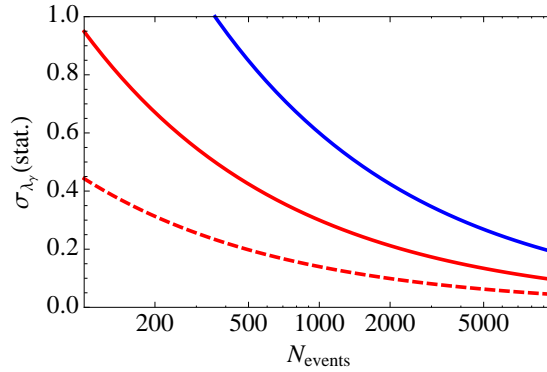


Figure 4.2: Dependence of the statistical error σ_λ on the total number of signal events of the decays $B^+ \rightarrow (K^+\pi^-\pi^+)_{K_1(1270)}\gamma$ and $B^0 \rightarrow (K^0\pi^+\pi^-)_{K_1(1270)}\gamma$ depending on the λ_γ determination method: the error of λ_γ which is determined by using the DDLR method (red) and the error determined from the up-down asymmetry (blue). Red dashed curve corresponds to the error of λ_γ determined by the DDLR method for $B^+ \rightarrow (K^0\pi^+\pi^0)_{K_1(1270)}\gamma$ and $B^0 \rightarrow (K^+\pi^-\pi^0)_{K_1(1270)}\gamma$ decays.

Finally, let us give a rough estimate for the event numbers expected by the future experiments, namely the SuperB factories and LHCb. Taking the exclusive branching fraction $\mathcal{B}(B^+ \rightarrow K_1^+(1270)\gamma) = 4.3 \times 10^{-5}$ and assuming that the decays $K_1 \rightarrow K\pi\pi$ are by $K^*\pi$ (16%) and $K\rho$ (42%) channels, we obtain the observable branching fraction of $\mathcal{B}(B^+ \rightarrow (K^+\pi^-\pi^+)_{K_1(1270)}\gamma) = 4.3 \times 10^{-5} \times (0.16 * 4/9 + 0.42 * 1/6) \simeq 0.6 \times 10^{-5}$ and $\mathcal{B}(B^+ \rightarrow (K^0\pi^+\pi^0)_{K_1(1270)}\gamma) = 4.3 \times 10^{-5} \times (2 * 0.16 * 2/9 + 0.42 * 1/3) \times 1/3 \simeq 0.3 \times 10^{-5}$

σ_{λ_γ} (statistical error)	$N_{events} = 10^3$	$N_{events} = 10^4$
$B^+ \rightarrow (K^+\pi^-\pi^+)_{K_1(1270)}\gamma$	± 0.18	± 0.06
$B^+ \rightarrow (K^0\pi^+\pi^0)_{K_1(1270)}\gamma$	± 0.12	± 0.04
$B^0 \rightarrow (K^0\pi^+\pi^-)_{K_1(1270)}\gamma$	± 0.18	± 0.06
$B^0 \rightarrow (K^+\pi^-\pi^0)_{K_1(1270)}\gamma$	± 0.12	± 0.04

Table 4.1: Sensitivity study of the polarization measurement with $B \rightarrow K_1(1270)\gamma$ in the DDLR method. Our estimates of the statistical errors to λ_γ in the case of SM (i.e. $\lambda_\gamma = +1$) is shown in this table. The event sample, 10^3 and 10^4 , roughly corresponds to the annual expected events of SuperB and LHCb, respectively. The systematic error due to the uncertainties from these hadronic parameters is not included and has to be carefully studied.

(here the last factor $1/3$ comes from the fact that K^0 is observed as $\pi^+\pi^-$ from the K_S -decay). In order to get a more realistic estimation of the required number of signal events at the future experiments, we take the total efficiency of the reconstruction and selection to be of the order of 0.1% as in the case of $B \rightarrow K^*\gamma$ and $B_s \rightarrow \phi\gamma$ at the LHCb experiment [74] and of the order of 1% at the B -factories² [13]. Then, we obtain the yield of the nominal data taking to be of the order of

$$\begin{aligned} N^{\text{LHCb}}(B^+ \rightarrow (K^+\pi^-\pi^+)_{K_1(1270)}\gamma) &\approx 5 \times 10^3 \\ N^{\text{LHCb}}(B^+ \rightarrow (K^0\pi^+\pi^0)_{K_1(1270)}\gamma) &\approx 2.5 \times 10^3 \end{aligned} \quad (4.5)$$

of signal events for an accumulated luminosity of 2 fb^{-1} at LHCb. The estimated annual yield at SuperB factories with 2 ab^{-1} of integrated luminosity is of the order of

$$\begin{aligned} N^{\text{SuperB}}(B^+ \rightarrow (K^+\pi^-\pi^+)_{K_1(1270)}\gamma) &\approx 1 \times 10^3 \\ N^{\text{SuperB}}(B^+ \rightarrow (K^0\pi^+\pi^0)_{K_1(1270)}\gamma) &\approx 0.5 \times 10^3 \end{aligned} \quad (4.6)$$

events, respectively. Thus, the event sample, 10^3 and 10^4 , studied in Table 4.1, roughly corresponds to the annual expected events of SuperB and LHCb, respectively. It should be noted that the decay modes including a neutral particle are difficult to study at LHCb, i.e. LHCb may well study the first decay channel in Table 4.1 whereas SuperB can study all of them reasonably well.

We want to underline that the above considerations assume a perfect knowledge of the decay observables. In practise, in order to be realistic, the experimental effects, such as measurement errors, backgrounds, reduced acceptance, etc., must be taken into

²This estimate is for the decay modes which contain only charged pion and K in the final state. For the decay modes which contain the neutral mesons, we expect lower sensitivity, in general. The realistic estimate requires more detailed simulations considering the experimental performance.

account. In practice, this can be done by constructing the reduced variable ω from decay distributions convoluted with functions describing the detector effects [14]

$$W'(s_{13}, s_{23}, \cos \theta) = \frac{D(f + \lambda_\gamma g)}{\int D(f + \lambda_\gamma g) ds_{13} ds_{23} d \cos \theta} \quad (4.7)$$

where $D(s_{13}, s_{23}, \cos \theta)$ describes the detector acceptance and efficiency. Thus, the photon polarization parameter can be extracted by comparing the experimental ω -distribution to the corrected theoretical distributions computed with the help of MC methods.

4.2 Theoretical uncertainties of the hadronic model and error on the polarization parameter

Up to now, we have not considered the systematic errors coming from the hadronic parameters. We must reiterate that our hadronic model applied in the above analysis is approximate; it depends on basic assumptions like the non-relativistic approximations inherent to the quark models. It depends also on parameters, some of them being internal to the full quark model, like the meson radii, and one being purely phenomenological, the mixing angle θ_{K_1} (we must note that there exists a correlation between the mixing angle, extracted from the data, and the chosen set of meson radii). It depends also on the set of experimental data which we claim to describe by such models as discussed in Chapter 3.

Let us explain how the errors in the hadronic model generate systematic errors or in another word, theoretical uncertainties, on λ_γ . Starting from the experimental distribution $\frac{d\Gamma}{ds_{13} ds_{23} d \cos \theta}$ we obtain the distribution of ω by calculating ω according to Eq. (2.59). In this formula, the function \mathcal{J} which determines ω for each event is fixed by the hadronic model (let us call it as ω^{model}). Thus, the λ_γ can be determined by knowing the hadronic model as well as the hadronic input parameter describing the K_1 strong decay:

$$\lambda_\gamma^{\text{obs}} = \frac{\langle \omega \rangle^{\text{model}}}{\langle \omega^2 \rangle^{\text{model}}} \quad (4.8)$$

Therefore, if we were using a “wrong” hadronic model, the extracted polarization parameter $\lambda_\gamma^{\text{obs}}$ would be different from the “true” value $\lambda_\gamma^{\text{th}}$. Having the hadronic model which we have applied to explain the K_1 strong decays relatively well as shown in Chapter 3, we would believe the model itself may not be too bad. On the other hand, the input parameters contain some uncertainties. In the following, we will estimate the systematic error on λ_γ caused by the uncertainties in the hadronic input parameters, namely the K_1 mixing angle θ_{K_1} and the “off-set” phase δ_ρ .

Similar to the estimate of the statistical error in the previous section, the errors generally depend on the assumed $\lambda_\gamma^{\text{th}}$ value. In this section, we evaluate the theoretical error in the case of

$$\lambda_\gamma^{\text{th}} = 0.5 \quad (4.9)$$

We chose this value since, as we will see in Chapter 5, our decay channel is most sensitive to the polarization parameter around this value.

4.2.1 Theoretical uncertainty due to the K_1 mixing angle

For the estimation of the uncertainty, related to our determination of the K_1 mixing angle (see previous chapter), we follow the procedure:

- First, we generate the MC sample of the “fake data” according to PDF (2.55) assuming $\lambda_\gamma^{\text{th}} = 0.5$ and fixing the mixing angle at its fitted central value $\theta_{K_1}^{\text{th}} = 60^\circ$. Since both ACCMOR and Belle collaborations observed a non-zero “off-set” phase of the order of 30° , we study the δ_ρ -dependence of λ_γ by testing three MC data sets: generated with $\delta_\rho^{\text{th}} = 0$ (i.e. pure quark model prediction) and $\delta_\rho^{\text{th}} = \pm 30^\circ$.
- Then, we randomly generate θ_{K_1} according to the Gaussian distribution with the mean value of 60° and the standard deviation of 10° .
 - For each generated value of θ_{K_1} we recalculate for each event the value of $\omega(s_{13}^i, s_{23}^i, \cos \theta^i)$ from Eq. (2.59) ($i = 1, \dots, N_{\text{events}}$) using the “fake data” generated on the first step.
 - Having calculated the ω ’s for each event at particular value of the randomly generated θ_{K_1} , we compute the ω -moments (i.e. the average values) and evaluate λ_γ :

$$\lambda_\gamma^{\text{obs}}(\theta_{K_1}) = \frac{\langle \omega \rangle}{\langle \omega^2 \rangle} \quad (4.10)$$

- Finally, we fill the histogram of $\lambda_\gamma^{\text{obs}}$ (Fig. 4.4). This normalized histogram provides us the PDF of the extracted polarization parameter as a function of θ_{K_1} .

One can see from Fig. 4.3 that within one standard deviation region of θ_{K_1} the discrepancy between three analyzed MC data, which were generated using $\delta_\rho^{\text{th}} = 0, \pm 30^\circ$, is rather small. The total deviation of $\lambda_\gamma^{\text{obs}}$ does not exceed 0.2; the calculated values of $\lambda_\gamma^{\text{obs}}$ lie within the interval $[0.3; 0.6]$ (note, the true value is supposed to be $\lambda_\gamma^{\text{th}} = 0.5$).

Allowing the K_1 -mixing angle to be varied according to Gaussian distribution with the central value of 60° and standard deviation of 10° , one finds that the systematic effect on the λ_γ measurement hardly reaches beyond 0.5 ± 0.2 region. We find from Fig. 4.4 that λ_γ is restricted to the following 68% CL intervals:

$$\lambda_\gamma^{\text{obs}} \in \begin{cases} [0.42; 0.60] & (\delta_\rho^{\text{th}} = 0) \\ [0.46; 0.54] & (\delta_\rho^{\text{th}} = -30^\circ) \\ [0.40; 0.64] & (\delta_\rho^{\text{th}} = 30^\circ) \end{cases} \quad (4.11)$$

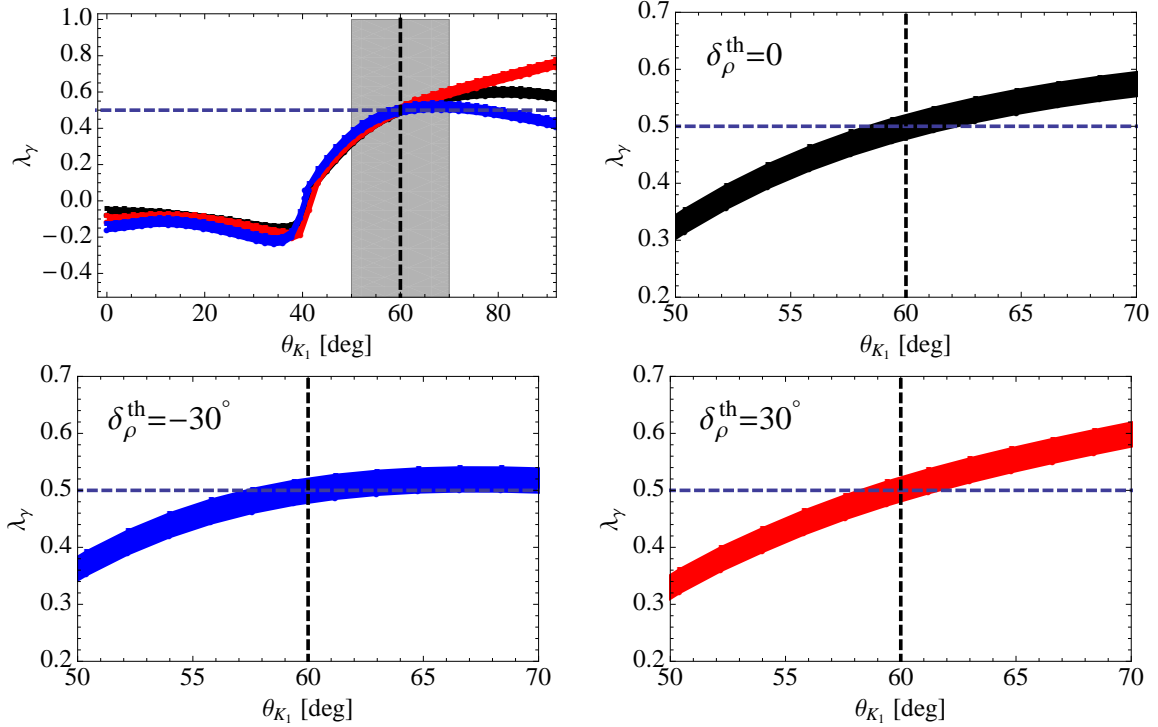


Figure 4.3: The mixing angle θ_{K_1} dependence of λ_γ obtained from the “fake data” which was generated using the fixed values $\lambda_\gamma^{\text{th}} = 0.5$ and $\theta_{K_1}^{\text{th}} = 60^\circ$. Black curve corresponds to the analysis of the MC data generated by using the pure 3P_0 quark model prediction with the “off-set” phase $\delta_\rho^{\text{th}} = 0$, while the blue and red curves correspond to the data generated with $\delta_\rho^{\text{th}} = -30^\circ$ and $\delta_\rho^{\text{th}} = +30^\circ$ respectively.

4.2.2 Theoretical uncertainty due to the “off-set” phase δ_ρ

Estimating the theoretical uncertainties, we take into account that the ACCMOR, BABAR and Belle collaborations observed a non-zero relative phase δ_ρ of the $K\rho$ and $K^*\pi$ channels (see the discussion of Section 3.4.3 of Chapter 3) which is of the order of 30° . Although our 3P_0 quark-pair-creation model predicts no complex phase (but it fixes the relative sign of the amplitudes), we test several “hadronic models” by adding by hands an additional complex “off-set” phase $\delta_\rho = \pm 30^\circ$ to our model prediction. The experimental values of the error to δ_ρ , measured by Belle collaboration [43] are of the order of 7° and surprisingly small error of 1° from the reanalysis of the ACCMOR data by BABAR collaboration [54]. To be conservative, we put the error of 10° in our study.

Similarly to the estimation of the uncertainty due to the K_1 mixing angle, we repeat the procedure to study the “off-set” phase δ_ρ effects:

- We generate the MC sample of the “fake data” according to PDF (2.55) assuming $\lambda_\gamma^{\text{th}} = 0.5$ and fixing the mixing angle at its fitted central value $\theta_{K_1}^{\text{th}} = 60^\circ$. As in

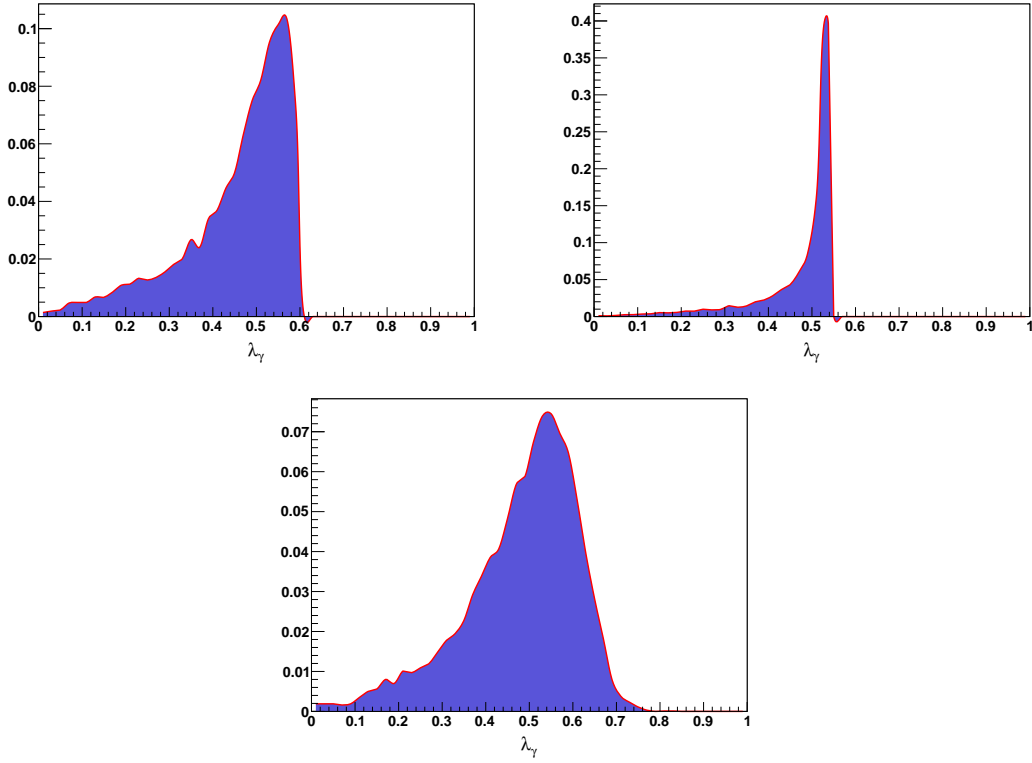


Figure 4.4: Normalized probability density function distribution of $\lambda_\gamma^{\text{obs}}$. The “true” value of the polarization parameter, used for the MC simulation, is set to be $\lambda_\gamma^{\text{th}} = 0.5$. The K_1 mixing angle is varied randomly according to Gaussian distribution with mean value $\theta_{K_1} = 60^\circ$ and standard deviation $\sigma_{\theta_{K_1}} = 10^\circ$. The “off-set” phase δ_ρ is set to zero (top-left), -30° (top-right) and $+30^\circ$ (bottom).

the previous case, we study the δ_ρ dependence of λ_γ by testing three MC data sets: generated with $\delta_\rho^{\text{th}} = 0$ and $\delta_\rho^{\text{th}} = \pm 30^\circ$.

- Then, we randomly generate δ_ρ according to the Gaussian distribution with the mean values $\delta_\rho^{\text{th}} = 0, \pm 30^\circ$ respectively and the standard deviation of 10° .
 - For each generated value of δ_ρ we recalculate for each event the value of $\omega(s_{13}^i, s_{23}^i, \cos \theta^i)$ from Eq. (2.59) ($i = 1, \dots, N_{\text{events}}$) using the “fake data” generated on the first step.
 - Having calculated the ω ’s for each event at particular value of the randomly generated δ_ρ , we compute the ω -moments (i.e. the average values) and evaluate λ_γ :

$$\lambda_\gamma^{\text{obs}}(\delta_\rho) = \frac{\langle \omega \rangle}{\langle \omega^2 \rangle} \quad (4.12)$$

- Finally, we fill the histogram of $\lambda_\gamma^{\text{obs}}$ (Fig. 4.6). This normalized histogram provides

us the PDF of the extracted polarization parameter as a function of δ_ρ .

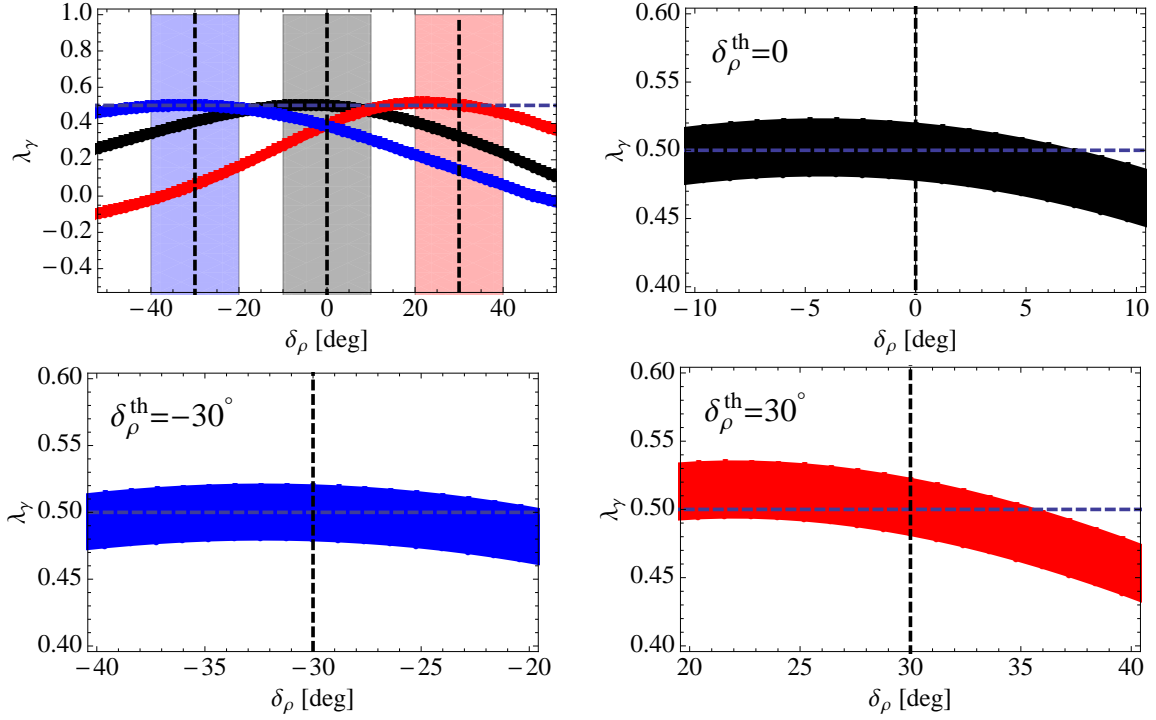


Figure 4.5: The “off-set” phase δ_ρ dependence of λ_γ obtained from the “fake data” which was generated using the fixed values $\lambda_\gamma^{\text{th}} = 0.5$ and $\theta_{K_1}^{\text{th}} = 60^\circ$. Black curve corresponds to the analysis of the MC data generated by using the pure 3P_0 quark model prediction with the “off-set” phase $\delta_\rho^{\text{th}} = 0$, while the blue and red curves correspond to the data generated with $\delta_\rho^{\text{th}} = -30^\circ$ and $\delta_\rho^{\text{th}} = +30^\circ$ respectively. The plots on the right and bottom represent the zoomed parts of gray, blue and red areas which correspond to $\delta_\rho^{\text{th}} \pm 10^\circ$ region.

Allowing δ_ρ to be varied according to Gaussian distribution with the central values $\delta_\rho^{\text{th}} = 0, \pm 30^\circ$ and standard deviation of 10° , one finds that the systematic effect on the λ_γ measurement hardly reaches beyond 5%. We find from Fig. 4.6 that λ_γ is restricted to the following 68% CL intervals:

$$\lambda_\gamma^{\text{obs}} \in \begin{cases} [0.46; 0.50] & (\delta_\rho^{\text{th}} = 0) \\ [0.48; 0.52] & (\delta_\rho^{\text{th}} = -30^\circ) \\ [0.48; 0.52] & (\delta_\rho^{\text{th}} = 30^\circ) \end{cases} \quad (4.13)$$

One has to notice that, allowing θ_{K_1} and δ_ρ vary within $\pm 10^\circ$ intervals around their central values $\theta_{K_1}^{\text{th}}$ and δ_ρ^{th} , there is a large gap between the largest possible value of the computed $\lambda_\gamma^{\text{obs}}$ (~ 0.6) and the SM prediction $\lambda_\gamma^{\text{SM}} \simeq 1$ (see Fig. 4.3 and 4.5). This fact is

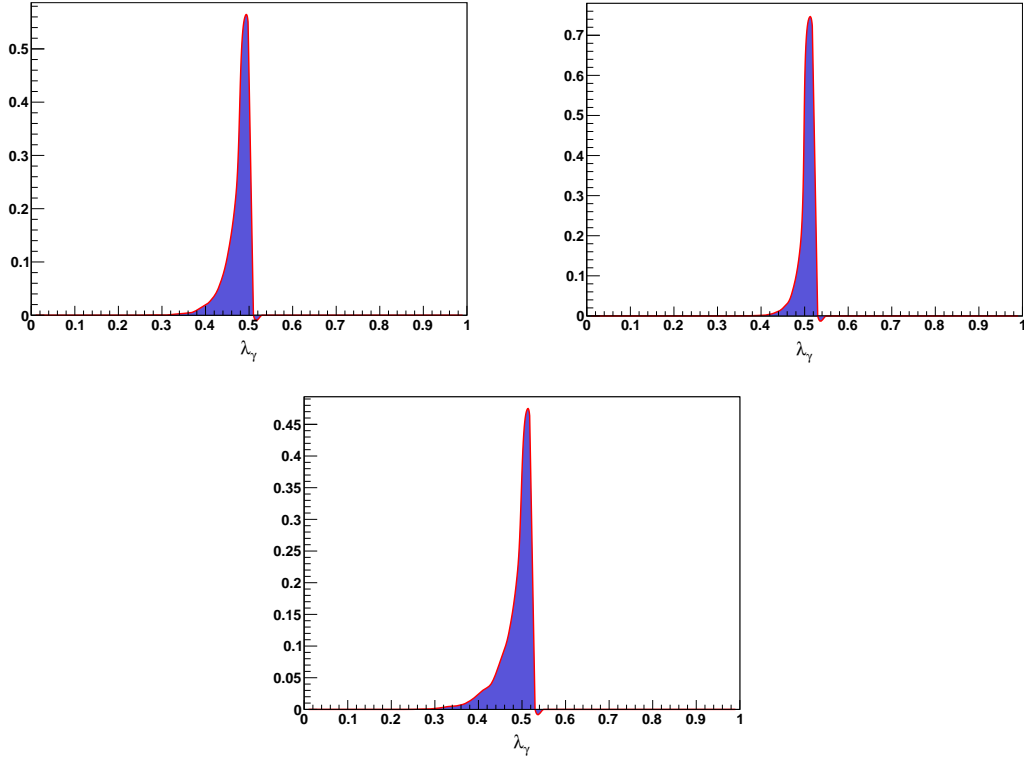


Figure 4.6: Normalized probability density function distribution of $\lambda_\gamma^{\text{obs}}$. The “true” value of polarization parameter, used for the MC simulation, is set to be $\lambda_\gamma^{\text{th}} = 0.5$. The K_1 mixing angle is fixed to be $\theta_{K_1} = 60^\circ$. The “off-set” phase δ_ρ is varied randomly according to Gaussian distribution with standard deviation $\sigma_{\delta_\rho} = 10^\circ$ and mean value equal to zero (top-left), -30° (top-right) and $+30^\circ$ (bottom).

rather encouraging since our study is concentrated on the search of NP beyond the SM with theoretical value of λ_γ sizebly different from $|\lambda_\gamma|^{\text{SM}} \simeq 1$. That implies that λ_γ will never be close to 1 which will allow us to exclude the SM prediction (see Chapter 5 for more details).

4.3 Discussion on the importance of the D -waves and the cut-off

In the end of this chapter we discuss the role of the cut-off β' in the λ_γ determination. Since there is no safe determination of this parameter it is important to emphasize its effect. For demonstration we generate two MC samples of $B^+ \rightarrow K_1^+(1270)\gamma \rightarrow K^+\pi^-\pi^+\gamma$ decays setting $\lambda_\gamma^{\text{th}} = 0.5$ and $\beta' = 3 \text{ GeV}^{-2}$.

- First, we test the case when the D -wave of the $K^*\pi$ channel is neglected in the MC generation (in the following we call it MC^(I)-sample). Then we recalculate ω

for each event setting $\beta' = 0$ and compute the ω -moments. This gives us the value $\lambda_\gamma^{\text{obs}(I)}$ which turns out to be

$$\lambda_\gamma^{\text{obs}(I)} \approx \lambda_\gamma^{\text{th}} = 0.50 \pm 0.02(\text{stat}) \quad (4.14)$$

- After that, we test the case when the D -wave of the $K^*\pi$ channel is taken into account in the MC generation (in the following we call it MC^(II)-sample). Then we recalculate ω for each event setting $\beta' = 0$ and compute the ω -moments. This gives us the value $\lambda_\gamma^{\text{obs}(I)}$ which turns out to be

$$\lambda_\gamma^{\text{obs}(II)} \simeq 0.35 \pm 0.02(\text{stat}) \quad (4.15)$$

i.e. $\delta\lambda_\gamma^{(II)}/\lambda_\gamma^{\text{th}} \simeq 0.3$.

Thus, as already discussed in the previous chapter, we conclude that having only the S -waves the role of the cut-off in our 3P_0 model is not significant. On the other hand, the choice of the cut-off becomes significant for the λ_γ estimation in the presence of the D -waves, which contribution to the interference terms becomes large for large momentum transfer in the quasi-two-body decay $K_1 \rightarrow K^*\pi$.

Chapter 5

Future prospects of the photon polarization measurement

In this chapter, we discuss the sensitivity of the future experiments, namely the SuperB factories and LHCb to λ_γ , using $B \rightarrow K_1(1270)\gamma \rightarrow (K\pi\pi)\gamma$. We also discuss the advantages and disadvantages of our method compared to the other methods of the polarization measurement using the other processes, such as $B \rightarrow K^*e^+e^-$, $B_d \rightarrow K^*\gamma$ and $B_s \rightarrow \phi\gamma$.

5.1 Comparison to the other methods

5.1.1 Up-down asymmetry of GGPR

One of the direct methods of the photon polarization determination methods, proposed by Gronau *et al.* [11, 12], is to study the angular distribution in the $B \rightarrow K\pi\pi\gamma$ decay and extract the polarization parameter λ_γ from the angular correlations among the final hadronic decay products $K\pi\pi$. An observable called up-down asymmetry is defined by Eq. (2.46) and represents the asymmetry between the measured number of signal events with the photons emitted above and below the $K\pi\pi$ decay plane in the K_1 reference frame. Having the theoretical prediction of \mathcal{J} , one can determine λ_γ .

Our conclusion, identical to the one for the angular fit, is that the statistical error on λ_γ is about twice the one in our method (see Fig. 4.2).

5.1.2 The angular analysis of $B \rightarrow K^*\ell^+\ell^-$

From the analysis of the angular distributions of the four-body final state in the $B^0 \rightarrow K^{*0}(\rightarrow K^-\pi^+)\ell^+\ell^-$ decay in the low $\ell^+\ell^-$ invariant mass region one can study various observables that involve different combinations of K^* spin amplitudes [75].

Working in the transversity basis

$$\mathcal{M}_\perp = \frac{\mathcal{M}_R - \mathcal{M}_L}{\sqrt{2}} \quad \mathcal{M}_\parallel = \frac{\mathcal{M}_R + \mathcal{M}_L}{\sqrt{2}} \quad (5.1)$$

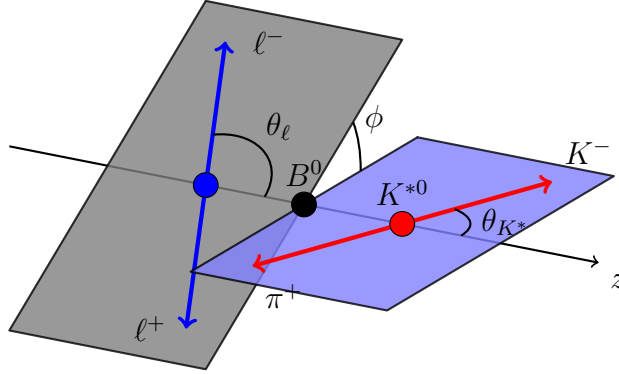


Figure 5.1: Definition of kinematical variables in the $B \rightarrow K^*(\rightarrow K\pi)\ell^+\ell^-$ decay.

one of the most promising observables, that has a small impact from the theoretical uncertainties, are two transverse asymmetries defined as [75, 76]

$$A_T^{(2)}(q^2) \equiv \frac{|\mathcal{M}_\perp|^2 - |\mathcal{M}_\parallel|^2}{|\mathcal{M}_\perp|^2 + |\mathcal{M}_\parallel|^2} = -\frac{2\text{Re}[\mathcal{M}_R\mathcal{M}_L^*]}{|\mathcal{M}_R|^2 + |\mathcal{M}_L|^2} \quad (5.2a)$$

$$A_T^{(im)}(q^2) \equiv \frac{2\text{Im}[\mathcal{M}_\perp\mathcal{M}_\parallel^*]}{|\mathcal{M}_\perp|^2 + |\mathcal{M}_\parallel|^2} = \frac{2\text{Im}[\mathcal{M}_R\mathcal{M}_L^*]}{|\mathcal{M}_R|^2 + |\mathcal{M}_L|^2} \quad (5.2b)$$

which can be experimentally extracted from the differential decay distribution as a function of the dilepton invariant mass q^2 and the angle ϕ between the dilepton-plane ($\ell^+\ell^-$) and the K^* -plane ($K\pi$)¹

$$\frac{d\Gamma}{dq^2 d\phi} = \frac{1}{2\pi} \frac{d\Gamma}{dq^2} \left[1 + \frac{1}{2} F_T(q^2) \left(A_T^{(2)}(q^2) \cos 2\phi + A_T^{(im)}(q^2) \sin 2\phi \right) \right] \quad (5.3)$$

where $F_T(q^2)$ is a fraction of the decay product with transversely polarized K^*

$$F_T(q^2) = \beta_\ell^2 \frac{|\mathcal{M}_\perp|^2 + |\mathcal{M}_\parallel|^2}{d\Gamma/dq^2}, \quad \text{with} \quad \beta_\ell = \sqrt{1 - \frac{4m_\ell^2}{q^2}} \quad (5.4)$$

Note that we assume that in the low $\ell^+\ell^-$ invariant mass region the $\mathcal{O}_{7\gamma}$ is dominating over the semileptonic \mathcal{O}_9 and \mathcal{O}_{10} operators defined as

$$\mathcal{O}_9 = \frac{e^2}{16\pi^2} (\bar{s}_{\alpha L} \gamma^\mu b_{\alpha L}) (\bar{\ell} \gamma_\mu \ell) \quad (5.5a)$$

$$\mathcal{O}_{10} = \frac{e^2}{16\pi^2} (\bar{s}_{\alpha L} \gamma^\mu b_{\alpha L}) (\bar{\ell} \gamma_\mu \gamma_5 \ell) \quad (5.5b)$$

¹The full angular quasi-three-body decay distribution can be found in the original paper by Kruger and Matias [75].

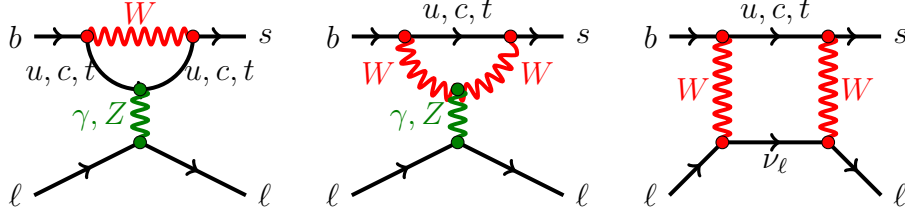


Figure 5.2: Typical diagrams in the full theory, from which the operators $\mathcal{O}_{9,10}$ (5.5) originate.

As a result, the K^* helicity amplitudes $\mathcal{M}_{L,R}$ can be identified with the decay amplitudes of $b \rightarrow s \gamma_{L,R}$ and are related to our polarization parameter as $\lambda_\gamma = \frac{|C_R|^2 - |C_L|^2}{|C_R|^2 + |C_L|^2}$. Therefore, the transverse asymmetry can be written as

$$A_T^{(2)}(0) = \frac{2\text{Re}[C_{7\gamma}^{eff} C_{7\gamma}^{\prime eff*}]}{|C_{7\gamma}^{eff}|^2 + |C_{7\gamma}^{\prime eff}|^2} \quad (5.6a)$$

$$A_T^{(im)}(0) = \frac{2\text{Im}[C_{7\gamma}^{eff} C_{7\gamma}^{\prime eff*}]}{|C_{7\gamma}^{eff}|^2 + |C_{7\gamma}^{\prime eff}|^2} \quad (5.6b)$$

Note that approximation of Eq. (5.6) is strictly valid only at $q^2 = 0$ and away from this point the expression for $A_T^{(2,im)}$ becomes much more complicated due to the non-negligible contributions from the terms proportional to $C_{9,10}^{(l)eff}$. In the SM, these asymmetries vanish due to the m_s/m_b chiral suppression:

$$A_T^{(2)}(0)^{\text{SM}} \simeq 2 \frac{C_{7\gamma}^{\prime eff(\text{SM})}}{C_{7\gamma}^{eff(\text{SM})}} \ll 1 \quad (5.7)$$

$$A_T^{(im)}(0)^{\text{SM}} = 0$$

The new analysis of the $B \rightarrow K^* e^+ e^-$ decay mode by the LHCb collaboration [77] shows that one can expect an annual signal yield of 200 to 250 events for 2 fb^{-1} in this q^2 -region $q^2 < 1 \text{ GeV}$. With this number, it is found that the LHCb can reach a precision of

$$\sigma(A_T^{(2)})_{\text{LHCb}} \sim 0.2 \quad (5.8)$$

corresponding to the statistical error on $|C_{7\gamma}^{\prime eff}/C_{7\gamma}^{eff}|$ to be $\sigma(|C_{7\gamma}^{\prime eff}/C_{7\gamma}^{eff}|) \sim 0.1$ [77].

By comparison we recall the expected number of events for the reaction $B \rightarrow K_1(1270)\gamma$, namely 10^4 signal events at 2 fb^{-1} . A priori it seems much more than the expected number of $B \rightarrow K^* e^+ e^-$.

However, it should be noticed that method of the transverse asymmetry in the semileptonic decay allows the direct measurement of the ratio

$$x \equiv \left| \frac{C_{7\gamma}'^{eff}}{C_{7\gamma}^{eff}} \right| \quad (5.9)$$

while our polarization parameter λ_γ

$$\lambda_\gamma \equiv \frac{|C_R|^2 - |C_L|^2}{|C_R|^2 + |C_L|^2} = \begin{cases} \frac{|x|^2 - 1}{|x|^2 + 1}, & \text{for } \bar{B} - \text{decays} \\ \frac{1 - |x|^2}{|x|^2 + 1}, & \text{for } B - \text{decays} \end{cases} \quad (5.10)$$

is sensitive only to the amplitude ratio square, x^2 . Therefore, the errors of these two methods are to be compared using the following equation:

$$\sigma_x = \frac{(1 + x^2)^2}{4x} \sigma_{\lambda_\gamma} \quad (5.11)$$

which shows that the sensitivity depends on the value of x . We should immediately notice that for verifying the SM value, $x \simeq 0$, the method accessible to x is much more advantageous than the one to x^2 : our λ_γ is in fact insensitive to the SM point (requiring an infinitesimal error). We plot Eq. (5.11) in Fig. 5.3. Let us look at the horizontal line of $\sigma_x = 0.1$, expected error on x with the $B \rightarrow K^* e^+ e^-$ measurement. One can see that our method, which has an estimated statistical error of the λ_γ determination $\sigma_{\lambda_\gamma} \lesssim 0.1$ (see Table 4.1), becomes more advantageous for the measured value of x above $x \sim 0.3$ (i.e. $|\lambda_\gamma| \lesssim 0.8$). Moreover, the same sensitivity to x can be achieved even having a larger error $\sigma_{\lambda_\gamma} \gtrsim 0.1$.

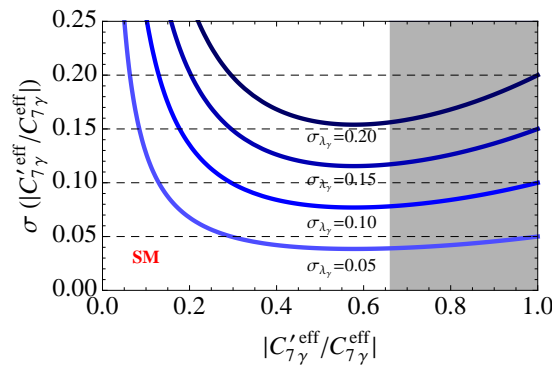


Figure 5.3: Comparison of the sensitivity of the two methods: the one directly determining $x \equiv |C_{7\gamma}'^{eff}/C_{7\gamma}^{eff}|$ and the other one determining x^2 such as our λ_γ (see Eq. (5.11)). One can see that when we assume the same errors for the both methods, a better significance can be obtained with the later method only for $x \gtrsim 0.3$. Gray region is excluded by the measurement of $\mathcal{B}(B \rightarrow X_s \gamma)$.

5.1.3 Methods invoking CP -asymmetries

An indirect method to measure the photon polarization is to study the time-dependent CP -asymmetry in the neutral B_q ($q = d, s$) mesons. For the generic radiative decay of the neutral B_q -meson into any hadronic self-conjugate state f^{CP} , $B_q(t) \rightarrow f^{CP}\gamma$, neglecting direct CP -violation and the small width difference between two B -mesons, the CP -asymmetry is given by [78]²

$$\begin{aligned}\mathcal{A}_{CP}(t) &\equiv \frac{\Gamma(\bar{B}(t) \rightarrow f^{CP}\gamma) - \Gamma(B(t) \rightarrow f^{CP}\gamma)}{\Gamma(\bar{B}(t) \rightarrow f^{CP}\gamma) + \Gamma(B(t) \rightarrow f^{CP}\gamma)} \\ &= -\xi \sin(2\psi) \sin(\phi_M - \phi_L - \phi_R) \sin(\Delta mt) = S_{f^{CP}} \sin(\Delta mt)\end{aligned}\quad (5.12)$$

where $\xi(= \pm 1)$ is the CP -eigenvalue of f^{CP} ; $\sin(2\psi)$ which is defined as

$$\sin(2\psi) \equiv \frac{2|\mathcal{M}_L\mathcal{M}_R|}{|\mathcal{M}_L|^2 + |\mathcal{M}_R|^2}, \quad (5.13)$$

parametrizes the relative amount of left- and right-polarized photons; ϕ_M is one in the $B_q - \bar{B}_q$ mixing; $\phi_{L,R}$ are the relative CP -odd weak phases in the $b \rightarrow s\gamma$ process, i.e.

$$\phi_{L,R} = \sin^{-1} \left(\frac{\text{Im}\mathcal{M}_{L,R}}{|\mathcal{M}_{L,R}|} \right) \quad (5.14)$$

These phases are $\phi_{L,R} = 0$, $\phi_d = 2\beta$, $\phi_s \simeq 0$ in the SM.

Note that here $\mathcal{M}_{L,R}$ denote the amplitudes of the left/right-handed photon emission in $\bar{B} \rightarrow \bar{K}^* \gamma_{L,R}$ respectively. Due the smallness of the right-handed amplitude, the SM predicts

$$\mathcal{A}_{CP}^{\text{SM}}(t) \simeq 0 \quad (5.15)$$

We should emphasise that $\mathcal{A}_{CP}(t)$ measures the combination of $x = |\mathcal{M}_R/\mathcal{M}_L|$ and the CP violating phases $\phi_{M,L,R}$ but not separately. *Thus, the value of x can be obtained from this measurement, only by having the value of the CP violating phases in the $b \rightarrow s\gamma$ as well as the B_q -mixing.*

The current world average for the asymmetry in the $B_d \rightarrow K_S \pi^0 \gamma$ process is [9]

$$S_{K_S \pi^0 \gamma}^{\text{exp}} = -0.15 \pm 0.20 \quad (5.16)$$

which is expected to be improved by the SuperB factory by reducing the error down to 2% [80]. The LHCb experiment is going to measure the $B_s \rightarrow \phi \gamma$ process. Based on the MC simulation for 2 fb^{-1} , it is claimed in [74] that LHCb will be able to measure x with the accuracy of $\sigma_x \simeq 0.1$. Therefore, similar to the case of $B \rightarrow K^* e^+ e^-$, our method using

²In fact, the non-negligible width difference $\Delta\Gamma_s$ in B_s -mesons leads to another measurable observable H which can be also sensitive to the right-handed currents (e.g. see Ref. [79]). This makes the formula (5.12) more complicated in the case of $B_s \rightarrow \phi \gamma$. However, for simplicity, for the present moment we neglect this term proportional to $\sinh(\frac{\Delta\Gamma_s}{2}t)$ but keep in mind its significance.

λ_γ can be more sensitive to $x \gtrsim 0.3$ (see Fig. 5.3). Again, it should be emphasised that although an observation $\mathcal{A}_{CP}(t) \neq 0$ in this method immediately indicates the existence of new physics, a quantitative determination of x is not possible unless we fix the new physics model, namely the CP violating phases in $b \rightarrow s\gamma$ as well as B_q -mixing.

5.2 New physics constraints combining various methods of the polarization determination

In this section we present an example of potential constraints for right-handed current contribution to the photon polarization by combining several possible polarization measurement methods, described in the previous section.

In Fig. 5.4, we show constraints on C_L and C_R , which are currently available or will be available in the future. The x - and y -axes are the real and imaginary parts of

$$x = \frac{C_{7\gamma}'^{eff}}{C_{7\gamma}^{eff}} = \frac{C_{7\gamma}'^{eff(SM)} + C_{7\gamma}'^{eff(NP)}}{C_{7\gamma}^{eff(SM)} + C_{7\gamma}^{eff(NP)}} \approx \frac{C_{7\gamma}'^{eff(NP)}}{C_{7\gamma}^{eff(SM)} + C_{7\gamma}^{eff(NP)}} \quad (5.17)$$

Note that the SM being left-handed photon contribution, the $C_{7\gamma}^{eff(SM)}$ and $C_{7\gamma}^{eff(NP)}$ contributions are coherently added in the denominator. It should be noted therefore, if the new physics contribution to the left-handed photons, i.e. $C_{7\gamma}^{eff(NP)}$, has the sign opposite to the sign of the $C_{7\gamma}^{eff(SM)}$, one could have a relative enhancement of the right-handed amplitude.

Here we put the constraints on the normalized real and imaginary parts of $C_{7\gamma}'^{eff}/C_{7\gamma}^{eff}$ assuming that the new physics affects only the right-handed photon emission amplitude (i.e. $C_{7\gamma}^{eff(NP)} = 0$, $C_{7\gamma}^{eff(SM)} = -0.304$).

First, we use the constraint coming from the measured branching ratio of the inclusive decay [9]

$$\mathcal{B}(B \rightarrow X_s \gamma)_{\text{exp}} = (3.55 \pm 0.24) \times 10^{-4} \quad (5.18)$$

The current bound is represented as white circle in Fig. 5.4. We can see from this figure that there is still a large allowed range for new physics.

The constraint from the time-dependent CP -asymmetry in $B^0 \rightarrow K_S \pi^0 \gamma$ is shown as black lines labeled with values of $S_{K_S \pi^0 \gamma}$ (top-left). We show the bound including $\pm 3\sigma$ error on the current experimental value [9]

$$S_{K_S \pi^0 \gamma}^{\text{exp}} = -0.15 \pm 0.2 \quad (5.19)$$

Note, that the diagonal constraint results from the factor $\sin(2\beta - \phi_R) = (\sin 2\beta \text{Re}[x] - \cos 2\beta \text{Im}[x])/|x|$ in Eq. (5.12).

Similarly, the labeled red circles (top-right) denote the constraints from potential measurement of the polarization parameter λ_γ in the $\bar{B} \rightarrow \bar{K}_1 \gamma$ decay. The labeled

blue and green curves represent the possible constraints from the transverse asymmetries $A_T^{(2)}$ (bottom-left) and $A_T^{(im)}$ (bottom-right) respectively at low dilepton mass in the $\overline{B} \rightarrow \overline{K}^* \ell^+ \ell^-$ decay. The interval of the lines represents the uncertainty for λ_γ and the transverse asymmetries which can be in principle achieved by LHCb:

$$\begin{aligned} \sigma(\lambda_\gamma) &\simeq 0.2 \\ \sigma(A_T^{(2)})_{\text{LHCb}} &\simeq \sigma(A_T^{(im)})_{\text{LHCb}} \simeq 0.2 \end{aligned} \quad (5.20)$$

The Fig. 5.4 shows that combining the measurements of $S_{K_S \pi^0 \gamma}$, λ_λ , $A_T^{(2)}$, $A_T^{(im)}$ will pin down the value of x very precisely in the future.

On Fig. 5.5 (left) we present the confidence level regions for the ratio $C_{7\gamma}'^{eff}/C_{7\gamma}^{eff}$ in the SM for the case when all the polarization quantities $\{S_{K_S \pi^0 \gamma}, \lambda_\gamma, A_T^{(2)}(0), A_T^{(im)}(0)\}$ are measured in future collider experiments. We assume $C_{7\gamma}^{eff}$ to be purely SM-like (i.e. $C_{7\gamma}^{eff(\text{NP})} = 0$, $C_{7\gamma}^{eff(\text{SM})} = -0.304$). Thus the CL represents the exclusion potential of SM points. The figure can simultaneously give an indication that the new physics models whose prediction for $C_{7\gamma}'^{eff}/C_{7\gamma}^{eff}$ stays within the CL circles can not be distinguished from the SM. Let us see the SUSY example. As briefly discussed in Section 1.4.2 the SUSY contribution to $C_{7\gamma}'^{eff}/C_{7\gamma}^{eff}$ in the mass insertion approximation can be given as Eq. (5.21). Then, inputting an example mass of gluino and squark as $m_{\tilde{g}} \simeq m_{\tilde{q}} = 500$ GeV, using Eq. (1.56) we find [81]

$$\begin{aligned} \frac{C_{7\gamma}'^{eff(\text{SUSY})}}{C_{7\gamma}^{eff(\text{SM})}} &= (134 + 2.7i)(\delta_{RL}^d)_{23} + (0.28 + 0.0057i)(\delta_{RR}^d)_{23} \\ &+ (80 + 1.6i)(\delta_{RL}^d)_{33}(\delta_{RR}^d)_{23} \end{aligned} \quad (5.21)$$

Recall, the large value in the coefficient of the first term in the numerator comes from the chiral-enhancement as discussed in subsection 1.4.2. We need to fix the SUSY breaking model in order to find the value of the mass insertions. Let us give a few examples (see Ref. [81] and references therein).

- **SUSY SO(10)**

$$\begin{aligned} (\delta_{RR}^d)_{23} &\simeq 0.5 + 0.5i \\ (\delta_{LL,LR,RL}^d)_{23} &\simeq 0 \end{aligned} \quad (5.22)$$

- **mSUGRA**

$$\begin{aligned} (\delta_{LL}^d)_{23} &\simeq 0.009 + 0.001i \\ (\delta_{RR,LR,RL}^d)_{23} &\simeq 0 \end{aligned} \quad (5.23)$$

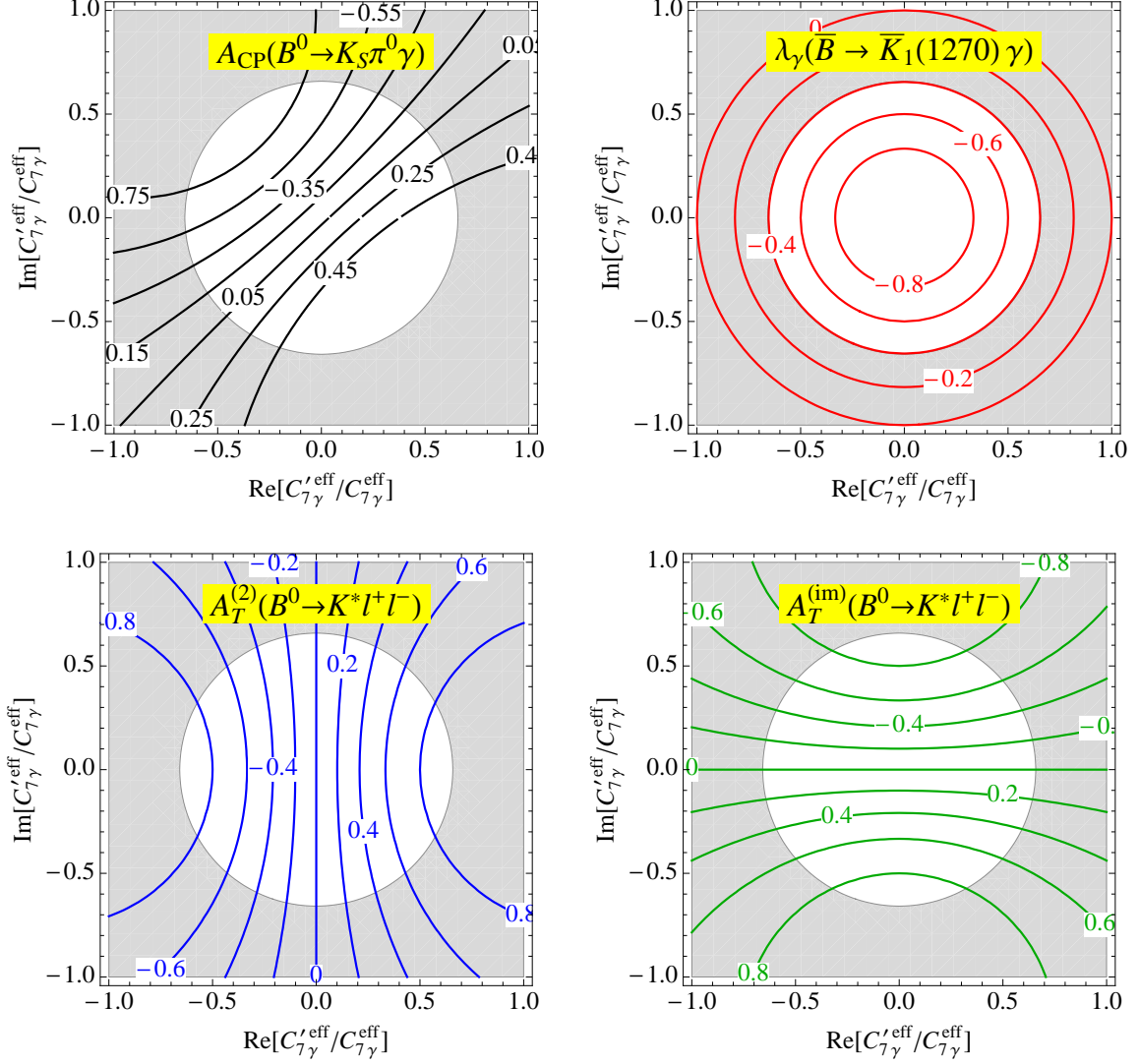


Figure 5.4: Constraints on the normalized real and imaginary parts of $C'_{\gamma\gamma}/C_{\gamma\gamma}^{eff}$ assuming $C_{\gamma\gamma}^{eff}$ to be purely SM-like (i.e. $C_{\gamma\gamma}^{eff(NP)} = 0$, $C_{\gamma\gamma}^{eff(SM)} = -0.304$). The white circle represents the constraint coming from the measured branching ratio $\mathcal{B}(B \rightarrow X_s \gamma)$. The constraint from the time-dependent CP asymmetry of $B^0 \rightarrow K_S \pi^0 \gamma$ is shown as black lines labeled with values of $S_{K_S \pi^0 \gamma}$ (top-left). Note that the current experimental bound is $S_{K_S \pi^0 \gamma}^{\text{exp}} = -0.15 \pm 0.2$ (we show our result in a range including $\pm 3\sigma$ error). Similarly, the labeled red circles (top right) denote the constraints from potential measurement of the polarization parameter λ_γ in the $\bar{B} \rightarrow \bar{K}_1 \gamma$ decay. The labeled blue and green curves represent the possible constraints from the transverse asymmetries $A_T^{(2)}$ (bottom-left) and $A_T^{(im)}$ (bottom-right) respectively at low dilepton mass in the $\bar{B} \rightarrow \bar{K}^* \ell^+ \ell^-$ decay.

- **Hermitian Yukawa**

$$\begin{aligned}(\delta_{RL}^d)_{23} &\simeq (\delta_{LR}^d)_{23} \simeq 0.002 + 0.005i \\ (\delta_{LL,RR}^d)_{23} &\simeq 0\end{aligned}\tag{5.24}$$

We plot the resulting x values from these models in Fig. 5.5. One can see that the Minimal Supergravity (mSUGRA) model is perfectly consistent with the SM prediction which is supposed to be centered at zero. Although the SUSY SO(10) model prediction is beyond the SM point, it is located within our predicted SM-like 99%CL bound³. The model with Hermitian Yukawa couplings is relatively far beyond of our predicted SM-like CL bounds. However, one can observe that all three considered MSSM models are still consistent with the current experimental bounds from $\mathcal{B}(B \rightarrow X_s \gamma)$ and $S_{K_S \pi^0 \gamma}$ which will be improved by LHCb and SuperB experiments.

³One has to note that this is an *example* and that the other set of SUSY parameters can make the point on the plot to be beyond the SM allowed region. This aspect requires a more detailed study and it has not been done in this thesis.

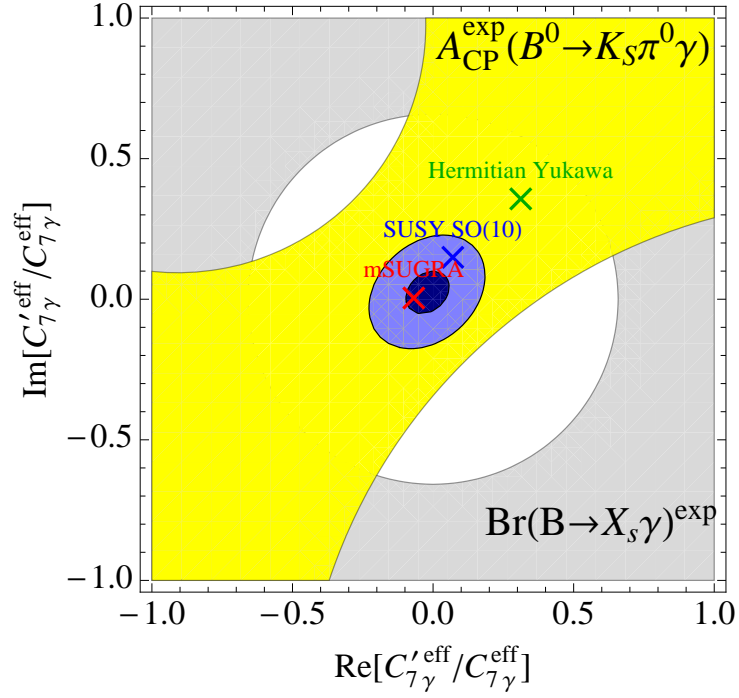


Figure 5.5: Dark and light blue regions represent the CL (68% and 99% respectively) regions for the ratio $C'_{7\gamma}/C_{7\gamma}^{eff}$ in the SM assuming $C_{7\gamma}^{eff}$ to be purely SM-like (i.e. $C_{7\gamma}^{eff(NP)} = 0$, $C_{7\gamma}^{eff(SM)} = -0.304$). The region bounds are obtained from the χ^2 fit of the constraints of the measured time-dependent CP -asymmetry in $B^0 \rightarrow K_S \pi^0 \gamma$ ($S_{K_S \pi^0 \gamma}^{exp} = -0.15 \pm 0.2$), the transverse asymmetries in $\bar{B} \rightarrow \bar{K}^* \ell^+ \ell^-$ (in our study we put the central values of $A_T^{(2)}$ and $A_T^{(im)}$ to be zero as predicted by the SM, while the errors are assumed to be $\sigma(A_T^{(2)}) = \sigma(A_T^{(im)}) = 0.2$) and from the λ_γ potential measurement in $\bar{B} \rightarrow \bar{K}_1 \gamma$ (we assume $\lambda_\gamma^{SM} = -1.0 \pm 0.2(\text{syst.})$). Gray region is excluded by the $\mathcal{B}(B \rightarrow X_s \gamma)$ measurement. Yellow region represents the $\pm 3\sigma$ region allowed by the current constraint from the time-dependent CP -asymmetry in $B \rightarrow K_S \pi^0 \gamma$.

Chapter 6

Conclusions

6.1 The general method of Gronau *et al.*: a critical view

- Although we are quite aware of the very important work accumulated in the study of competing methods since its proposal in 2002, we have estimated that the method, proposed by Gronau *et al.* for measuring the photon polarisation in FCNC through the $B \rightarrow K_{\text{res}}\gamma \rightarrow K\pi\pi\gamma$ processes, has several interests and advantages and deserves further investigation and update. A good news has been the observation of the unexpected large rate for the transition $B \rightarrow K_1(1270)\gamma$ in 2005, by Belle collaboration. Additional information has been provided in the study of $B \rightarrow K\rho\gamma$ time-dependent CP -asymmetry by the same collaboration. Moreover, in view of the importance of the issue of the structure of FCNC, we feel that it is worth exploring and exploiting several complementary approaches. Having worked and discussed a good deal, we conclude that the application of the method is appreciably more complex than expected first by Gronau *et al.*.

Nevertheless, it appears still worth to emphasize first its advantages. The advantage of the method of Gronau *et al.* for determining the photon polarization can be summarized as follows. The method is very simple in principle. It relies on the study of the process $B \rightarrow K_{\text{res}}\gamma \rightarrow K\pi\pi\gamma$ and allows to extract the photon polarisation by fitting one normalized angular distribution $a(1 + \cos^2 \theta) + P_\gamma b \cos \theta$ where P_γ is the photon polarisation parameter defined as

$$P_\gamma \equiv \frac{|\Gamma(\bar{B} \rightarrow \bar{K}\pi\pi\gamma_R)|^2 - |\Gamma(\bar{B} \rightarrow \bar{K}\pi\pi\gamma_L)|^2}{|\Gamma(\bar{B} \rightarrow \bar{K}\pi\pi\gamma_R)|^2 + |\Gamma(\bar{B} \rightarrow \bar{K}\pi\pi\gamma_L)|^2} \quad (6.1)$$

and a, b are purely hadronic quantities and functions of the Dalitz plot variables, characterising the three-body decays of the K_{res} -resonances (note that this implies the sum over all possible K_{res} -states, e.g. $K_1(1270/1400)$, $K^*(1410)$, $K_2^*(1430)$, that decay to the common $\bar{K}\pi\pi$ final state). A detailed knowledge of a and b allows the precise determination of P_γ .

In the case when one can isolate one of the K_{res} 's, the photon polarisation is directly equal to the parameter characterising the electroweak interaction mixture of abnormal (right-handed) helicity in the effective Hamiltonian, λ_γ , due to the cancellation of the common form factor in the ratio (6.1):

$$P_\gamma = \lambda_\gamma \quad (\text{for one isolated resonance}) \quad (6.2)$$

Therefore, the problem of the $B \rightarrow K_1$ transition and the further K_1 -decays description is reduced to a purely strong interaction problem of the K_1 -decays, which have already been studied in detail in the literature.

On the other hand, the method has encountered some drawbacks and difficulties:

- In particular, it must be said that the photon polarisation parameter λ_γ is quadratic in the helicity amplitudes. Then, in order to observe the “abnormal” helicity (which could be an indication of physics beyond the SM), C_R/C_L should be large, i.e. $|\lambda_\gamma|$ must be significantly different from the SM-value, or the accuracy of the λ_γ -measurement has to be good.
- Although it is quite simple in its principle, the method is revealed to be more complex in practice, because one has to know the strong decays in a rather detailed way. In particular, the relative phases of various intermediate decay channels and the relevant quantity $\text{Im}[\vec{n} \cdot (\vec{\mathcal{J}} \times \vec{\mathcal{J}}^*)]$ are very important.
- The fact that the $K_1(1270)$ -resonance, not considered by Gronau *et al.*, is produced with a rather large branching ratio, seems on the one hand quite positive, since it allows to have a relatively large statistics. But on the other hand, it complicates the analysis since the pattern of decays of this resonance is much more complex.

In this thesis, we have tried to face this situation by two main contributions :

1. Improving the accuracy of the polarization parameter determination by recourse to the DDLR method, developed by Davier *et al.*, which is precisely well suited for the problem at hand due to the linear dependence on λ_γ of the decay distribution. It amounts to determine optimally λ_γ by exploiting not only the pure angular distribution, but also the additional information from the whole Dalitz plot and without having to perform a complex multidimensional fit.
2. Improving also as much as possible the treatment of the strong K_1 -decays by introducing the input of quark models into our knowledge of the K_1 -decays. We concentrate on the $B \rightarrow K_1(1270)\gamma$ decay. We leave aside for the moment a possible $K_1(1400)\gamma$ -contribution, which seems to be small according to the observation of Belle collaboration and to our estimations. Yet, in the strong interaction decay analysis, we must address the full system of the two resonances because of the well known phenomenon of mixing between the two states, and since, in the main experiments (i.e. in diffractive production), they are strongly entangled.

Then, we applied this improved knowledge of the hadronic side to estimate the errors (statistical as well as theoretical ones) on the polarisation measurement.

6.2 Improvement of statistical errors by the DDLR method

The fact that the normalised distribution of the number of events depends linearly on the polarisation parameter allows us to use the DDLR method. This has the great advantage of reducing the multidimensional problem of fitting the polarisation over the whole Dalitz plot and angle θ to a simple one-dimensional fit of one variable ω defined in our case by Eq. (2.59). We have given an explicit expression for the new ω -distribution and demonstrated that the polarisation is exactly given by ratios of two moments of the distribution:

$$\lambda_\gamma = \frac{\langle \omega^{2n-1} \rangle}{\langle \omega^{2n} \rangle} \quad (6.3)$$

with arbitrary $n \geq 1$.

At the present moment, there is no data available. However, we can discuss the method by generating “fake” data with an assumed value of the polarisation, and compare this one with the one deduced from the moments. The statistical error can also be evaluated either by an explicit formula (which is very complex and, in practise, is unknown) or by random sampling from the dispersion of the moments ratio using the MC simulation. Then, a strong conclusion is that **the statistical error is reduced by a factor 2 with respect to the method of Gronau *et al.***

6.3 The treatment of the full system of the K_1 -decays

6.3.1 Critical view of the experimental analyses of the K_1 -system of strong decays

Not only the strong decay pattern of $K_1(1270)$ is quite complex, but, not surprisingly, it is then difficult to analyze the whole system experimentally. In spite of many efforts, we have found that much information is missing and that certain weaknesses may be suspected in various analyses (which imply many theoretical assumptions, like the prescription of Nauenberg and Pais for the quasi-two-body phase space). In addition, the interpretation of width in the presence of nearby quasi-two body thresholds (like in $K_1(1270) \rightarrow K\rho$) is delicate.

6.3.2 A semi-theoretical treatment of the K_1 -system of strong decays

In view of this, it has appeared necessary to assess the present experimental studies by a more theoretical treatment. In lack of more fundamental treatments, we have resorted to the quark model approach, which, although approximate, is at the basis of our whole understanding of spectroscopy. The 3P_0 quark-pair-creation model for decays presents the advantage of handling in a simple way the whole set of $L = 1$ decays. On the other hand, experimental inputs are still required to fix the crucial K_1 mixing angle. We have determined this angle by comparing our theoretical predictions for the partial widths and the ones deduced from the K -matrix formalism.

6.4 Theoretical errors on the polarisation measurement

It appears that the polarisation measurement through the ω -moments will be sensitive to several errors in the modelling of the hadronic K_1 -decays, which will change the value of the moments corresponding to a given λ_γ . These errors include those affecting the relative phase of the $K\rho/K^*\pi$ -amplitudes ratio, the magnitude and phase of the D -waves, and the damping factor. After fixing the parameters from our theoretical considerations, we try to estimate some remaining uncertainties: in particular, the one coming from the uncertainty on the K_1 mixing angle, and the effect of a possible “off-set” phase in strong decay S -waves (which are not deducible from theory, but apparently present in data).

6.5 The need for improvements of our experimental knowledge and some future prospects

From our whole discussion, it appears clearly that an important improvement of our experimental knowledge on the strong K_1 -decays is required in order to obtain a better accuracy in the photon polarisation determination.

Indeed, we have observed a sensitivity of λ_γ to various model parameters, whose values, in our mixed approach, depend both on certain experimental data and on the theoretical model of the decays. It is important to recall that there is no fundamental theoretical treatment, and that our theoretical model is based on quark models, which being much valuable contains essential approximations, i.e. ones that can not be improved systematically. In addition, the quark model does not provide any prediction for the decays involving non- $q\bar{q}$ intermediate state like $\kappa(800)$ or purely continuum $K\pi\pi$ -state.

Then it seems that progress should come mainly from better and more complete determination of the magnitude and phases of the various couplings by experiment. Certainly, the experiments with production of K_1 by strong interaction scattering (as the old ones of SLAC and ACCMOR) have much larger statistics for decays involving K_1 than present

at B -factories. Yet there is little prospect of them being redone, and they have also their own weakness in the fact that the production process is rather complex. There is some hope that a new detailed study could be made in B -decays. Encouraging examples have been coming from both BABAR and Belle experiments. A new study of $B \rightarrow K_1 \psi$ with angular analysis in the angle θ could yield directly the crucial quantity $Im[\vec{n} \cdot (\vec{\mathcal{J}} \times \vec{\mathcal{J}}^*)]$ up to a multiplicative constant. The analyses could be guided by our semi-theoretical and approximate investigation, which, for instance, emphasizes the need to take into account the D -waves.

Appendix A

Renormalization and running of the Wilson coefficients

In this appendix we present a brief description of general concepts of the renormalization group evolution and scale running of the Wilson coefficients following the lectures of A. Buras [16].

A.1 Renormalization and operator mixing

One has to note that the Wilson coefficients do not depend only on the scale μ like the usual gauge couplings but also on the renormalization scheme used for the local operators. It is not surprising that the local operators \mathcal{O}_i , as the usual vertices in the field theory, must be renormalized when the quantum QED and QCD corrections are taken into account. Hence, the matrix elements $\langle \mathcal{O}_i(\mu) \rangle$ are renormalization scheme dependent and this dependence (as well as the scale μ dependence) must be cancelled by the one of $C_i(\mu)$ since the physical amplitudes must be scheme independent.

The renormalization procedure is the process of relating the unphysical (bare) and physical (renormalized) parameters like couplings or masses and rewrite the observables as functions of the physical quantities. In the SM, which is a renormalized theory, all divergences can be absorbed into the renormalization constants Z and can be removed by introducing a finite number of counterterms in the Lagrangian. In general, one can have many different local operators \mathcal{O}_i with the same quantum numbers which can mix under renormalization. In this case the relationship between bare and renormalized operators has the form

$$\mathcal{O}_i^{(bare)} = Z_{ij} \mathcal{O}_j \tag{A.1}$$

Since the bare operator is μ independent

$$0 = \mu \frac{d}{d\mu} \mathcal{O}_i^{(bare)} = \left(\mu \frac{d}{d\mu} Z_{ij} \right) \mathcal{O}_j + Z_{ij} \left(\mu \frac{d}{d\mu} \mathcal{O}_j \right) \tag{A.2}$$

what gives

$$\mu \frac{d}{d\mu} \mathcal{O}_j = -\gamma_{ji} \mathcal{O}_i \quad (\text{A.3})$$

where

$$\gamma_{ji} = Z_{jk}^{-1} \left(\mu \frac{d}{d\mu} Z_{ki} \right) \quad (\text{A.4})$$

Here γ_{ij} is called the anomalous dimension matrix. It can be calculated order by order in the coupling constant from the renormalization constants Z .

Due to the renormalization group invariance, the physical amplitudes must be independent on the scales μ at which the heavy quark masses are defined or the other heavy particles are integrated out. The scale independence of the weak Hamiltonian implies that

$$\left(\mu \frac{d}{d\mu} C_j \right) \mathcal{O}_j - C_j \gamma_{ji} \mathcal{O}_i = 0 \quad (\text{A.5})$$

This gives us the Renormalization Group Equation (RGE) for the Wilson coefficients:

$$\mu \frac{d}{d\mu} C_i = \gamma_{ji} C_j \quad (\text{A.6})$$

The solution of this equation is

$$C_i(\mu) = \exp \left[\int_{g(M_W)}^{g(\mu)} \frac{\gamma^T}{\beta(g)} dg \right]_{ij} C_j(M_W) \quad (\text{A.7})$$

where the β -function that describes the running of the couplings constant is defined in the standard way:

$$\beta(g) = \mu \frac{dg}{d\mu} \quad (\text{A.8})$$

A.2 $b \rightarrow s\gamma$ at Leading Logarithmic Approximation

The renormalization matrix Z and, consequently, the anomalous dimension matrix can be perturbatively expanded in powers of α_s :

$$Z = 1 + \frac{\alpha_s}{4\pi} Z^{(1)} + \frac{\alpha_s^2}{4\pi} Z^{(2)} + \dots \quad (\text{A.9a})$$

$$\gamma(\alpha_s) = \gamma^{(0)} \frac{\alpha_s}{4\pi} + \gamma^{(1)} \left(\frac{\alpha_s}{4\pi} \right)^2 + \dots \quad (\text{A.9b})$$

The 6×6 submatrix of $\gamma^{(0)}$ describing mixing of $\mathcal{O}_1, \dots, \mathcal{O}_6$ and the 2×2 submatrix for $(\mathcal{O}_{7\gamma}, \mathcal{O}_{7g})$ follow from one-loop computations. On the other hand, the entries in the anomalous dimension matrix representing the mixing between $(\mathcal{O}_1, \dots, \mathcal{O}_6)$ and $(\mathcal{O}_{7\gamma}, \mathcal{O}_{7g})$

sectors at leading order appears at two-loop level. Consequently, to calculate the coefficients $C_7(\mu_b)$ and $C_8(\mu_b)$ at leading logarithmic approximation, two-loop computations of $O(e g_s^2)$ and $O(g_s^3)$ are required. Going beyond the leading order, the two-loop mixing between $\mathcal{O}_{7\gamma}$ and \mathcal{O}_{7g} plus the three-loop mixing between these two sets of operators enter matrix $\gamma^{(1)}$ in the next-to-leading order analysis.

Expanding Eq. (A.7) in terms of α_s , the Wilson coefficients can be written as

$$C_j(\mu) = C_j^{(0)}(\mu) + \frac{\alpha_s(\mu)}{4\pi} C_j^{(1)}(\mu) + \dots \quad (\text{A.10})$$

Due to the mixing of the operators it is convenient to introduce the so-called “effective coefficients” for the operators \mathcal{O}_7 and \mathcal{O}_8 . One observes at leading order that in any regularization scheme one can write the one-loop matrix elements of the four-quark operators ($\mathcal{O}_1, \dots, \mathcal{O}_6$) can be written as

$$\langle s\gamma | \mathcal{O}_i | b \rangle_{\text{one-loop}} = y_i \langle s\gamma | \mathcal{O}_{7\gamma} | b \rangle_{\text{tree}} \quad (i = 1, \dots, 6) \quad (\text{A.11a})$$

$$\langle sg | \mathcal{O}_i | b \rangle_{\text{one-loop}} = z_i \langle sg | \mathcal{O}_{8g} | b \rangle_{\text{tree}} \quad (i = 1, \dots, 6) \quad (\text{A.11b})$$

with y_i, z_i coming from purely short-distance part of the one-loop diagrams. The vectors \vec{y} and \vec{z} can be considered as the effect of mixing of order α_s^0 among $\mathcal{O}_{1,\dots,6}$ and magnetic operators. In the naive dimensional regularization (NDR) scheme they are $\vec{y} = (0, 0, 0, 0, -1/3, -1)$ and $\vec{z} = (0, 0, 0, 0, 1, 0)$. Defining the “effective coefficients” as

$$\begin{aligned} C_7^{(0)eff}(\mu_b) &= C_7^{(0)}(\mu_b) + \sum_{i=1}^6 y_i C_i^{(0)}(\mu_b) \\ C_8^{(0)eff}(\mu_b) &= C_8^{(0)}(\mu_b) + \sum_{i=1}^6 z_i C_i^{(0)}(\mu_b) \end{aligned} \quad (\text{A.12})$$

the amplitude of the inclusive $b \rightarrow s\gamma$ process will be of the form

$$\mathcal{M}(b \rightarrow s\gamma)_{\text{LO}} = -\frac{4G_F}{\sqrt{2}} V_{tb} V_{ts}^* C_{7\gamma}^{(0)eff}(\mu_b) \langle s\gamma | \mathcal{O}_{7\gamma} | b \rangle_{\text{tree}} \quad (\text{A.13})$$

One has to note that the regularization scheme dependence of $C_i(\mu)$ is cancelled by a corresponding regularization scheme dependence in $\gamma^{(0)}$. Consequently, the quantity $C_{7\gamma}^{eff}(\mu)$ is scheme-independent.

The evolution of $C_i^{(0)eff}(\mu)$

$$\mu \frac{d}{d\mu} C_i^{(0)eff}(\mu) = \frac{\alpha_s}{4\pi} \gamma_{ji}^{(0)eff} C_j^{(0)eff}(\mu) \quad (\text{A.14})$$

is driven by the effective anomalous dimension matrix

$$\gamma_{ji}^{(0)eff} = \begin{cases} \gamma_{j7}^{(0)} + \sum_{k=1}^6 y_k \gamma_{jk}^{(0)} - y_j \gamma_{77}^{(0)} - z_j \gamma_{87}^{(0)} & i = 7, \quad j = 1, \dots, 6 \\ \gamma_{j8}^{(0)} + \sum_{k=1}^6 z_k \gamma_{jk}^{(0)} - z_j \gamma_{88}^{(0)} & i = 8, \quad j = 1, \dots, 6 \\ \gamma_{ji}^{(0)} & \text{otherwise} \end{cases} \quad (\text{A.15})$$

At LO the anomalous dimension 8×8 matrix for the $\mathcal{O}_1, \dots, \mathcal{O}_8$ operator basis is given by [16]

$$\gamma_{ji}^{(0)} = \begin{pmatrix} -2 & 6 & 0 & 0 & 0 & 0 & 0 & 3 \\ 6 & -2 & -\frac{2}{9} & \frac{2}{3} & -\frac{2}{9} & \frac{2}{3} & \frac{416}{81} & \frac{70}{27} \\ 0 & 0 & -\frac{22}{9} & \frac{22}{3} & -\frac{4}{9} & \frac{4}{3} & -\frac{464}{81} & \frac{140}{27} + 3f \\ 0 & 0 & 6 - \frac{2f}{9} & -2 + \frac{2f}{3} & -\frac{2f}{9} & \frac{2f}{3} & \frac{416}{81}u - \frac{232}{81}d & 6 + \frac{70}{27}f \\ 0 & 0 & 0 & 0 & 2 & -6 & \frac{32}{9} & -\frac{14}{3} - 3f \\ 0 & 0 & -\frac{2f}{9} & \frac{2f}{3} & -\frac{2f}{9} & -16 + \frac{2f}{3} & \frac{200}{81}d - \frac{448}{81}u & -4 - \frac{119}{27}f \\ 0 & 0 & 0 & 0 & 0 & 0 & \frac{32}{9} & 0 \\ 0 & 0 & 0 & 0 & 0 & 0 & -\frac{32}{9} & \frac{28}{3} \end{pmatrix} \quad (\text{A.16})$$

where u and d are the numbers of active up- and down-type quark flavours at a certain scale μ respectively and $f = u + d$.

The initial conditions for the coefficients at a large scale μ_W are obtained from a matching of the effective and the full theory. In the SM $C_i^{(0)}(\mu_W)$ read as follows:

$$\begin{aligned} C_{1,3,\dots,6}^{(0)}(\mu_W) &= 0 \\ C_2^{(0)}(\mu_W) &= 1 \\ C_7^{(0)}(\mu_W) &= -\frac{1}{2}D'_0(x_t) \\ C_8^{(0)}(\mu_W) &= -\frac{1}{2}E'_0(x_t) \end{aligned} \quad (\text{A.17})$$

where the one-loop functions $D'_0(x_t)$ and $E'_0(x_t)$ have the standard definition [15]

$$\begin{aligned} D'_0(x_t) &= -\frac{x_t^2(3x_t - 2)}{2(x_t - 1)^4} \ln x_t + \frac{x_t(8x_t^2 + 5x_t - 7)}{12(x_t - 1)^3} \\ E'_0(x_t) &= \frac{3x_t^2}{2(x_t - 1)^4} \ln x_t + \frac{x_t(x_t^2 - 5x_t - 2)}{4(x_t - 1)^3} \end{aligned} \quad (\text{A.18})$$

with $x_t = m_t^2/M_W^2$.

i	1	2	3	4	5	6	7	8
a_i	$\frac{14}{23}$	$\frac{16}{23}$	$\frac{6}{23}$	$-\frac{12}{23}$	0.4086	-0.4230	-0.8994	0.1456
h_i	2.2996	-1.0880	$-\frac{3}{7}$	$-\frac{1}{14}$	-0.6494	-0.0380	-0.0185	-0.0057
\bar{h}_i	0.8623	0	0	0	-0.9135	0.0873	-0.0571	0.0209
k_{1i}	0	0	$\frac{1}{2}$	$-\frac{1}{2}$	0	0	0	0
k_{2i}	0	0	$\frac{1}{2}$	$\frac{1}{2}$	0	0	0	0
k_{3i}	0	0	$-\frac{1}{14}$	$\frac{1}{6}$	0.0510	-0.1403	-0.0113	0.0054
k_{4i}	0	0	$-\frac{1}{14}$	$-\frac{1}{6}$	0.0984	0.1214	0.0156	0.0026
k_{5i}	0	0	0	0	-0.0397	0.0117	-0.0025	0.0304
k_{6i}	0	0	0	0	0.0335	0.0239	-0.0462	-0.0112

Table A.1: “Magic numbers” taken from Ref. [16].

Finally, the leading order results for Wilson coefficients of all operators that are present in the effective Hamiltonian can be written in analytic form [16] as follows:

$$C_j^{(0)}(\mu_b) = \sum_{i=1}^8 k_{ji} \eta^{a_i} \quad (j = 1, \dots, 6) \quad (\text{A.19a})$$

$$C_7^{(0)eff}(\mu_b) = \eta^{\frac{16}{23}} C_7^{(0)}(\mu_W) + \frac{8}{3} \left(\eta^{\frac{14}{23}} - \eta^{\frac{16}{23}} \right) C_8^{(0)}(\mu_W) + C_2^{(0)} \sum_{i=1}^8 h_i \eta^{a_i} \quad (\text{A.19b})$$

$$C_8^{(0)eff}(\mu_b) = \eta^{\frac{14}{23}} C_8^{(0)}(\mu_W) + C_2^{(0)} \sum_{i=1}^8 \bar{h}_i \eta^{a_i} \quad (\text{A.19c})$$

where $\eta = \frac{\alpha_s(\mu_W)}{\alpha_s(\mu_b)}$. The numbers a_i , k_{ji} , h_i and \bar{h}_i are given in Table A.1. It is useful to write α_s at LO as

$$\alpha_s(\mu_b) = \frac{\alpha_s(M_Z)}{1 - \beta_0 \frac{\alpha_s(M_Z)}{2\pi} \ln \left(\frac{M_Z}{\mu_b} \right)} \quad (\text{A.20})$$

Appendix B

Watson's theorem

Final state interactions play an important role in the test of CP and T violation. A test for T violation is to observe a T -odd correlation of the form of triple product like $\vec{p}_1 \cdot [\vec{p}_2 \times \vec{p}_3]$. In the contrast with the partial decay rate difference which is used to test CP violation a T -odd correlation can be produced by by final state interactions even if the T invariance is not violated. Watson's theorem that relates the final state interaction phase of the decay products and the elastic scattering phase, can be illustrated on the following example.

The amplitude for the decay $A \rightarrow B + C$ induced by weak interactions Hamiltonian can be written as [36]

$$\langle BC; \text{out} | \mathcal{H}_{weak} | A; \text{in} \rangle = A e^{i\delta_s} \quad (\text{B.1})$$

where δ_s is the phase generated by strong interactions. If T is conserved A is real.

Assuming that

- the weak Hamiltonian is invariant under the time-reversal:

$$T \mathcal{H}_{weak} T^{-1} = \mathcal{H}_{weak} \quad (\text{B.2})$$

- with the time-reversal operator T is anti-unitary, i.e.

$$\langle \text{out} | T^\dagger T | \text{in} \rangle = \langle \text{out} | \text{in} \rangle^* = \langle \text{in} | \text{out} \rangle \quad (\text{B.3})$$

we can write

$$\langle BC; \text{out} | \mathcal{H}_{weak} | A; \text{in} \rangle = \langle BC; \text{out} | T^\dagger T \mathcal{H}_{weak} T^{-1} T | A; \text{in} \rangle^* = \langle BC; \text{in} | \mathcal{H}_{weak} | A; \text{in} \rangle^* \quad (\text{B.4})$$

since for a single particle state A there is no distinction between “in” and “out” states. Then we can insert a complete set of “out” states:

$$\langle BC; \text{out} | \mathcal{H}_{weak} | A; \text{in} \rangle = \sum_n (\langle BC; \text{in} | n; \text{out} \rangle \langle n; \text{out} | \mathcal{H}_{weak} | A; \text{in} \rangle)^* \quad (\text{B.5})$$

The S -matrix element for the elastic $B + C \rightarrow B + C$ scattering is given by the standard formula

$$S_{elastic} \equiv \langle BC; \text{out} | BC; \text{in} \rangle = e^{2i\delta_{elastic}} \quad (\text{B.6})$$

where $\delta_{elastic}$ is the BC elastic scattering phase. Thus, the $A \rightarrow B + C$ decay amplitude (B.5) can be written as

$$\langle BC; \text{out} | \mathcal{H}_{weak} | A; \text{in} \rangle = e^{2i\delta_{elastic}} \langle BC; \text{out} | \mathcal{H}_{weak} | A; \text{in} \rangle^* = A e^{i(2\delta_{elastic} - \delta_s)} \quad (\text{B.7})$$

Comparing Eqs. (B.7) and (B.1), we immediately find

$$\delta_s = \delta_{elastic} \quad (\text{B.8})$$

Eq. (B.8) gives the desired formulation of the Watson's theorem: *the phase generated by the strong interactions coincides with the S -wave elastic scattering of decay products below the first threshold taken at the mass of the decaying particle.*

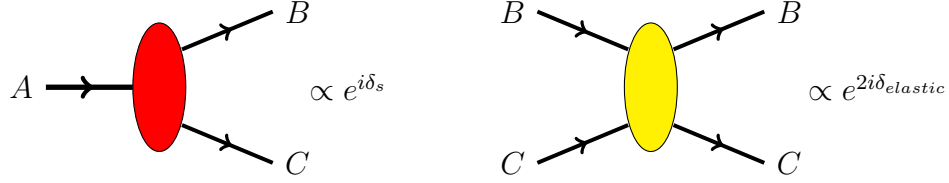


Figure B.1: bc strong final state interaction in the decay of particle A (left) and elastic BC scattering (right).

Appendix C

K -matrix formalism

C.1 General formalism for the overlapping resonances

In Ref. [82] the role of the K -matrix formalism is explained in detail, in a form precisely suited to match to our quark model approach.

In potential theory formalism, the T -matrix elements T_{ij} for transition between the continuum two-body states i and j (i.e. scattering) via the overlapping resonances $\{a^0, b^0, \dots\}$ forming the intermediate states can be written as [82]

$$T_{ij} = f_{ia^0} \Pi_{a^0 b^0} f_{b^0 j} \quad (\text{C.1})$$

where the elements of the resonance propagator matrix are parametrized as

$$\Pi_{a^0 b^0} = \left(M - i \frac{\Gamma}{2} - m \right)_{a^0 b^0}^{-1} \quad (\text{C.2})$$

where m is the total energy in the center of mass frame and M is a Hermitian mass matrix and Γ is a Hermitian width matrix, given by

$$\Gamma_{a^0 b^0} = \sum_i 2\rho_{ii} f_{a^0 i} f_{i b^0} \quad (\text{C.3})$$

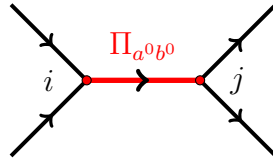


Figure C.1: Transition from state i to state j via set of overlapping resonance states described by the propagator $\Pi_{a^0 b^0}$.

The states $\{a^0, b^0, \dots\}$ are the “bare” resonance states as they exist before either the coupling to the continuum channels i or direct coupling between the states is turned on.

Therefore, they are bound states. The factor ρ_{ii} the diagonal element of is the phase-space factor matrix (3.33) for channel i , and f are the matrix elements between the bare states a^0 and the continuum states i . Some comments must be made concerning the phase space matrix. First, it is a diagonal matrix as can be seen from Eq. (3.33). Second, in usual calculations ρ_{ij} is a real quantity but which vanishes below the threshold. However, in some works including the work by Daum *et al.* the phase space is defined below the threshold by analytic continuation in the complex plane [69].

If the potential is Hermitian $f_{a^0 i} = f_{i a^0}^*$ and if the time reversal is valid one can choose the couplings f to be real and such that $f_{a^0 i} = f_{i a^0}$.

The matrices M and Γ do not in general commute and they can not be diagonalized simultaneously by a unitary transformation. But it is possible to diagonalize one of them, in particular M , by a unitary¹ matrix U :

$$U_{a' a^0}^{-1} M_{a^0 b^0} U_{b^0 b'} = M'_{a' b'} = m_{a'} \delta_{a' b'} \quad (\text{C.4})$$

Thus U transforms the set of base states $\{a^0, b^0, \dots\}$ to a new set $\{a', b', \dots\}$. This set of states diagonalize M and are called the *mass-mixed states*. Note that they are not the physical states which diagonalize $M - i\Gamma/2$.

Defining the new rotated couplings as

$$f_{i a'} = f_{i a^0} U_{a^0 a'}, \quad f_{b' j} = U_{b' b^0}^{-1} f_{b^0 j} \quad (\text{C.5})$$

the T -matrix has the form

$$T_{ij} = f_{i a'} \Pi'_{a' b'} f_{b' j} \quad (\text{C.6})$$

where

$$\begin{aligned} \Pi'^{-1}_{a' b'} &= \left(U^{-1} M U - \frac{i}{2} U^{-1} \Gamma U - m \right)_{a' b'} \\ &= (m_{a'} - m) \delta_{a' b'} - \frac{i}{2} \sum_i 2\rho_{ii} f_{a' i} f_{i b'} = D_{a' b'}^{-1} - \Sigma_{a' b'} \end{aligned} \quad (\text{C.7})$$

with

$$D_{a' b'}^{-1} = (M' - m)_{a' b'} = (m_{a'} - m) \delta_{a' b'}, \quad \Sigma_{a' b'} = \frac{i}{2} \Gamma'_{a' b'} = i \sum_i \rho_{ii} f_{a' i} f_{i b'} \quad (\text{C.8})$$

Eq. (C.7) can be written in the matrix form

$$\Pi' = D + \Pi' \Sigma D \quad (\text{C.9})$$

which can be iterated as

$$\Pi' = D + D \Sigma D + D \Sigma D \Sigma \Pi + \dots \quad (\text{C.10})$$

¹As discussed in the next section when the M -matrix is symmetric the transformation is orthogonal which is the case of the T -invariant interactions.

Substituting the iterated form of Π' from Eq. (C.10) in Eq. (C.6), one obtains

$$\begin{aligned} T_{ij} &= f_{ia'} D_{a'b'} f_{b'j} + f_{ia'} D_{a'c'} \Sigma_{c'd'} D_{d'b'} f_{b'j} + \dots \\ &= f_{ia'} D_{a'b'} f_{b'j} + f_{ia'} D_{a'c'} \left(i \sum_k \rho_{kk} f_{c'k} f_{kd'} \right) D_{d'b'} f_{b'j} + \dots \\ &= K_{ij} + i \sum_k K_{ik} \rho_{kk} K_{kj} + \dots \end{aligned} \quad (\text{C.11})$$

which is the iterated form of

$$T = K(1 - i\rho K)^{-1} \quad (\text{C.12})$$

Eq. (C.12) is the standard expression for the T -matrix in terms of the K -matrix, which is defined as

$$K_{ij} = f_{ia'} D_{a'b'} f_{b'j} = \sum_{a'} \frac{f_{ia'} f_{a'j}}{m_{a'} - m} \quad (\text{C.13})$$

Note that this is not the most general form of the K -matrix. Quite often in addition to the pole terms one introduces additional non-resonant terms (e.g. terms polynomial in the mass m) to Eq. (C.13). Remote wide resonances can contribute similarly to the continuum if we consider restricted range of m . One has to point out that in the experimental analyses we are discussing [45, 68] only the two K_1 resonance contributions are considered, what is a rather strong assumption.

The physical states of the system which have definite mass and lifetime are neither $\{a^0, b^0, \dots\}$ nor $\{a', b', \dots\}$ but the eigenstates $\{a^{ph}, b^{ph}, \dots\}$ of the full operator $M - i\Gamma/2$:

$$\left(M - i\frac{\Gamma}{2} \right) |a^{ph}\rangle = m_{a^{ph}} |a^{ph}\rangle \quad (\text{C.14})$$

where $m_{a^{ph}}$ is complex. These states have a definite mass $Re(m_{a^{ph}})$ and lifetime $\tau^{-1} = -2Im(m_{a^{ph}})$. Of course, these masses $m_{a^{ph}}$ are also the poles of the T -matrix in the form of (C.1) in the potential theory formalism and (C.6) in the K -matrix formalism at the eigenvalues $m = m_{a^{ph}}$.

In order to relate the T -matrix elements, expressed in the physical state and K -matrix bases, one has to diagonalize the matrix $m_{a'} \delta_{a'b'} - \Sigma_{a'b'}$:

$$V_{a^{ph}a'}^{-1} (m_{a'} \delta_{a'b'} - \Sigma_{a'b'}) V_{b'b^{ph}} = m_{a^{ph}} \delta_{a^{ph}b^{ph}} \quad (\text{C.15})$$

One has to note that since $M - i\frac{\Gamma}{2}$ is not Hermitian, the transformation matrix V , which relates the K -matrix and T -matrix states, is not unitary though it is (complex) orthogonal since the matrices are symmetric.

Rotating the K -matrix couplings $f_{ia'}$ to the couplings to the physical mass eigenstates $f_{ia^{ph}}$

$$f_{ia^{ph}} = f_{ia'} V_{a'a^{ph}}, \quad f_{b^{ph}j} = V_{b^{ph}a'}^{-1} f_{a'j} \quad (\text{C.16})$$

the T -matrix (C.6) can be rewritten in terms of the physical states:

$$T_{ij} = f_{ia^{ph}} \Pi'_{a^{ph} b^{ph}} f_{b^{ph} j} = \sum_{a^{ph}} \frac{f_{ia^{ph}} f_{a^{ph} j}}{m_{a^{ph}} - m} \quad (\text{C.17})$$

where

$$\Pi'^{-1}_{a^{ph} b^{ph}} = (m_{a^{ph}} - m) \delta_{a^{ph} b^{ph}} \quad (\text{C.18})$$

The physical masses and widths of the overlapping resonances can be determined from Eq. (C.15):

$$\begin{aligned} M_{a^{ph}} &= \text{Re}(m_{a^{ph}}(m)) = \text{Re} \left(\sum_{a'} V_{a^{ph} a'}^{-1} m_{a'} V_{a' a^{ph}} - i \sum_k \rho_{kk} f_{a^{ph} k} f_{k a^{ph}} \right) \\ \Gamma_{a^{ph}} &= -2\text{Im}(m_{a^{ph}}(m)) = -2\text{Im} \left(\sum_{a'} V_{a^{ph} a'}^{-1} m_{a'} V_{a' a^{ph}} - i \sum_k \rho_{kk} f_{a^{ph} k} f_{k a^{ph}} \right) \end{aligned} \quad (\text{C.19})$$

Note that there is a contribution to the mass due to the complex part of $\rho_{ij}(m)$ below the threshold.

C.2 Relation of the couplings in the K -matrix method and the quark model

In this section we identify in a systematic approach the couplings deduced from the 3P_0 quark model, including the mixing of K_1 resonances, with the couplings introduced in the K -matrix formalism by Bowler *et al.* [68]. To justify this identification, we establish the connection between the formalism, introduced in the previous section, and the quark model.

1. To make explicit the discussion in Ref. [82], we distinguish two types of interactions:

- The first type of interactions is described by Hamiltonian H_0 , which describes the $q\bar{q}$ potential of the bound states of mesons, $\{a^0, b^0, \dots\}$. It generates the initial meson masses and wave functions which are used to calculate the matrix elements of meson decays in the quark model (see next item).
- The second type of interactions, described by Hamiltonian H' , represents the interaction vertices connecting these bound states to the continuum of all possible states of two interacting mesons, $\{i, j, \dots\}$:

$$f_{a^0 i} = \langle a^0 | H' | i \rangle \quad (\text{C.20})$$

We commonly call these vertex interactions “couplings”. These couplings can be precisely calculated within the 3P_0 quark-pair-creation model. With adequate choice of phases of the wave functions of the bound states the couplings can be set to be real.

2. No direct interaction is assumed between two mesons. Nevertheless, there is rescattering since a meson pair can annihilate into one bound state and then be created again from the decay of this bound state. This rescattering process can be iterated arbitrary number of times, what is equivalent to a resummation of meson loops between the initial and final vertices (see Fig. C.2).

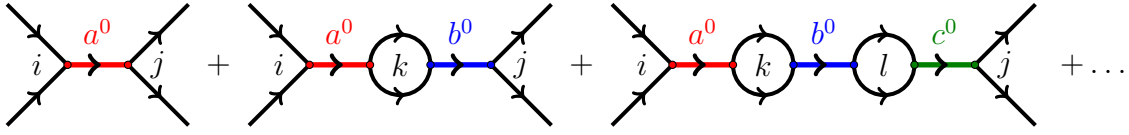


Figure C.2: Rescattering process.

All these possible processes can be resummed into a matrix propagator $\Pi_{a^0 b^0}$ (C.2) connecting two vertices. Defining the “bare” scattering amplitude for the first diagram in Fig. C.2

$$T_{ij}^{a^0(0)} = \frac{f_{ia^0} f_{a^0 j}}{m_{a^0} - m} \quad (\text{C.21})$$

this leads to the scattering amplitude (C.1):

$$\begin{aligned} T_{ij} &= \sum_{a^0} T_{ij}^{a^0(0)} + \sum_{a^0, k, b^0} T_{ik}^{a^0(0)} I_k T_{kj}^{b^0(0)} + \sum_{a^0, k, b^0, l, c^0} T_{ik}^{a^0(0)} I_k T_{kl}^{b^0(0)} I_l T_{lj}^{c^0(0)} + \dots \\ &= \sum_{a^0, b^0} f_{ia^0} \Pi_{a^0 b^0} f_{b^0 j} \end{aligned} \quad (\text{C.22})$$

where I_k denotes the loop integral.

The mass matrix $M - i\Gamma/2$ in $\Pi_{a^0 b^0}$ (C.2) is in general non-diagonal. It contains

- the initial diagonal mass matrix $\text{diag}(m_{a^0}, m_{b^0}, \dots)$ of the bound states;
- the contribution of the loops for each possible channel, which can be non-diagonal since common two-body channels can couple to two different bound states. The loop integrals contain real and imaginary parts, which appear only when a two-body channel is open at the energy m .

3. Now the mass matrix must be diagonalized in two steps as explained in the previous section. Thus, one first diagonalises the real part, M , then one passes to a diagonalization of the full new matrix, $M' - i\Gamma'/2$.

- (a) Diagonalisation of the real part of the denominator of $\Pi_{a^0b^0}$ matrix, M , leads to the introduction of the new diagonal mass matrix (see Eq. (C.4))

$$M'(m) = \text{diag}(m_{a'}, m_{b'}, \dots) \quad (\text{C.23})$$

This mass diagonalization implies a simultaneous rotation of the couplings (C.5). If there exists only one resonance which couples to the initial and final states, no rotation is needed. In this case all bare couplings $\{f_{a^0i}\}$ coincide with the ones of the K -matrix, $\{f_{a'i}\}$. Thus, one can relate them with couplings calculated in the quark model. Otherwise, when there are two possible overlapping resonances, namely the two K_1 's, we have to make a rotation and introduce a mixing angle. We notice then that we have introduced an arbitrary rotation angle θ_{K_1} in our model computations which allows us to identify the set of the observed K -matrix couplings with the theoretical ones by the fit of data with our model predictions. This identification means that:

- the effect of the real part of the loops, i.e. $\text{Re}(I_k)$ in Eq. (C.22), are taken into account in our model;
- mixing angle θ_{K_1} is not predicted by the model but is simply adjusted to data;
- introduction of the mixing angle θ_{K_1} can also take into account the uncalculated rotation of the pure spin states K_{1A} and K_{1B} into the eigenstates of Hamiltonian H_0 due to the spin-orbit forces [83].

- (b) The second step consists the diagonalization of the new mass matrix

$$\left(M' - i\frac{\Gamma'}{2}\right)_{a'b'} = m_{a'}\delta_{a'b'} - i\sum_i \rho_{ii}(m)f_{a'i}f_{ib'} \quad (\text{C.24})$$

This leads to the physical mass eigenstates and to the Breit-Wigner parametrization with energy-dependent width. This new rotation that accomplishes the last transformation into the physical states must have a complex and the angle of this rotation must have a complex phase. This would lead to the complex couplings of the mass eigenstates to set of continuum states. As we have already mentioned in the text, this rotation seems to be rather small.

4. Let us now discuss the dependence of various variables on the energy m . In principle, all the masses and couplings, produced by two previous steps are dependent on m because of the loop effects. However, as regards the mass matrix, its real and imaginary parts have rather different behaviour depending on m . In first approximation, the real part of the mass matrix, which includes the sum of the large number of loops, varies slowly with m and can be considered as constants. This is what was done in the analysis of Daum *et al.*. On the contrary, the imaginary part, which corresponds to the partial widths of the opened channels, is a rapidly varying function near the threshold.

In principle, one can go beyond the approximation of the real part of the mass matrix by taking into account that there is some variation near the threshold. This is obtained by analytic continuation of the phase space through the threshold. This effect is included in the prescription of Naunberg and Pais of the complex phase space. This corresponds to having imaginary part of the widths generating a m -dependent mass shift. For instance, for the K -matrix width one have

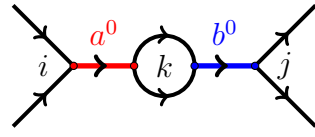
$$\Gamma_{a'b'}(m) = \sum_i \rho_{ii}(m) f_{a'i} f_{ib'} \quad (\text{C.25})$$

where the phase-space factor $\rho_{ij}(m)$ can be complex in general.

Finally, one obtains for the physical states that the physical masses of $K_1(1270/1400)$ are varying slowly as functions of m while the physical widths are rapidly changing functions; moreover the mass of $K_1(1270)$ has a more rapid variation around the peak due to the closeness of the K_1 -mass to the $K\rho$ threshold (see Fig. C.4).

C.3 Watson's theorem: another view

One can introduce “bubble” diagrams of rescattering as depicted on the figure below:

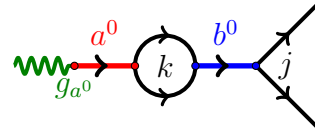


$$= \frac{f_{ia^0} f_{a^0 k}}{m_{a^0} - m} I_k \frac{f_{kb^0} f_{b^0 j}}{m_{b^0} - m} = T_{ik}^{a^0(0)} I_k T_{kj}^{b^0(0)} \quad (\text{C.26})$$

where I_k denote the loop integral which has a complex phase. Now, summing the series of such “bubble” diagrams with the initial production of resonance a^0 , we obtain

$$\begin{aligned} T_{ij}^{a^0} &= T_{ij}^{a^0(0)} + \sum_{k,b^0} T_{ik}^{a^0(0)} I_k T_{kj}^{b^0(0)} + \sum_{k,b^0,l,c^0} T_{ik}^{a^0(0)} I_k T_{kl}^{b^0(0)} I_l T_{lj}^{c^0(0)} + \dots \\ &= T^{(0)} (1 - IT^{(0)})^{-1} \end{aligned} \quad (\text{C.27})$$

For the production of the resonance one can follow the same procedure:



$$= \frac{g_{a^0} f_{a^0 k}}{m_{a^0} - m} I_k \frac{f_{kb^0} f_{b^0 j}}{m_{b^0} - m} = F^{a^0(0)} I_k T_{kj}^{b^0(0)} \quad (\text{C.28})$$

where g_{a^0} is the resonance production constant. The summation of the “bubble” diagrams gives

$$\begin{aligned} F^{a^0} &= F^{a^0(0)} + \sum_{k,b^0} F^{a^0(0)} I_k T_{kj}^{b^0(0)} + \sum_{k,b^0,l,c^0} F^{a^0(0)} I_k T_{kl}^{b^0(0)} I_l T_{lj}^{c^0(0)} + \dots \\ &= F^{a^0(0)} (1 - IT^{(0)})^{-1} \end{aligned} \quad (\text{C.29})$$

Comparing Eqs. (C.27) and (C.29), one can notice that since the couplings $f_{a^0 k}$ are taken to be real, the complex phase comes from the loop integrals I_k and, moreover, is the same for the rescattering and production. In the case of one resonance, the Watson's theorem formulation is the following: *the production and the scattering phases are the same below the first inelastic threshold*. If there are several resonances, coupled to the same decay channels, the formulation of Watson's theorem can be treated at the matrix level.

C.4 Re-interpreting the ACCMOR result

In order to determine our model parameters and the K_1 mixing angle from comparison of the predicted partial decay widths of the K_1 meson decays into the dominant $K^*\pi$ and $K\rho$ channels with the measured experimental values, we use the fitted K -matrix parameters extracted by Daum *et al.* from Ref. [45] (see Table C.2).

Using the definition of the K_1 mixing by Daum *et al.* (which is different from (3.1) that we use)

$$\begin{aligned} |K_1(1270)\rangle &= -|K_{1A}\rangle \sin \theta_{K_1} + |K_{1B}\rangle \cos \theta_{K_1} \\ |K_1(1400)\rangle &= |K_{1A}\rangle \cos \theta_{K_1} + |K_{1B}\rangle \sin \theta_{K_1} \end{aligned} \quad (\text{C.30})$$

the dominant S -wave K -matrix couplings of the K_1 's to the states $K^*\pi$ (channel 1) and $K\rho$ (channel 2) are given as [45]

$$\begin{aligned} f_{a'1} &= \frac{1}{2}\gamma_+ \cos \theta_{K_1} + \sqrt{\frac{9}{20}}\gamma_- \sin \theta_{K_1} \\ f_{b'1} &= -\frac{1}{2}\gamma_+ \sin \theta_{K_1} + \sqrt{\frac{9}{20}}\gamma_- \cos \theta_{K_1} \\ f_{a'2} &= \frac{1}{2}\gamma_+ \cos \theta_{K_1} - \sqrt{\frac{9}{20}}\gamma_- \sin \theta_{K_1} \\ f_{b'2} &= -\frac{1}{2}\gamma_+ \sin \theta_{K_1} - \sqrt{\frac{9}{20}}\gamma_- \cos \theta_{K_1} \end{aligned} \quad (\text{C.31})$$

where γ_+ and γ_- are the reduced $SU(3)$ couplings for K_{1A} (F -type) and K_{1B} (D -type) respectively. Their fitted experimental values are given in Table C.1. The indices a' and b' denote the upper and lower K_1 resonances.

$m_{a'}$, GeV/ c^2	$m_{b'}$, GeV/ c^2	γ_+	γ_-	$\tilde{\theta}_{K_1}$
1.4 ± 0.02	1.17 ± 0.02	0.78 ± 0.1	0.54 ± 0.1	$64^\circ \pm 8^\circ$

Table C.1: Fitted K -matrix pole masses, S -wave reduced $SU(3)$ couplings and mixing angle for K_{1A} (F -type) and K_{1B} (D -type), taken from Ref. [45] (low t data). The indices a' and b' denote the upper and lower K_1 resonances.

$f_{a'1}$	$f_{b'1}$	$f_{a'2}$	$f_{b'2}$	$f_{a'3}$	$f_{b'3}$
0.50 ± 0.07	-0.19 ± 0.09	-0.15 ± 0.10	-0.51 ± 0.06	0	0.32

Table C.2: K -matrix couplings, calculated from Eq. (C.31) using the fitted parameters from Table C.1. The indices a' and b' denote the upper and lower K_1 resonances decaying into $K^*\pi$ (channel 1) and $K\rho$ (channel 2) hadronic states respectively. The coupling to the $K_0^*(1430)\pi$ channel, where $K_0^*(1430)$ resonance is supposed to have the mass $1.25 \text{ GeV}/c^2$ and width $600 \text{ MeV}/c^2$, f_{b3} is taken from Ref. [54].

Using the experimental values of the K -matrix couplings from Table C.2 and performing the diagonalization of the complex mass matrix (C.24), we observed that

- The variation of the absolute values and phases of the new rotated physical couplings $\{f_{a^{ph}i}, f_{b^{ph}i}\}$ around the masses at the peak of Breit-Wigner (i.e. $m \sim 1.27 \text{ GeV}/c^2$ and $1.4 \text{ GeV}/c^2$) turn out to be small (see Fig. C.3).
- Contribution of the complex phase space for energy below the decay threshold (which implies $\rho_{ij}(m) \rightarrow i|\rho_{ij}(m)|$) is very small for diagonalized physical mass of $K_1(1400)$ (see Fig. C.4). But one observes a threshold effect for $K_1(1270)$ near $m \sim 1.2 \text{ GeV}/c^2$. However, the mass variation of $M_{K_1}(m)$ around the peak of Breit-Wigner can be considered not so significant.
- One can see from Fig. C.4 that, contrary to $M_{K_1}(m)$ dependence, the width $\Gamma_{K_1}(m)$ is a rapidly varying function of the energy m .
- Non-diagonal elements of the mass matrix (C.24) are sufficiently small compared to the diagonal ones. One can see from Fig. C.4 that the difference between the properly diagonalized masses and widths (C.19) (blue/red curves), which are calculated in terms of the rotated physical couplings, and the real and imaginary parts of the diagonal elements of (C.24) (green/orange curves) is insignificant. As a consequence, our assumption for the partial widths

$$\Gamma_{a^{ph}i}(M_{peak}) \simeq \Gamma_{a'i}(M_{peak}) = \Gamma_{a'i}^{QPCM}(M_{peak}) \quad (\text{C.32})$$

seems to be reasonable. This means that we can use the experimental measured K -matrix couplings in order to calculate the partial decay widths and fit our model parameters, namely quark-pair-creation constant γ and the mixing angle θ_{K_1} , which can further be used for the \mathcal{J} function computation.

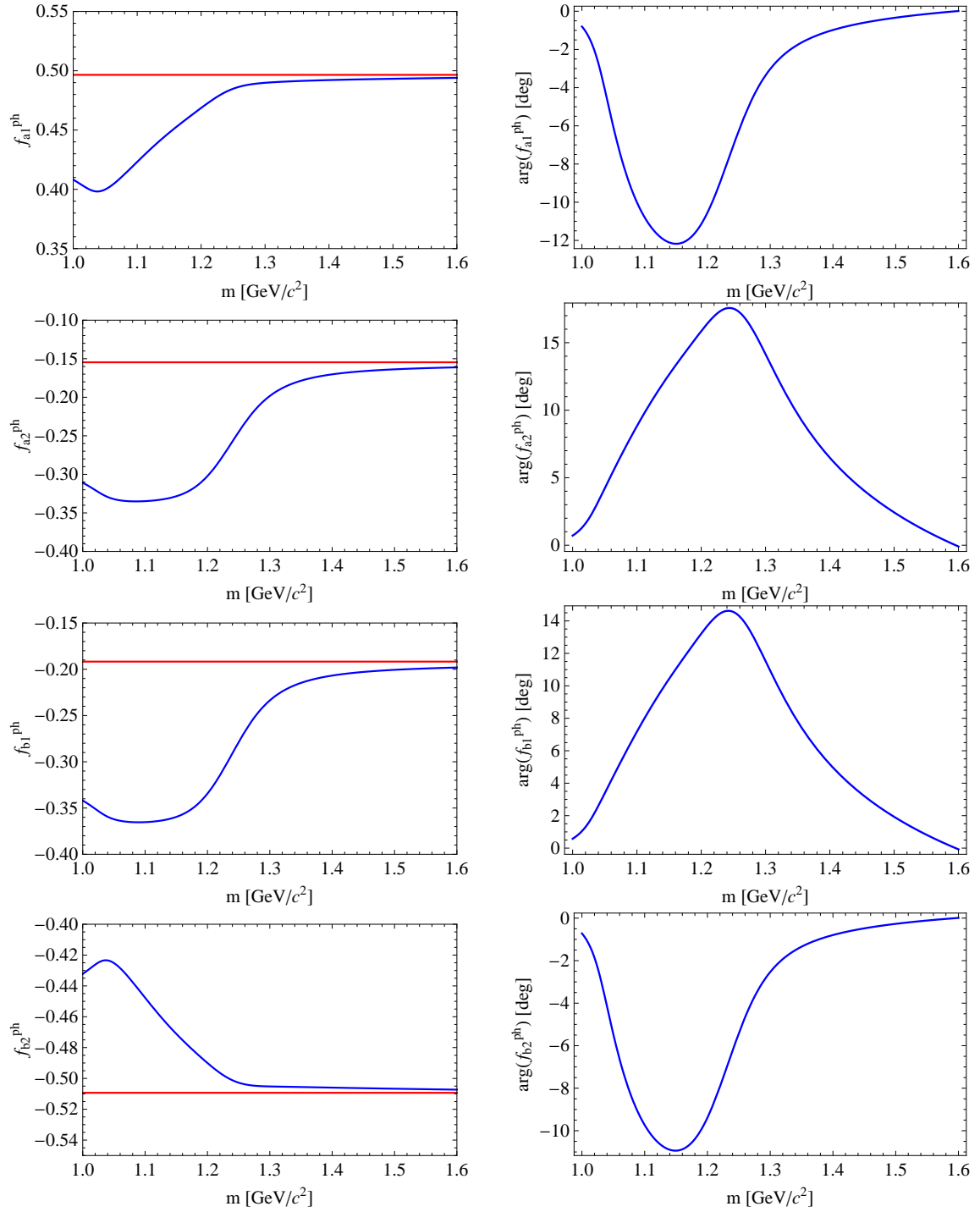


Figure C.3: Energy dependence of the physical couplings (blue). The red lines represent the values of the real couplings for the *K*-matrix states, fitted by ACCMOR collaboration [45].

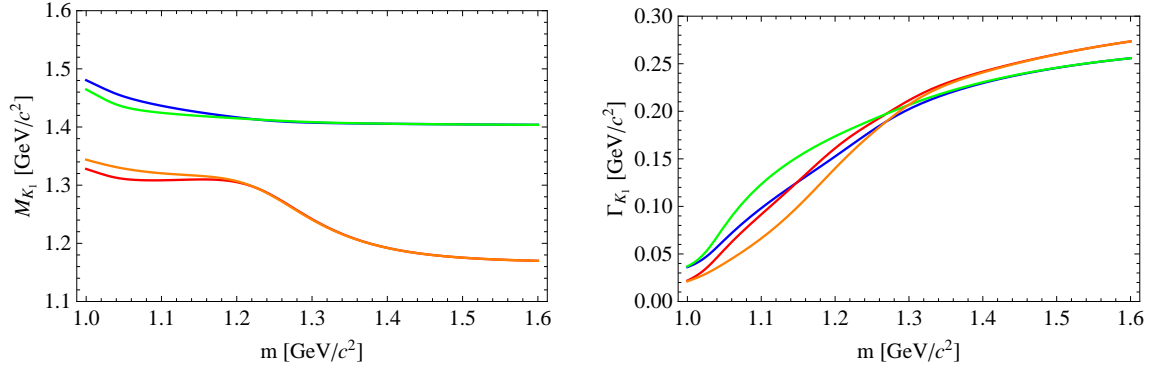


Figure C.4: Energy dependence of the mass (left) and width (right) of $K_1(1270)$ (red, orange) and $K_1(1400)$ (blue, green). Red and blue curves correspond to the masses and total widths of the physical eigenstates, i.e. diagonal mass matrix elements (C.19) which are calculated in terms of the rotated physical couplings. Orange and green curves represent the leading diagonal elements of the complex mass matrix $(M' - i\Gamma'/2)_{a'b'}$ (C.7) in the K -matrix eigenstate basis. The D -wave contribution is not taken into account due to the absence of knowledge of the corresponding couplings.

Appendix D

QPCM

D.1 Spacial integrals in QPCM

For the decay $A \rightarrow B + C$ (see Fig. 3.1) the spacial integrals are given by

$$\begin{aligned}
 I_m^{(ABC)} &= \int d^3\vec{k}_1 d^3\vec{k}_2 d^3\vec{k}_3 d^3\vec{k}_4 \delta(\vec{k}_1 + \vec{k}_2 - \vec{k}_A) \delta(\vec{k}_2 + \vec{k}_3 - \vec{k}_B) \delta(\vec{k}_4 + \vec{k}_1 - \vec{k}_C) \delta(\vec{k}_3 + \vec{k}_4) \\
 &\quad \times \mathcal{Y}_1^m(\vec{k}_3 - \vec{k}_4) \psi^{(A)}(\vec{k}_1 - \vec{k}_2) \psi^{(B)}(\vec{k}_2 - \vec{k}_3) \psi^{(C)}(\vec{k}_4 - \vec{k}_1) \\
 &= \frac{1}{8} \int d^3\vec{k} \mathcal{Y}_1^m(\vec{k}_B - \vec{k}) \psi^{(A)}(\vec{k}_B + \vec{k}) \psi^{(B)}(-\vec{k}) \psi^{(C)}(\vec{k})
 \end{aligned} \tag{D.1}$$

where ψ 's are the normalized Fourier transforms of harmonic oscillator meson wave functions. The wave functions for the ground ($L = 0$) and orbitally excited ($L = 1$) meson states are defined as

$$\begin{aligned}
 \psi_0^{(i)}(\vec{k}) &= \frac{R_i^{3/2}}{\pi^{3/4}} \exp\left(-\frac{\vec{k}^2 R_i^2}{8}\right) \quad (L = 0) \\
 \psi_1^{m(i)}(\vec{k}) &= \sqrt{\frac{2}{3}} \frac{R_i^{5/2}}{\pi^{1/4}} \mathcal{Y}_1^m(\vec{k}) \exp\left(-\frac{\vec{k}^2 R_i^2}{8}\right) \quad (L = 1, L_z = m) \\
 \mathcal{Y}_1^m(\vec{k}) &= |\vec{k}| Y_1^m(\hat{\vec{k}}) = (\vec{\varepsilon}_m \vec{k}) \sqrt{\frac{3}{4\pi}}
 \end{aligned} \tag{D.2}$$

Here R_i is the meson wave function radius and $\vec{\varepsilon}_m$ are the A -polarization vectors, defined as

$$\vec{\varepsilon}_0 = \begin{pmatrix} 0 \\ 0 \\ 1 \end{pmatrix}, \quad \vec{\varepsilon}_{\pm 1} = \mp \frac{1}{\sqrt{2}} \begin{pmatrix} 1 \\ \mp i \\ 0 \end{pmatrix} \tag{D.3}$$

Performing the integration over \vec{k} one obtains for the orbitally excited axial-vector

meson decay into pseudoscalar and vector mesons in the A -meson reference frame:

$$I_m^{(ABC)} = -\frac{4\sqrt{3}}{\pi^{5/4}} \frac{R_A^{5/2}(R_B R_C)^{3/2}}{(R_A^2 + R_B^2 + R_C^2)^{5/2}} \left((\vec{\varepsilon}_m \cdot \vec{\varepsilon}_{-m}) - (\vec{\varepsilon}_m \cdot \vec{k}_B)(\vec{\varepsilon}_{-m} \cdot \vec{k}_B) \right. \\ \left. \times \frac{(2R_A^2 + R_B^2 + R_C^2)(R_B^2 + R_C^2)}{4(R_A^2 + R_B^2 + R_C^2)} \right) \exp \left[-\vec{k}_B^2 \frac{R_A^2(R_B^2 + R_C^2)}{8(R_A^2 + R_B^2 + R_C^2)} \right] \quad (\text{D.4})$$

Setting \vec{k}_B along z -axis, the integrals become

$$I_0^{(ABC)} = -\frac{4\sqrt{3}}{\pi^{5/4}} \frac{R_A^{5/2}(R_B R_C)^{3/2}}{(R_A^2 + R_B^2 + R_C^2)^{5/2}} \left(1 - \vec{k}_B^2 \frac{(2R_A^2 + R_B^2 + R_C^2)(R_B^2 + R_C^2)}{4(R_A^2 + R_B^2 + R_C^2)} \right) \\ \times \exp \left[-\vec{k}_B^2 \frac{R_A^2(R_B^2 + R_C^2)}{8(R_A^2 + R_B^2 + R_C^2)} \right] \quad (\text{D.5}) \\ I_1^{(ABC)} = \frac{4\sqrt{3}}{\pi^{5/4}} \frac{R_A^{5/2}(R_B R_C)^{3/2}}{(R_A^2 + R_B^2 + R_C^2)^{5/2}} \exp \left[-\vec{k}_B^2 \frac{R_A^2(R_B^2 + R_C^2)}{8(R_A^2 + R_B^2 + R_C^2)} \right]$$

For the vector meson ground state decay into two pseudoscalar mesons the spacial integral is

$$I_m^{(ABC)} = \frac{\sqrt{6}}{\pi^{5/4}} (\vec{\varepsilon}_m \cdot \vec{k}_C) \frac{(R_A R_B R_C)^{3/2} (2R_A^2 + R_B^2 + R_C^2)}{(R_A^2 + R_B^2 + R_C^2)^{5/2}} \\ \times \exp \left[-\vec{k}_C^2 \frac{R_A^2(R_B^2 + R_C^2)}{8(R_A^2 + R_B^2 + R_C^2)} \right] \quad (\text{D.6})$$

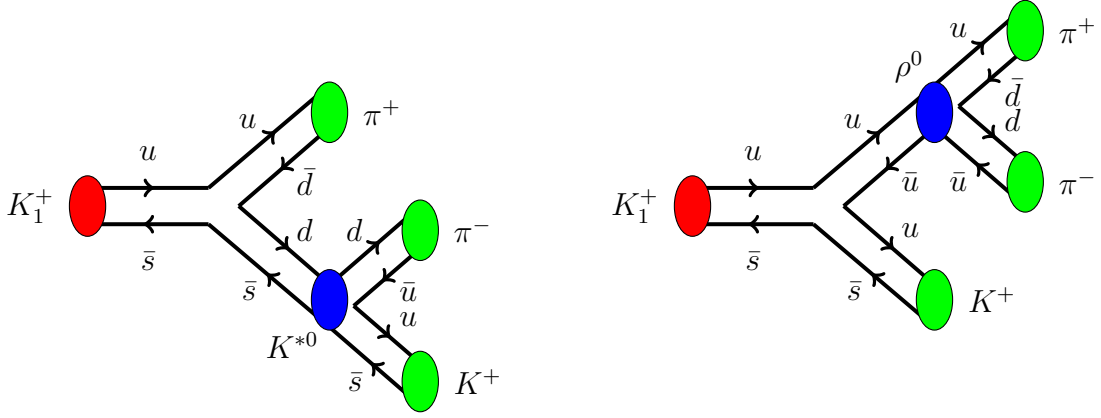
D.2 Fixing the relative signs for tree-body decay

D.2.1 Clebsch-Gordan coefficients

We decided to use the convention “down→up” (see Fig. D.1). For instance, for the case of $K_1^+ \rightarrow K^+ \pi^- \pi^+$ decay that implies that we take the Clebsch-Gordan coefficients as

$$(K^{*0} \pi^+ | K_1^+) = (1/2, -1/2; 1, 1 | 1/2, 1/2) = -\sqrt{\frac{2}{3}} \\ (K^+ \pi^- | K^{*0}) = (1/2, 1/2; -1, 1 | -1/2, 1/2) = +\sqrt{\frac{2}{3}} \\ (K^+ \rho^0 | K_1^+) = (1/2, 1/2; 1, 0 | 1/2, 1/2) = +\frac{1}{\sqrt{3}} \\ (\pi^- \pi^+ | \rho^0) = (1, -1; 1, 1 | 1, 0) = -\frac{1}{\sqrt{2}} \quad (\text{D.7})$$

This gives the signs of the amplitudes listed in Table 3.2 and the coefficients $-2/3$ for $K^* \pi$ and $-1/\sqrt{6}$ for ρK contributions in Eq. 24 from Ref. [11].

Figure D.1: $K_1^+ \rightarrow K^+ \pi^- \pi^+$ decay

D.2.2 Determination of the relative sign of $g_{K^*K\pi}$ and $g_{\rho\pi\pi}$

Following the definition in the work of Gronau *et al.*, the total amplitude of the two possible channels is written as

$$\begin{aligned} \mathcal{M}^{(a)} &= \varepsilon_\mu^{(K_1)} T_{K^*\pi}^{\mu\nu} \varepsilon_\nu^{(K^*)*} g_{K^*K\pi} \varepsilon_\sigma^{(K^*)} (p_{\pi^-} - p_{K^+})^\sigma \\ \mathcal{M}^{(b)} &= \varepsilon_\mu^{(K_1)} T_{K\rho}^{\mu\nu} \varepsilon_\nu^{(\rho)*} g_{\rho\pi\pi} \varepsilon_\sigma^{(\rho)} (p_{\pi^+} - p_{\pi^-})^\sigma \end{aligned} \quad (\text{D.8})$$

where $T_{VP}^{\mu\nu}$ is the hadronic tensor, parametrized in terms of the form factors f_V , h_V (or equivalently the S and D partial wave amplitudes).

Now, using the same Clebsch-Gordan coefficients, defined above in Eq. (D.7), one can write the amplitude of the $V \rightarrow PP$ decay, calculated the general tensor Lorenz-invariant form in the vector meson reference frame:

$$\begin{aligned} \mathcal{M}(K^{*0} \rightarrow K^+ \pi^-) &= -\sqrt{\frac{2}{3}} g_{K^*K\pi} (\vec{\varepsilon}_{K^*} \cdot (\vec{p}_{\pi^-} - \vec{p}_{K^+})) = \sqrt{\frac{8}{3}} g_{K^*K\pi} (\vec{\varepsilon}_{K^*} \cdot \vec{p}_{K^+}) \\ \mathcal{M}(\rho^0 \rightarrow \pi^- \pi^+) &= \sqrt{\frac{1}{2}} g_{\rho\pi\pi} (\vec{\varepsilon}_\rho \cdot (\vec{p}_{\pi^+} - \vec{p}_{\pi^-})) = -\sqrt{2} g_{\rho\pi\pi} (\vec{\varepsilon}_\rho \cdot \vec{p}_{\pi^-}) \end{aligned} \quad (\text{D.9})$$

Taking into account all the spin and isospin couplings, the QPCM prediction is

$$\begin{aligned} \mathcal{M}_m^{\text{QPCM}}(K^{*0} \rightarrow K^+ \pi^-) &= -\frac{1}{6} \gamma I_m^{(K^*K\pi)} = -\frac{1}{6} \gamma \tilde{I}^{(K^*K\pi)} (\vec{\varepsilon}_m \cdot \vec{p}_{K^+}) \\ \mathcal{M}_m^{\text{QPCM}}(\rho^0 \rightarrow \pi^- \pi^+) &= -\frac{1}{3\sqrt{2}} \gamma I_m^{(\rho\pi\pi)} = -\frac{1}{3\sqrt{2}} \gamma \tilde{I}^{(\rho\pi\pi)} (\vec{\varepsilon}_m \cdot \vec{p}_{\pi^-}) \end{aligned} \quad (\text{D.10})$$

where $\tilde{I}^{(VPP)}$ can be defined from Eq. (D.6)¹.

¹One has to be careful with the choice of the momentum, i.e. \vec{p}_C or $\vec{p}_B = -\vec{p}_C$, since it changes the sign of the P -wave amplitude.

Now, doing a matching between two approaches and factorizing out the common factor $\vec{\varepsilon} \cdot \vec{p}_i$, we can write the following equations:

$$\begin{aligned} \sqrt{\frac{8}{3}} g_{K^* K \pi} &= -\frac{1}{6} \gamma \tilde{I}^{(K^* K \pi)} \\ -\sqrt{2} g_{\rho \pi \pi} &= -\frac{1}{3\sqrt{2}} \gamma \tilde{I}^{(\rho \pi \pi)} \end{aligned} \quad (\text{D.11})$$

Since $\tilde{I}^{(VPP)}$ is a positive function, one can see that

$$\text{sign}(g_{K^* K \pi}) = -\text{sign}(g_{\rho \pi \pi})$$

and in the $SU(3)$ limit $\frac{g_{\rho \pi \pi}}{g_{K^* K \pi}} = -\sqrt{\frac{8}{3}}$.

One can notice that the choice of the order in the isospin factors of the vector meson decay into two pseudoscalars in Eq. (D.7) well fixes the relative sign of the g_{VPP} couplings. Moreover, this method makes the calculation of the quasi-two-body decay amplitude independent on the intermediate vector meson state (K^* , ρ) wave function sign (which, in principle, can be arbitrary in the quasi-two-body calculation since the final state is not the same)!

D.3 Partial Wave Amplitudes

With the quark models one can directly calculate the amplitudes with definite spin or helicity states. An experiment can measure the partial wave amplitudes of particular quantum numbers of the final state. Since both canonical (orbital) and helicity approaches give complete description of the process, one can find the relation between two representations for the decay of the initial at-rest state $|J, M\rangle$ with spin J and spin projection M on to the z -axis into two particles with spins $s_{1,2}$, helicities $\lambda_{1,2}$, total spin S and relative orbital momentum L [44]:

$$\mathcal{M}_{\lambda_1 \lambda_2}^{JM}(\Omega_1) = N_J f_{\lambda_1 \lambda_2}^J D_{M, \lambda_1 - \lambda_2}^{J*}(\Omega_1) \quad (\text{D.12})$$

with the normalization factor $N_J = \sqrt{\frac{2J+1}{4\pi}}$.

The observed number of events is given by

$$\sum_{M, \lambda_i, \lambda'_i} \int \mathcal{M}_{\lambda_1 \lambda_2}^{JM}(\Omega_1) \mathcal{M}_{\lambda'_1 \lambda'_2}^{JM*}(\Omega_1) d\Omega_1 = 4\pi \sum_{\substack{\lambda_i, \lambda'_i \\ \lambda_1 - \lambda_2 = \lambda'_1 - \lambda'_2}} N_J^2 f_{\lambda_1 \lambda_2}^J f_{\lambda'_1 \lambda'_2}^{J*} \quad (\text{D.13})$$

The recoupling from the canonical to the helicity representation is

$$N_J f_{\lambda_1 \lambda_2}^J = \sum_{L, S} \sqrt{2L+1} (L, 0; S, \lambda_1 - \lambda_2 | J, \lambda_1 - \lambda_2) (s_1, \lambda_1; s_2, -\lambda_2 | S, \lambda_1 - \lambda_2) A_L \quad (\text{D.14})$$

The two-body decay of the axial-vector meson into vector and pseudoscalar mesons can proceed in S and D -waves. Using $J = 1$, $\lambda_1 = \lambda_V$, $\lambda_2 = 0$, the helicity amplitudes in the A reference frame can be written in terms of partial wave amplitudes:

$$N_1 f_{\lambda_V 0}^1 = \sum_{L=0,2} \sqrt{2L+1} (L, 0; 1, \lambda_V | 1, \lambda_V) A_L \quad (\text{D.15})$$

Setting \vec{k}_V along z -direction (i.e. $\theta_V = 0$), the helicity amplitudes are

$$\begin{aligned} \mathcal{M}_{00}^{10} &= N_1 f_{00}^1 = A_S - \sqrt{2} A_D \\ \mathcal{M}_{\pm 1, 0}^{1, \pm 1} &= N_1 f_{\pm 1, 0}^1 = A_S + \frac{1}{\sqrt{2}} A_D \end{aligned} \quad (\text{D.16})$$

By-turn, the partial wave amplitudes are related to the helicity amplitudes as following:

$$\begin{aligned} A_S &= \frac{1}{3} (2\mathcal{M}_{10}^{11} + \mathcal{M}_{00}^{10}) \\ A_D &= \frac{\sqrt{2}}{3} (\mathcal{M}_{10}^{11} - \mathcal{M}_{00}^{10}) \end{aligned} \quad (\text{D.17})$$

Summing over the final and averaging over the initial spin states, the partial width is then given by

$$\Gamma(A \rightarrow VP) = (|A_S|^2 + |A_D|^2) PS_2 \quad (\text{D.18})$$

For the V -decay into two pseudoscalar mesons P_1 and P_2 in the P -wave the decay amplitude will be given by

$$\mathcal{M}_{00}^{1M}(\Omega_1) = N_1 f_{00}^1 D_{M,0}^{1*}(\Omega_1) \quad (\text{D.19})$$

where the helicity amplitude is $N_1 f_{00}^1 = \sqrt{3} a_P$.

Correspondingly, averaging over the V -spin states, the partial width is then given by

$$\Gamma(V \rightarrow P_1 P_2) = |A_P|^2 PS_2 \quad (\text{D.20})$$

D.4 Phase space convention

The non-relativistic partial width is given by

$$\Gamma(A \rightarrow BC) = 2\pi |\mathcal{M}_{A \rightarrow BC}^{(NR)}|^2 \times PS_2^{(NR)} \quad (\text{D.21})$$

where two-body non invariant phase space can be written as

$$PS_2^{(NR)} = \int d^3 \vec{k}_B d^3 \vec{k}_C \delta^3(\vec{k}_B + \vec{k}_C) \delta(E_B + E_C - m_A) = 4\pi \frac{E_B E_C k_C}{m_A} \quad (\text{D.22})$$

Since QPCM is in principle a non-relativistic model and we are using the relativistic Lorentz-invariant tensor formalism to describe $B \rightarrow K_1 \gamma$ decay, one has to make some kind of continuation. In order to do that one has to

- Use relativistic kinematics (i.e. $E_i^2 = \vec{k}_i^2 + m_i^2$).
- Use relativistic Breit-Wigner forms.
- Make the non-relativistic decay amplitudes to be “relativistic” correcting the phase space:

$$\Gamma(A \rightarrow BC) = \frac{1}{8\pi} \frac{k_C}{m_A^2} |\mathcal{M}_{A \rightarrow BC}^{(R)}|^2 = 8\pi^2 \frac{E_B E_C k_C}{m_A} |\mathcal{M}_{A \rightarrow BC}^{(NR)}|^2$$

from where one immediately obtains the relation between the amplitudes

$$\mathcal{M}_{A \rightarrow BC}^{(R)} = 8\pi^{3/2} \sqrt{E_B E_C m_A} \mathcal{M}_{A \rightarrow BC}^{(NR)} \quad (\text{D.23})$$

Here E_i, \vec{k}_i are the energies and momentum in the A -reference frame.

Appendix E

Some notes on statistics

E.1 Maximum likelihood method

Let $F(x, a)$ be some function of a variable x and an unknown parameter a . Lets measure the value of F at some different x_i : $y_i \pm \sigma_i$. The central limit theorem (CLT) states that the mean of a sufficiently large number of independent random identically distributed variables, each with finite mean and variance, will be approximately normally distributed. So according to CLT, the measurement y_i is assumed to be Gaussian distributed with mean $F(x_i, a)$ and variance σ_i and the likelihood function can be written as

$$\mathcal{L}(a) = \prod_{i=1}^N \frac{1}{\sqrt{2\pi\sigma_i^2}} \exp \left[-\frac{(y_i - F(x_i, a))^2}{2\sigma_i^2} \right] \quad (\text{E.1})$$

and the log likelihood

$$\ln \mathcal{L}(a) = -\sum_{i=1}^N \frac{[y_i - F(x_i, a)]^2}{2\sigma_i^2} + \sum_{i=1}^N \ln \frac{1}{\sqrt{2\pi\sigma_i^2}} \quad (\text{E.2})$$

Using the method of maximum likelihood, the “true” value or estimator \hat{a} can be found from the following equation:

$$\left. \frac{\partial \ln \mathcal{L}}{\partial a} \right|_{a=\hat{a}} \equiv 0 \quad (\text{E.3})$$

To estimate the error one can expand the log likelihood around \hat{a} :

$$\ln \mathcal{L}(a) = \ln \mathcal{L}(\hat{a}) + \frac{1}{2} \left. \frac{\partial^2 \ln \mathcal{L}}{\partial a^2} \right|_{a=\hat{a}} (a - \hat{a})^2 + \mathcal{O}((a - \hat{a})^3) \quad (\text{E.4})$$

It is easy to see from Eq. (E.4) that if the derivatives $\partial^k \mathcal{L} / \partial a^k = 0$ for $k > 2$, parameter a has the normal distribution. Assuming a is Gaussian distributed with mean value \bar{a} and

standard deviation σ_a

$$\mathcal{L}(a) = \frac{1}{\sqrt{2\pi\sigma_a^2}} \exp \left[-\frac{(a - \bar{a})^2}{2\sigma_a^2} \right] \quad (\text{E.5})$$

it is easy to show that the likelihood maximization condition (Eq. (E.3)) gives

$$\bar{a} \equiv \hat{a} \quad (\text{E.6})$$

Taking the second derivative

$$\frac{\partial^2 \ln \mathcal{L}}{\partial a^2} = -\frac{1}{\sigma_a^2} \quad (\text{E.7})$$

whence it follows that the variance of the mean value is

$$\sigma_a = \left(-\frac{\partial^2 \mathcal{L}}{\partial a^2} \Big|_{a=\bar{a}} \right)^{-1/2} \quad (\text{E.8})$$

In many practical cases the situation when $F(x, a)$ is a linear function of a takes place. In this particular case it is obvious that $\mathcal{L}(a)$ will have a Gaussian distribution (E.5) (since the product of Gaussians always remains a Gaussian) and Eq. (E.6)-(E.8) will be valid.

E.2 General DDLR method

We review the DDLR method [14]. Let $\{\xi\}$ be the set of experimentally observed parameters that describes the kinematics of the four-body decay (Dalitz variables, angles that determine the orientation of the four-body system, invariant masses of the resonances and intermediate isobars, etc.). Then the normalized decay distribution has the following form:

$$W(\xi) = f(\xi) + \lambda_\gamma g(\xi) \quad (\text{E.9})$$

where the functions f and g satisfy the conditions

$$\int g d\xi = 0, \quad \int f d\xi = 1, \quad f \geq 0, \quad |g| \leq f \quad (\text{E.10})$$

The first condition in Eq. (E.10), $\int g d\xi = 0$, expresses the fact that the decay width does not depend on the polarization, while the second one is the probability normalization condition. The two last conditions, $f \geq 0$ and $|g| \leq f$, represent the positive character of W which is proportional to the matrix element squared.

For a sample of N measured events the likelihood function \mathcal{L} can be defined as

$$\mathcal{L} = \prod_{i=1}^N (f(\xi_i) + \lambda_\gamma g(\xi_i)) \quad (\text{E.11})$$

However it is more convenient to use the logarithmic likelihood

$$\begin{aligned}\ln \mathcal{L} &= \sum_{i=1}^N \ln[f(\xi_i)(1 + \lambda_\gamma \omega_i)] \\ &= \sum_{i=1}^N \ln(1 + \lambda_\gamma \omega_i) + \text{other terms independent on } \lambda_\gamma\end{aligned}\tag{E.12}$$

One can see from Eq. (E.12) that the quantity

$$\omega_i = \frac{g(\xi_i)}{f(\xi_i)}\tag{E.13}$$

contains all information to measure the polarization and depends only on the kinematic variables.

Using the method of maximum likelihood, the true polarization parameter λ_γ maximizes \mathcal{L} and consequently can be determined as the solution of the equation

$$\frac{\partial \ln \mathcal{L}}{\partial \lambda_\gamma} = \sum_{i=1}^N \frac{\omega_i}{1 + \lambda_\gamma \omega_i} = N \left\langle \frac{\omega}{1 + \lambda_\gamma \omega} \right\rangle = 0\tag{E.14}$$

The standard error of the optimal mean value of λ_γ is also determined as a function of ω -variable:

$$\frac{1}{\sigma_{\lambda_\gamma}^2} = -\frac{\partial^2 \ln \mathcal{L}}{\partial^2 \lambda_\gamma} = \sum_{i=1}^N \frac{\omega_i^2}{(1 + \lambda_\gamma \omega_i)^2} = N \left\langle \left(\frac{\omega}{1 + \lambda_\gamma \omega} \right)^2 \right\rangle\tag{E.15}$$

For the small values of λ_γ ¹ the likelihood maximization is equivalent to a moment method:

$$\left\langle \frac{\omega}{1 + \lambda_\gamma \omega} \right\rangle \approx \langle \omega \rangle - \lambda_\gamma \langle \omega^2 \rangle = 0\tag{E.16}$$

and hence the polarization parameter can be determined as

$$\lambda_\gamma \approx \frac{\langle \omega \rangle}{\langle \omega^2 \rangle}\tag{E.17}$$

On the other side, one can write the new PDF of the ω -distribution as

$$W'(\omega) = \varphi(\omega)(1 + \lambda_\gamma \omega)\tag{E.18}$$

where $\varphi(\omega)$ is an unknown function, which is very hard to determine analytically. This requires to perform a numerical MC simulation. However, in some particular cases $\varphi(\omega)$

¹ τ -polarization is of the order of 0.1 and the expansion in terms of λ_γ is reasonable, while in our case $\lambda_\gamma \simeq \pm 1$ in the SM. But one can see from Fig. 2.3 that ω is concentrated around 0, so one can assume that such expansion can be used.

turns out to be an even function of ω (one can see from Eq. (2.56c) $f(s_{13}, s_{23}, \cos \theta)$ is an even function of $\cos \theta$ while $\omega(s_{13}, s_{23}, \cos \theta)$ is an odd one).

Then, one can easily demonstrate by integration over the interval $-1 \leq \omega \leq 1$ that λ_γ can be expressed as ratios of odd over even momenta:

$$\lambda_\gamma = \frac{\langle \omega^{2n-1} \rangle}{\langle \omega^{2n} \rangle} \quad (n \geq 1) \quad (\text{E.19})$$

where the moments are defined as

$$\langle \omega^n \rangle \equiv \int_{-1}^1 \omega^n W'(\omega) d\omega \quad (\text{E.20})$$

Therefore, the expression obtained by DDLR for small λ_γ (E.17) seems exact.

Here we provide a demonstration that, indeed, $\varphi(\omega)$ is the even function of ω in the case of polarization measurement in the $B \rightarrow K_1 \gamma$ decay.

The normalization condition for our PDFs, $W(s_{13}, s_{23}, \cos \theta)$ (Eq. (2.55)) and $W'(\omega)$ (Eq. (E.18)) can be written as

$$\int W(s_{13}, s_{23}, \cos \theta) ds_{13} ds_{23} d\cos \theta = 1 \quad (\text{E.21a})$$

$$\int_{-1}^1 W'(\omega) d\omega = 1 \quad (\text{E.21b})$$

This normalization equation (E.21) can be modified by inserting the integration over new “independent” variable ω , defined by Eq. (2.59), and be identified with the new $W'(\omega)$ function:

$$\int_{-1}^1 d\omega \underbrace{\int W(s_{13}, s_{23}, \cos \theta) \delta \left(\omega - r_{\mathcal{J}} \frac{2 \cos \theta}{1 + \cos^2 \theta} \right) ds_{13} ds_{23} d\cos \theta}_{W'(\omega)} = 1 \quad (\text{E.22})$$

whith

$$r_{\mathcal{J}}(s_{13}, s_{23}) = \frac{\text{Im}[\vec{n} \cdot (\vec{\mathcal{J}} \times \vec{\mathcal{J}}^*)]}{|\vec{\mathcal{J}}|^2} \quad (\text{E.23})$$

Using the well known property of the delta-function

$$\delta(y(x)) = \sum_k \frac{\delta(x - x_k)}{|y'(x_k)|}, \quad y(x_k) \equiv 0 \quad (\text{E.24})$$

one can write

$$\delta\left(\omega - r_{\mathcal{J}} \frac{2 \cos \theta}{1 + \cos^2 \theta}\right) = \frac{1}{2|r_{\mathcal{J}}|} \sum_{+,-} \frac{(1 + \cos^2 \theta_{\pm})^2}{1 - \cos^2 \theta_{\pm}} \delta(\cos \theta - \cos \theta_{\pm}) \quad (\text{E.25})$$

with

$$\cos \theta_{\pm} = \frac{r_{\mathcal{J}} \pm \sqrt{r_{\mathcal{J}}^2 - \omega^2}}{\omega} \quad (\text{E.26})$$

Note that only one of these two solutions satisfies the condition $|\cos \theta_{\pm}| \leq 1$ depending on the sign of $r_{\mathcal{J}}$ (see Fig. E.1). However, it is easy to notice that

$$\cos^2 \theta_{\pm} = \frac{(|r_{\mathcal{J}}| - \sqrt{r_{\mathcal{J}}^2 - \omega^2})^2}{\omega^2} \quad (\text{E.27})$$

satisfies $|\cos \theta_{\pm}| \leq 1$ for both positive and negative values of $r_{\mathcal{J}}$.

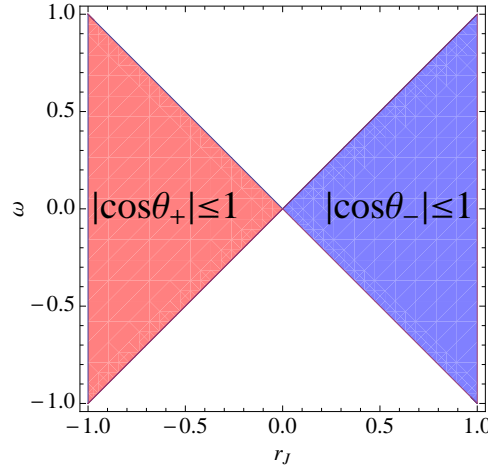


Figure E.1: Allowed regions for the $r_{\mathcal{J}}-\omega$ space coming from the requirement $|\cos \theta_{\pm}| \leq 1$.

Therefore, using Eq. (E.27) and integrating Eq. (E.22) over $\cos \theta$, we obtain

$$\begin{aligned} W'(\omega) &= \int \frac{|\vec{\mathcal{J}}|^2}{4I} \frac{(1 + \cos^2 \theta_{\pm})^3}{2|r_{\mathcal{J}}|(1 - \cos^2 \theta_{\pm})} (1 + \lambda_{\gamma}\omega) ds_{13} ds_{23} \\ &= \int \frac{|\vec{\mathcal{J}}|^2}{2I} \frac{r_{\mathcal{J}}^2}{\sqrt{r_{\mathcal{J}}^2 - \omega^2} (|r_{\mathcal{J}}| - \sqrt{r_{\mathcal{J}}^2 - \omega^2})^2} (1 + \lambda_{\gamma}\omega) ds_{13} ds_{23} \end{aligned} \quad (\text{E.28})$$

One can easily see from Eq. (E.28) that $\varphi(\omega)$

$$\varphi(\omega) = \int \frac{|\vec{\mathcal{J}}|^2}{2I} \frac{r_{\mathcal{J}}^2}{\sqrt{r_{\mathcal{J}}^2 - \omega^2} (|r_{\mathcal{J}}| - \sqrt{r_{\mathcal{J}}^2 - \omega^2})^2} ds_{13} ds_{23} \quad (\text{E.29})$$

is indeed the even function of ω as desired.

Bibliography

- [1] N. Cabibbo, “Unitary Symmetry and Leptonic Decays”, *Phys. Rev. Lett.* **10** (1963) 531–533.
- [2] M. Kobayashi and T. Maskawa, “CP Violation in the Renormalizable Theory of Weak Interaction”, *Prog. Theor. Phys.* **49** (1973) 652–657.
- [3] L. Wolfenstein, “Parametrization of the Kobayashi-Maskawa Matrix”, *Phys. Rev. Lett.* **51** (1983) 1945.
- [4] **LEP Working Group for Higgs boson searches** Collaboration, R. Barate *et al.*, “Search for the standard model Higgs boson at LEP”, *Phys. Lett.* **B565** (2003) 61–75, [arXiv:hep-ex/0306033](#).
- [5] **CDF and DØ** Collaboration, T. Aaltonen *et al.*, “Combined CDF and DØ Upper Limits on Standard Model Higgs Boson Production with up to 8.2 fb⁻¹ of Data”, [arXiv:1103.3233 \[hep-ex\]](#).
- [6] N. Arkani-Hamed, S. Dimopoulos, and G. R. Dvali, “The hierarchy problem and new dimensions at a millimeter”, *Phys. Lett.* **B429** (1998) 263–272, [arXiv:hep-ph/9803315](#).
- [7] L. Randall and R. Sundrum, “A large mass hierarchy from a small extra dimension”, *Phys. Rev. Lett.* **83** (1999) 3370–3373, [arXiv:hep-ph/9905221](#).
- [8] S. L. Glashow, J. Iliopoulos, and L. Maiani, “Weak Interactions with Lepton-Hadron Symmetry”, *Phys. Rev.* **D2** (1970) 1285–1292.
- [9] **Heavy Flavor Averaging Group** Collaboration, D. Asner *et al.*, “Averages of b -hadron, c -hadron, and τ -lepton properties”, [arXiv:1010.1589 \[hep-ex\]](#).
- [10] M. Misiak *et al.*, “The first estimate of $\mathcal{B}(\overline{B} \rightarrow X_s \gamma)$ at $O(\alpha_s^2)$ ”, *Phys. Rev. Lett.* **98** (2007) 022002, [arXiv:hep-ph/0609232](#).
- [11] M. Gronau and D. Pirjol, “Photon polarization in radiative B decays”, *Phys. Rev.* **D66** (2002) 054008, [arXiv:hep-ph/0205065](#).
- [12] M. Gronau, Y. Grossman, D. Pirjol, and A. Ryd, “Measuring the photon helicity in radiative B decays”, *Phys. Rev. Lett.* **88** (2002) 051802, [arXiv:hep-ph/0107254](#).

- [13] **Belle** Collaboration, H. Yang *et al.*, “Observation of $B^+ \rightarrow K_1(1270)^+\gamma$ ”, *Phys. Rev. Lett.* **94** (2005) 111802, [arXiv:hep-ex/0412039](#).
- [14] M. Davier, L. Duflot, F. Le Diberder, and A. Roug  , “The Optimal method for the measurement of τ polarization”, *Phys. Lett.* **B306** (1993) 411.
- [15] T. Inami and C. S. Lim, “Effects of Superheavy Quarks and Leptons in Low-Energy Weak Processes $K_L \rightarrow \mu\bar{\mu}$, $K^+ \rightarrow \pi^+\nu\bar{\nu}$ and $K^0 \leftrightarrow \bar{K}^0$ ”, *Prog. Theor. Phys.* **65** (1981) 297.
- [16] A. J. Buras, “Weak Hamiltonian, CP violation and rare decays”, [arXiv:hep-ph/9806471](#).
- [17] S. W. Bosch and G. Buchalla, “Constraining the unitarity triangle with $B \rightarrow V\gamma$ ”, *JHEP* **01** (2005) 035, [arXiv:hep-ph/0408231](#).
- [18] M. Matsumori and A. I. Sanda, “The mixing-induced CP asymmetry in $B \rightarrow K^*\gamma$ decays with perturbative QCD approach”, *Phys. Rev.* **D73** (2006) 114022, [arXiv:hep-ph/0512175](#).
- [19] B. Grinstein, Y. Grossman, Z. Ligeti, and D. Pirjol, “The photon polarization in $B \rightarrow X\gamma$ in the Standard Model”, *Phys. Rev.* **D71** (2005) 011504, [arXiv:hep-ph/0412019](#).
- [20] B. Grinstein and D. Pirjol, “The CP asymmetry in $B^0(t) \rightarrow K_S\pi^0\gamma$ in the Standard Model”, *Phys. Rev.* **D73** (2006) 014013, [arXiv:hep-ph/0510104](#).
- [21] A. Khodjamirian, R. Ruckl, G. Stoll, and D. Wyler, “QCD estimate of the long-distance effect in $B \rightarrow K^*\gamma$ ”, *Phys. Lett.* **B402** (1997) 167–177, [arXiv:hep-ph/9702318](#).
- [22] P. Ball and R. Zwicky, “Time-dependent CP asymmetry in $B \rightarrow K^*\gamma$ as a (quasi)null test of the Standard Model”, *Phys. Lett.* **B642** (2006) 478–486, [arXiv:hep-ph/0609037](#).
- [23] P. Ball and R. Zwicky, “ $B_{d,s} \rightarrow \rho, \omega, K^*, \phi$ Decay Form Factors from Light-Cone Sum Rules Revisited”, *Phys. Rev.* **D71** (2005) 014029, [arXiv:hep-ph/0412079](#).
- [24] P. Ball and R. Zwicky, “ $B \rightarrow K^*\gamma$ vs $B \rightarrow \rho\gamma$ and $|V_{td}/V_{ts}|$ ”, [arXiv:hep-ph/0608009](#).
- [25] **Belle** Collaboration, Y. Ushiroda *et al.*, “Time-dependent CP asymmetries in $B^0 \rightarrow K_S^0\pi^0\gamma$ transitions”, *Phys. Rev.* **D74** (2006) 111104, [arXiv:hep-ex/0608017](#).
- [26] **BABAR** Collaboration, B. Aubert *et al.*, “Measurement of Time-Dependent CP Asymmetry in $B^0 \rightarrow K_S^0\pi^0\gamma$ Decays”, *Phys. Rev.* **D78** (2008) 071102, [arXiv:0807.3103 \[hep-ex\]](#).

- [27] L. L. Everett, G. L. Kane, S. Rigolin, L.-T. Wang, and T. T. Wang, “Alternative approach to $b \rightarrow s\gamma$ in the uMSSM”, *JHEP* **01** (2002) 022, [arXiv:hep-ph/0112126](#).
- [28] W. Altmannshofer *et al.*, “Symmetries and Asymmetries of $B \rightarrow K^*\mu^+\mu^-$ Decays in the Standard Model and Beyond”, *JHEP* **01** (2009) 019, [arXiv:0811.1214 \[hep-ph\]](#).
- [29] J. Foster, K.-i. Okumura, and L. Roszkowski, “New constraints on SUSY flavour mixing in light of recent measurements at the Tevatron”, *Phys. Lett.* **B641** (2006) 452–460, [arXiv:hep-ph/0604121](#).
- [30] T. Goto, Y. Okada, T. Shindou, and M. Tanaka, “Patterns of flavor signals in supersymmetric models”, *Phys. Rev.* **D77** (2008) 095010, [arXiv:0711.2935 \[hep-ph\]](#).
- [31] T. Aushev *et al.*, “Physics at Super B Factory”, [arXiv:1002.5012 \[hep-ex\]](#).
- [32] E. Lunghi and J. Matias, “Huge right-handed current effects in $B \rightarrow K^*(K\pi)\ell^+\ell^-$ in supersymmetry”, *JHEP* **04** (2007) 058, [arXiv:hep-ph/0612166](#).
- [33] S. P. Martin, “A Supersymmetry Primer”, [arXiv:hep-ph/9709356](#).
- [34] L. J. Hall, V. A. Kostelecky, and S. Raby, “New Flavor Violations in Supergravity Models”, *Nucl. Phys.* **B267** (1986) 415.
- [35] F. Gabbiani, E. Gabrielli, A. Masiero, and L. Silvestrini, “A complete analysis of FCNC and CP constraints in general SUSY extensions of the standard model”, *Nucl. Phys.* **B477** (1996) 321–352, [arXiv:hep-ph/9604387](#).
- [36] I. I. Y. Bigi and A. I. Sanda, “CP violation”, *Camb. Monogr. Part. Phys. Nucl. Phys. Cosmol.* **9** (2000) 1–382.
- [37] **Particle Data Group** Collaboration, K. Nakamura *et al.*, “Review of particle physics”, *J. Phys.* **G37** (2010) 075021.
- [38] D. Atwood, T. Gershon, M. Hazumi, and A. Soni, “Clean Signals of CP-violating and CP-conserving New Physics in $B \rightarrow PV\gamma$ Decays at B Factories and Hadron Colliders”, [arXiv:hep-ph/0701021](#).
- [39] V. D. Orlovsky and V. I. Shevchenko, “On the photon polarization in radiative $B \rightarrow \phi K\gamma$ decay”, *Phys. Rev.* **D77** (2008) 093003, [arXiv:0708.4302 \[hep-ph\]](#).
- [40] H. Hatanaka and K.-C. Yang, “ $B \rightarrow K_1\gamma$ Decays in the Light-Cone QCD Sum Rules”, *Phys. Rev.* **D77** (2008) 094023, [arXiv:0804.3198 \[hep-ph\]](#).
- [41] J.-P. Lee, “Radiative $B \rightarrow K_1$ decays in the light-cone sum rules”, *Phys. Rev.* **D74** (2006) 074001, [arXiv:hep-ph/0608087](#).

- [42] S. Nishida, “New results on $B \rightarrow V\gamma$ decays”, Sep, 2008. International Workshop on the CKM Unitarity Triangle (CKM2008).
- [43] Belle Collaboration, H. Guler *et al.*, “Study of the $K^+\pi^+\pi^-$ Final State in $B^+ \rightarrow J/\psi K^+\pi^+\pi^-$ and $B^+ \rightarrow \psi' K^+\pi^+\pi^-$ ”, *Phys. Rev.* **D83** (2011) 032005, [arXiv:1009.5256 \[hep-ex\]](#).
- [44] S. U. Chung, “Spin formalisms”, <http://cdsweb.cern.ch/search?sysno=000097856CER>. Lectures given in Academic Training Program of CERN, 1969-1970.
- [45] ACCMOR Collaboration, C. Daum *et al.*, “Diffractive production of strange mesons at 63 GeV”, *Nucl. Phys.* **B187** (1981) 1.
- [46] R. K. Carnegie, R. J. Cashmore, W. M. Dunwoodie, T. A. Lasinski, and D. W. G. S. Leith, “ $Q_1(1290)$ and $Q_2(1400)$ Decay Rates and their SU(3) Implications”, *Phys. Lett.* **B68** (1977) 287.
- [47] CERN-College de France-Madrid-Stockholm Collaboration, S. Rodeback *et al.*, “ Q_1 production by hypercharge exchange in π^-p interactions at 3.95 GeV/c”, *Zeit. Phys.* **C9** (1981) 9.
- [48] D. Aston *et al.*, “The strange meson resonances observed in the reaction $K^-p \rightarrow \bar{K}^0\pi^+\pi^-n$ at 11 GeV/c”, *Nucl. Phys.* **B292** (1987) 693.
- [49] M. Suzuki, “Strange axial-vector mesons”, *Phys. Rev.* **D47** (1993) 1252–1255.
- [50] TPC/Two Gamma Collaboration, D. A. Bauer *et al.*, “Measurement of the kaon content of three prong τ decays”, *Phys. Rev.* **D50** (1994) 13–17.
- [51] ALEPH Collaboration, R. Barate *et al.*, “Study of τ decays involving kaons, spectral functions and determination of the strange quark mass”, *Eur. Phys. J.* **C11** (1999) 599–618, [arXiv:hep-ex/9903015](#).
- [52] OPAL Collaboration, G. Abbiendi *et al.*, “A study of three-prong τ decays with charged kaons”, *Eur. Phys. J.* **C13** (2000) 197–212, [arXiv:hep-ex/9908013](#).
- [53] CLEO Collaboration, D. M. Asner *et al.*, “Resonance structure of $\tau^- \rightarrow K^-\pi^+\pi^-\nu_\tau$ decays”, *Phys. Rev.* **D62** (2000) 072006, [arXiv:hep-ex/0004002](#).
- [54] BABAR Collaboration, B. Aubert *et al.*, “Measurement of branching fractions of B decays to $K_1(1270)\pi$ and $K_1(1400)\pi$ and determination of the CKM angle α from $B^0 \rightarrow a_1(1260)^\pm\pi^\mp$ ”, *Phys. Rev.* **D81** (2010) 052009, [arXiv:0909.2171 \[hep-ex\]](#).
- [55] H. G. Blundell, S. Godfrey, and B. Phelps, “Properties of the Strange Axial Mesons in the Relativized Quark Model”, *Phys. Rev.* **D53** (1996) 3712–3722, [arXiv:hep-ph/9510245](#).

- [56] S. Godfrey and N. Isgur, “Mesons in a Relativized Quark Model with Chromodynamics”, *Phys. Rev.* **D32** (1985) 189–231.
- [57] H. J. Lipkin, *Lie groups for pedestrians*. North-Holland Publishing Company, Amsterdam, 1966.
- [58] G. L. Kane, “Some Consequences of $SU(3)$ and Charge-Conjugation Invariance for K -Meson Resonances”, *Phys. Rev.* **156** (1967) 1738–1741.
- [59] G. L. Kane and H. S. Mani, “Interference of Kaon Resonances”, *Phys. Rev.* **171** (1968) 1533–1539.
- [60] L. Micu, “Decay rates of meson resonances in a quark model”, *Nucl. Phys.* **B10** (1969) 521–526.
- [61] R. D. Carlitz and M. Kislinger, “Regge amplitude arising from $SU(6)_W$ vertices”, *Phys. Rev.* **D2** (1970) 336–342.
- [62] A. Le Yaouanc, L. Oliver, O. Pène, and J. Raynal, “Naive quark pair creation model of strong interaction vertices”, *Phys. Rev.* **D8** (1973) 2223–2234.
- [63] R. Kokoski and N. Isgur, “Meson Decays by Flux Tube Breaking”, *Phys. Rev.* **D35** (1987) 907.
- [64] H. G. Blundell and S. Godfrey, “The $\xi(2220)$ revisited: Strong decays of the 1^3F_2 1^3F_4 $s\bar{s}$ mesons”, *Phys. Rev.* **D53** (1996) 3700–3711, [arXiv:hep-ph/9508264](#).
- [65] E. W. Colglazier and J. L. Rosner, “Quark graphs and angular distributions in positive parity meson decays”, *Nucl. Phys.* **B27** (1971) 349–371.
- [66] A. Barbaro-Galtieri. Proceedings of the Erice Summer School (1971), p.581.
- [67] B. Silvestre-Brac and C. Gignoux, “Unitary effects in spin orbit splitting of P wave baryons”, *Phys. Rev.* **D43** (1991) 3699–3708.
- [68] M. G. Bowler, J. B. Dainton, A. Kaddoura, and I. J. R. Aitchison, “A Two Resonance Analysis of the $Q(K\pi\pi)$ Enhancement”, *Nucl. Phys.* **B74** (1974) 493.
- [69] M. Nauenberg and A. Pais, “Woolly Cusps”, *Phys. Rev.* **126** (1962) no. 1, 360–364.
- [70] W. R. Frazer and A. W. Hendry, “S-Matrix Poles Close to Threshold”, *Phys. Rev.* **134** (1964) B1307–B1314.
- [71] **CKMfitter Group** Collaboration, J. Charles *et al.*, “CP violation and the CKM matrix: Assessing the impact of the asymmetric B factories”, *Eur. Phys. J.* **C41** (2005) 1–131, [arXiv:hep-ph/0406184](#).
- [72] W. Dunwoodie. private communication.

- [73] S. Descotes-Genon and B. Moussallam, “The $K_0^*(800)$ scalar resonance from Roy-Steiner representations of πK scattering”, *Eur. Phys. J.* **C48** (2006) 553, [arXiv:hep-ph/0607133](#).
- [74] S. Barsuk *et al.*, “The road map for the radiative decays of beauty hadrons at LHCb”, Feb, 2009. <http://cdsweb.cern.ch/record/1163013>. LHCb public note.
- [75] F. Kruger and J. Matias, “Probing new physics via the transverse amplitudes of $B^0 \rightarrow K^{*0}(\rightarrow K^-\pi^+)\ell^+\ell^-$ at large recoil”, *Phys. Rev.* **D71** (2005) 094009, [arXiv:hep-ph/0502060](#).
- [76] D. Becirevic and E. Schneider, “On transverse asymmetries in $B \rightarrow K^*\ell^+\ell^-$ ”, *Nucl. Phys.* **B854** (2012) 321–339, [arXiv:1106.3283 \[hep-ph\]](#). * Temporary entry *.
- [77] J. Lefrançois and M.-H. Schune, “Measuring the photon polarization in $b \rightarrow s\gamma$ using the $B \rightarrow K^*e^+e^-$ decay channel”, Tech. Rep. CERN-LHCb-PUB-2009-008, CERN, Geneva, Jun, 2009.
- [78] D. Atwood, M. Gronau, and A. Soni, “Mixing-induced CP asymmetries in radiative B decays in and beyond the standard model”, *Phys. Rev. Lett.* **79** (1997) 185–188, [arXiv:hep-ph/9704272](#).
- [79] F. Muheim, Y. Xie, and R. Zwicky, “Exploiting the width difference in $B_s \rightarrow \phi\gamma$ ”, *Phys. Lett.* **B664** (2008) 174–179, [arXiv:0802.0876 \[hep-ph\]](#).
- [80] **SuperB** Collaboration, M. Bona *et al.*, “SuperB: A High-Luminosity Asymmetric e^+e^- Super Flavor Factory. Conceptual Design Report”, [arXiv:0709.0451 \[hep-ex\]](#).
- [81] S. Khalil and E. Kou, “On supersymmetric contributions to the CP asymmetry of the $B \rightarrow \phi K_S$ ”, *Phys. Rev.* **D67** (2003) 055009, [arXiv:hep-ph/0212023](#).
- [82] I. J. R. Aitchison, “ K -matrix formalism for overlapping resonances”, *Nucl. Phys.* **A189** (1972) 417–423.
- [83] S. Godfrey and R. Kokoski, “The Properties of P Wave Mesons with One Heavy Quark”, *Phys. Rev.* **D43** (1991) 1679–1687.

Acknowledgements

Looking back, I am surprised how the time has flown by in a wink and at the same time very grateful for all I have received throughout these three years. It has certainly shaped me as a person and has led me where I am now. I would like to express my thanks to everyone who have been very helpful to me during the time it took me to write this thesis.

In the beginning I would like to thank Laboratoire de l'Accélérateur Linéaire, Laboratoire de Physique Théorique and Université Paris-Sud 11 (and in particular Achille Stocchi and Henk Hilhorst) for their hospitality and the opportunity to accomplish this thesis.

First and foremost I want to thank my supervisor from LAL, Emi Kou. It has been an honor to be her first PhD student. I am deeply grateful to Alain Le Yaouanc, my supervisor from LPT. I appreciate all their patience, contributions, ideas to make my PhD experience productive and stimulating. Their guidance helped me a lot in all the time of research and writing of this thesis. I have enormous gratitude for their concern about me and their assistance in resolving numerous scientific and administrative problems appeared during these three years of PhD. Domo arigato gozaimasu Emi, merci beaucoup Alain!

For this dissertation I would like to thank the reporters, Aldo Deandrea and Tim Gershon, who kindly agreed to read this manuscript, their comments were really helpful. I am also grateful to the other members of my jury committee, Jérôme Charles, Ulrich Ellwanger, Svjetlana Fajfer and Marie-Hélène Schune whose contribution cannot be overestimated.

I am particularly indebted to the director of LAL, Achille Stocchi, a person without whom this thesis (as well as my arrival in France) would not take place. Through him, I found myself a place as a master and later as a PhD student at Université Paris-Sud 11. I gratefully acknowledge for his invaluable help, concern and support during the whole period of my education, PhD research and stay in France. Tante grazie di tutto Achille!

I also want to thank Andrey Golutvin and Vanya Belyaev, my supervisors of my M.Sc. thesis when I studied in MIPT. Under their supervision I started doing particle physics being a bachelor student in ITEP. And although I decided to leave experimental physics and move to Paris to do my PhD in theoretical physics after my graduation, the time I spent at CERN working in the LHCb collaboration during several years and the experience and knowledge I acquired working with Andrey and Vanya were very-very useful for me in future.

Far too many people to mention individually have assisted in so many ways during my work at LPT and LAL. They all have my sincere gratitude. In particular, I would like to thank Asmaa Abada, Damir Becirevic, Michel Davier, Sebastien Descotes-Genon, Laurent Duflot, Jaques Lefrançois, François Le Diberder, Anne-Marie Lutz, Nejc Kosnik, Luis Oliver, Olivier Pène, Marie-Hélène Schune.

I have enormous gratitude to Damir Becirevic, with whom I started studying B -physics during my stage de pré-thèse being a master student. Thank you very much, Damir, for being always ready to help and for your concern! Our physics discussions were very useful and helpful for me, I learned a lot.

My warm, sincere thanks to François Le Diberder and Laurent Duflot for their precious help in understanding the basics of the DDLR method and some aspects of statistical methods. It gave me tools that turned out to be essential in my PhD research. I also want to thank Denis Bernard for his suggested idea to try to apply the original DDLR method to our case.

The collaboration with the LHCb group of LAL was extremely useful for the work of this thesis. In particular, I would like to thank Marie-Hélène Schune and Jaques Lefrançois wholeheartedly for very nice collaboration.

I want to thank William Dunwoodie, Eli Ben-Haim, Pablo del Amo Sanchez, Li-Jin and Sandrine Emery for the discussions of the experimental aspects of the $K_1 \rightarrow K\pi\pi$ decays.

My stay in France was made enjoyable in large part due to the many friends that became a part of my life. I am grateful for time spent with friends and buddies, I will never forget for our memorable life in Paris. I would like to thank all PhD students from LAL and LPT with whom it was a pleasure to share doctoral studies and students life: Julien Baglio, Rémi Bardenet, Yannis Bardoux, Adrien Besse, Charles Bouchart, Leonid Burmistrov, Iryna Chaikovska, Antonin Coutant, Denis Derkach, Philippe Doublet, Ilya Drebot, Andreas Goudelis, Aurélien Martens, Michelle Nicol, Joachim Rambeau, Guillaume Toucas, Viktor Yakovenko, Cédric Weiland. I would like to thank in particular Aurélien, Denis and Leonid who have helped me along the way in programming and teaching me some of the experimental statistical techniques. The years spent in Paris would not have been as wonderful without my friends from our Russian-Ukrainian “mafia”: Denis, Lenya, Ira, Ilya, Misha D., Misha R., Slava, Vitya, Veronika, Julya, Natasha and Denis C..

Lastly, and most importantly, I wish to thank my parents. They bore me, raised and supported me. I am infinitely grateful to them for that since my childhood they trained me to discipline and to work hard and a lot. This acquired habit has become very indispensable in my entire life. Without my parents support I would not be able to be where I am now.

My apologies to those who have not been cited amongst these lines. Thanks to all of you!